TESIS DE LA UNIVERSIDAD
DE ZARAGOZA

2021

260

Gabriele Nasello

Bone regeneration in patient-specific scaffolds from microfluidics to computational simulation

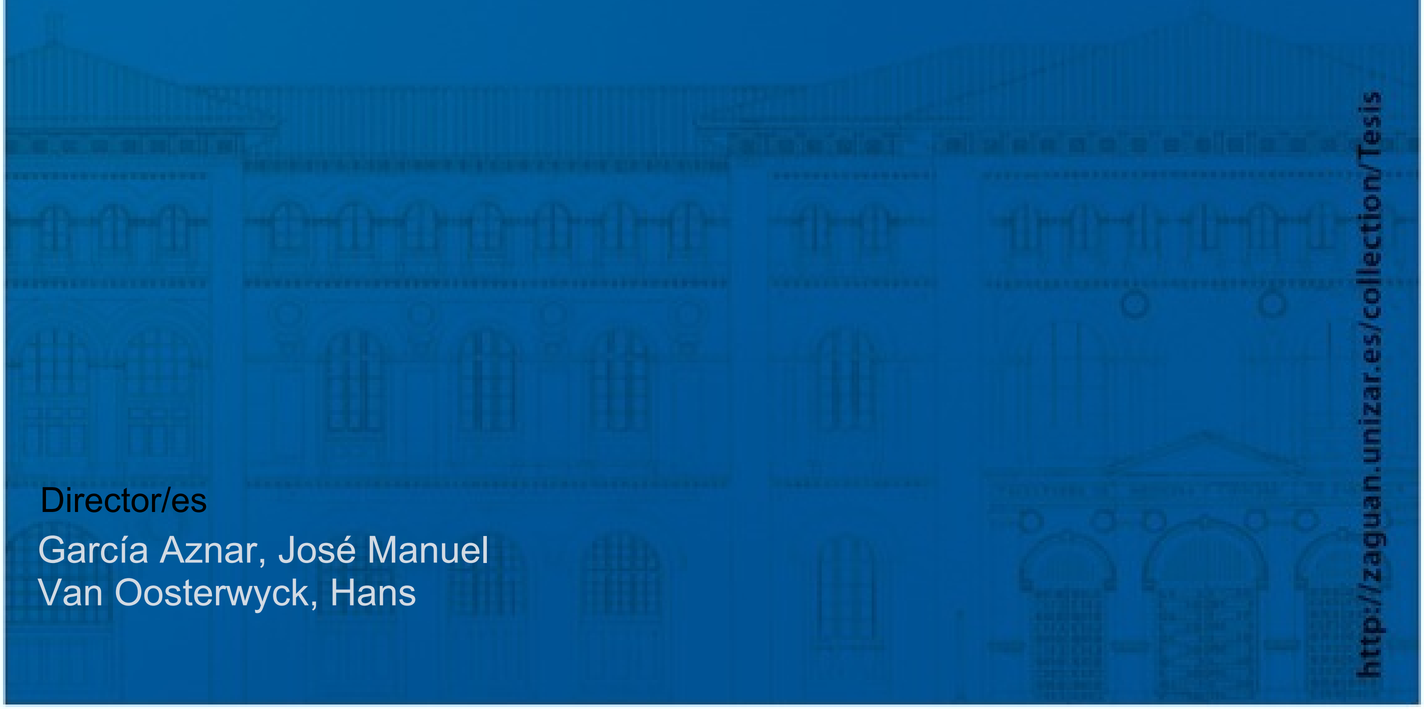

Director/es

García Aznar, José Manuel
Van Oosterwyck, Hans

http://zaguan.unizar.es/collection/Tesis

ISSN 2254-7606

Prensas de la Universidad
Universidad Zaragoza

© Universidad de Zaragoza
Servicio de Publicaciones

ISSN 2254-7606

Tesis Doctoral

BONE REGENERATION IN PATIENT-SPECIFIC SCAFFOLDS FROM MICROFLUIDICS TO COMPUTATIONAL SIMULATION

Autor

Gabriele Nasello

Director/es

García Aznar, José Manuel
Van Oosterwyck, Hans

UNIVERSIDAD DE ZARAGOZA
Escuela de Doctorado

Programa de Doctorado en Ingeniería Biomédica

2021

Repositorio de la Universidad de Zaragoza – Zaguan http://zaguan.unizar.es

Universidad Zaragoza
1542

KU LEUVEN

BONE REGENERATION IN PATIENT-SPECIFIC SCAFFOLDS

FROM MICROFLUIDICS TO COMPUTATIONAL SIMULATION

GABRIELE NASELLO

DOCTORAL DISSERTATION
SUPERVISORS:
PROF. J. M. GARCÍA AZNAR
PROF. H. VAN OOSTERWYCK

Instituto Universitario de Investigación
de Ingeniería de Aragón
Universidad Zaragoza

KU LEUVEN

Bone regeneration in patient-specific scaffolds

From microfluidics to computational simulation

Gabriele NASELLO

Supervisors:
Prof. J.M. García Aznar
Prof. H. Van Oosterwyck

Jury members:
Prof. R. Puers, chair
Prof. M.A. Pérez
Prof. L. Geris
Dr. G. Reilly
Prof. S. Hofmann
Dr. A. Carlier
Prof. S. Checa
Dr. T. Vaughan

Dissertation presented in partial fulfillment of the requirements for the degree of Doctor in Biomedical Engineering at Universidad de Zaragoza and the degree of Doctor in Engineering Science (PhD): Mechanical Engineering at KU Leuven

March 2021

Copyright © 2021 - Gabriele Nasello.

All rights reserved. No part of the publication may be reproduced in any form by print, photoprint, microfilm, electronic or any other means without written permission from the author.

Cover design by Gabriele Nasello.

This research is part of the CuraBone project and conducted with financial support of the European Union's Horizon 2020 research and innovation programme under the Marie Skłodowska-Curie grant agreement No 722535 (CuraBone project).

Abstract

Musculoskeletal disorders and related bone diseases are one of the major causes of pain and disability, resulting in a social and economical burden for our society. When the joint function is impaired or bone defects are too large for bone grafts, prosthetic implants are the gold standard to replace the defective tissues or fill the gap, however there is the clinical need of implants remaining active for longer period of time and reducing revision rates. To address the higher durability of orthopedic implants, three-dimensional (3D) printed implants have recently emerged to fabricate patient-specific porous surfaces at the bone-implant surface, thus enhancing the implant biological integration and fixation. The translation of regenerative medicine principles to orthopedic solutions can define a new generation of implants completing the transition from inert materials to bioactive scaffolds guiding the bone regeneration process. In the short-term, regenerative 3D printed orthopedic scaffolds are likely to increase osteointegration, while in the long-term they aim to degrade once the host tissue is fully repaired. The global objective of this thesis was to evaluate the regenerative potential associated to 3D printed bone scaffolds for patient-specific orthopedic applications.

The first study aimed at determining the role of the host mechanical environment on the bone regeneration process guided by 3D printed bone scaffolds in load-bearing applications. A computational model of mechano-driven bone regeneration in porous scaffolds was developed and based on the subject specificity, implantation site and sensitivity to the mechanical environment. Bone ingrowth in porous titanium scaffolds was then simulated in the distal femur and proximal tibia of three goats and compared to experimental results. The results showed that bone ingrowth shifted from a homogeneous distribution pattern, when scaffolds were in contact with trabecular bone, to a localized bone ingrowth when scaffolds were implanted in a diaphyseal location. Overall, the dependence of the osteogenic response on the host biomechanics suggested that, from a mechanical perspective, the regenerative potential depended on both the scaffold and the host environment.

The second study of this thesis aimed at evaluating the patient-specific osteogenic activity in a controlled *in vitro* environment where human bone cells, isolated from individual subjects, mimic the essential traits of the bone formation process. Traditional *in vitro* systems already showed that primary human osteoblasts embedded in a 3D fibrous collagen matrix differentiate into osteocytes under specific conditions. Therefore, it was hypothesized that translating this environment to the organ-on-a-chip scale creates a minimal functional unit to recapitulate osteoblast maturation towards osteocytes and matrix mineralization. Primary human osteoblasts were seeded in a type I collagen hydrogel, to establish the role of cell seeding density on their differentiation into osteocytes. Results showed that cells cultured at higher density exhibit dendritic morphology, increase dendrite length over time, stop proliferating, upregulate alkaline phosphatase activity and express osteocyte markers. This study revealed that microengineered systems are a functional strategy to create a patient-specific bone tissue model and investigate the individual osteogenic potential of the patient bone cells.

Taken together, the results of this thesis emphasize the importance of using multiple modeling systems when investigating the *in vivo* regeneration process guided by patient-specific bone scaffolds. Both actors of a cell-free *in situ* regenerative strategy, namely the scaffold and the patient, have a significant effect on the final regenerative outcome and needs to be modeled. Advanced *in vitro* and *in silico* techniques, combined with *in vivo* data, evaluate distinctive aspects of the bone regeneration process for patient-specific applications. Future personalized tissue engineering strategies could rely on the integration of those models to ultimately mitigate variability in the bone regeneration process guided by a patient-specific scaffold.

Resumen

Los trastornos musculoesqueléticos y sus correspondientes enfermedades óseas son una de las principales causas de dolor y discapacidad, así como una carga social y económica para nuestra sociedad. Cuando la función articular se ve afectada o los defectos óseos son demasiado grandes para los injertos óseos, los implantes protésicos son el método estándar para tratar los trastornos musculoesqueléticos graves, aunque existe la necesidad clínica de que los implantes permanezcan activos durante un período de tiempo más largo y reduzcan las tasas de revisión. Para abordar la mayor durabilidad de los implantes ortopédicos, recientemente han surgido implantes impresos en tres dimensiones (3D) para fabricar superficies porosas específicas del paciente en la superficie del hueso-implante, mejorando así la fijación biológica del implante. La traslación de los principios de la medicina regenerativa a la ortopedia permitiría definir una nueva generación de implantes que completen la transición de materiales inertes a andamios bioactivos que guíen el proceso de regeneración ósea. A corto plazo, es probable que los andamios ortopédicos regenerativos impresos en 3D aumenten la vida útil del implante, mientras que a largo plazo puedan degradarse una vez que el tejido huésped esté completamente reparado. El objetivo global de esta tesis es evaluar el potencial regenerativo asociado a los andamiajes óseos impresos en 3D para aplicaciones ortopédicas específicas del paciente.

Para ello, el primer estudio tuvo como objetivo determinar el papel del entorno mecánico del huésped en el proceso de regeneración ósea guiado por andamios óseos impresos en 3D en aplicaciones de carga. Se desarrolló un modelo computacional de regeneración ósea impulsada por un mecanismo en andamios porosos y se basó en la especificidad del sujeto, el sitio de implantación y la sensibilidad al entorno mecánico. A continuación, se simuló el crecimiento óseo en el interior de andamiajes porosos de titanio implantados en el fémur distal y la tibia proximal de tres cabras y se comparó con los resultados experimentales. Los resultados mostraron que el crecimiento óseo en el interior cambió de un patrón de distribución homogéneo, cuando los andamios estaban en contacto con el hueso trabecular, a un crecimiento óseo localizado cuando los andamios se implantaron en una ubicación diafisaria. En general, la dependencia de la respuesta osteogénica de la biomecánica del huésped sugirió que, desde una perspectiva mecánica, el potencial regenerativo dependía tanto del andamio como del entorno del huésped.

El segundo estudio de esta tesis tuvo como objetivo evaluar la actividad osteogénica específica del paciente en un entorno controlado *in vitro* donde las células óseas humanas, aisladas de sujetos individuales, imitan los rasgos esenciales del proceso de formación ósea. Los sistemas *in vitro* tradicionales ya permitieron demostrar que los osteoblastos humanos primarios embebidos en una matriz fibrada de colágeno se diferencian en osteocitos en condiciones específicas. Por lo tanto, se planteó la hipótesis de que la traslación de este entorno a la escala de órgano en un chip crea una unidad funcional mínima para recapitular la maduración de los osteoblastos hacia los osteocitos y la mineralización de la matriz. Con este propósito, se sembraron osteoblastos humanos primarios en un hidrogel de colágeno de tipo I, para conocer mejor el papel de la densidad de siembra de células en su diferenciación a osteocitos. Los resultados muestran que las células cultivadas a mayor densidad aumentan la longitud de la dendrita con el tiempo, dejan de proliferar, exhiben morfología dendrítica, regulan positivamente la actividad de la fosfatasa alcalina y expresan marcadores de osteocitos. Este estudio reveló que los sistemas de microfluídica son una estrategia funcional que permite crear un modelo de tejido óseo específico del paciente e investigar el potencial osteogénico individual de las células óseas del paciente.

En conjunto, los resultados de esta tesis enfatizan la importancia de utilizar un sistema de modelado múltiple al investigar el proceso de regeneración *in vivo* guiado por armazones óseos específicos adecuados al paciente. Ambos actores de una estrategia regenerativa libre de células *in situ*, a saber, el andamio y el paciente, tienen un efecto significativo en el resultado regenerativo final y necesitan ser modelados. Las técnicas avanzadas de *in vitro* e *in silico*, combinadas con datos de *in vivo*, evalúan aspectos distintivos del proceso de regeneración ósea para aplicaciones específicas del paciente. Las futuras estrategias personalizadas de ingeniería de tejidos podrían depender de la integración de esos modelos para mitigar en última instancia la variabilidad en el proceso de regeneración ósea guiado por un andamio específico para el paciente.

Beknopte samenvatting

Musculoskeletale aandoeningen en aanverwante botziekten zijn één van de belangrijkste oorzaken van pijn en handicaps, evenals een sociale en economische last voor onze samenleving. Wanneer de gewrichtsfunctie verzwakt is of botdefecten te groot zijn voor bottransplantaten, zijn prothetische implantaten de gouden standaard voor de behandeling van ernstige aandoeningen van het bewegingsapparaat, hoewel er de klinische behoefte is dat implantaten langer meegaan en revisiepercentages verminderen. Om een hogere duurzaamheid van orthopedische implantaten te bekomen, zijn recent driedimensionale (3D) geprinte implantaten ontwikkeld om patiëntspecifieke poreuze oppervlakken op het bot-implantaatoppervlak te fabriceren, waardoor de biologische fixatie van het implantaat wordt verbeterd. De vertaling van de principes van regeneratieve geneeskunde naar orthopedie kan een nieuwe generatie implantaten mogelijk maken die de overgang van inerte materialen naar bioactieve scaffolds die het botregeneratieproces ondersteunen, betekenen. Op korte termijn kunnen regeneratieve 3D-geprinte orthopedische scaffolds de levensduur van het implantaat waarschijnlijk verlengen, terwijl ze op lange termijn moeten degraderen zodra het gastheerweefsel volledig is hersteld. Het globale doel van dit proefschrift was om het regeneratieve potentieel te evalueren dat geassocieerd is met 3D-geprinte botscaffolds voor patiëntspecifieke orthopedische toepassingen.

De eerste studie was gericht op het bepalen van de rol van de mechanische omgeving van de gastheer op het botregeneratieproces ondersteund door 3D-geprinte botscaffolds in last dragende toepassingen. Een computationeel model van mechanisch gestimuleerde botregeneratie in poreuze scaffolds werd ontwikkeld en gebaseerd op de specificiteit van het onderwerp, de implantatieplaats en de gevoeligheid voor de mechanische omgeving. Botingroei in poreuze titanium scaffolds werd vervolgens gesimuleerd in het distale femur en proximale tibia van drie geiten en vergeleken met experimentele resultaten. De resultaten toonden aan dat botingroei verschoof van een homogeen distributiepatroon, wanneer scaffolds in contact waren met trabeculair bot, naar een plaatselijke botgroei wanneer scaffolds op een diafysaire locatie werden geïmplanteerd. Over het algemeen suggereerde de afhankelijkheid van de osteogene respons van de biomechanica van de gastheer dat, vanuit een mechanisch perspectief, het regeneratieve potentieel afhing van zowel de scaffold als de gastomgeving.

De tweede studie van dit proefschrift was gericht op het evalueren van de patiëntspecifieke osteogene activiteit in een gecontroleerde *in vitro* omgeving waar menselijke botcellen, geïsoleerd uit individuele proefpersonen, de essentiële eigenschappen van het botvormingsproces nabootsen. Traditionele *in vitro* systemen toonden al aan dat primaire menselijke osteoblasten ingebed in een 3D-fibreuze collageenmatrix onder specifieke omstandigheden differentiëren tot osteocyten. Daarom werd verondersteld dat het vertalen van deze omgeving naar de organ-on-a-chip-schaal een minimale functionele eenheid creëert om osteoblastrijping te recapituleren naar osteocyten en matrixmineralisatie. Primaire menselijke osteoblasten werden gezaaid in een type I collageenhydrogel, om de rol van celzaaidichtheid op hun differentiatie tot osteocyten te onderzoeken. De resultaten tonen aan dat cellen die onder een hogere zaai dichtheid zijn gekweekt, dendriet lengte in de loop van de tijd verhogen, de proliferatie stoppen, een dendritische morfologie vertonen, de alkalische fosfatase-activiteit verhogen en osteocytmarkers tot expressie brengen. Deze studie toonde aan dat micro-ontwikkelde systemen een functionele strategie zijn om een patiëntspecifiek botweefselmodel te creëren en het individuele osteogene potentieel van de botcellen van de patiënt te onderzoeken.

Alles bij elkaar genomen, benadrukken de resultaten van dit proefschrift het belang van het gebruik van meervoudige modelleersystemen bij het onderzoeken van het *in vivo* regeneratieproces, ondersteund door patiëntspecifieke botscaffolds. Beide actoren van een celvrije *in situ* regeneratieve strategie, namelijk de scaffold en de patiënt, hebben een significant effect op het uiteindelijke regeneratieve resultaat en moeten gemodelleerd worden. Geavanceerde *in vitro* en *in silico* technieken, gecombineerd met *in vivo* data, evalueren verschillende aspecten van het botregeneratieproces voor patiëntspecifieke toepassingen. Toekomstige gepersonaliseerde tissue engineering-strategieën hebben baat bij de integratie van die modellen om uiteindelijk de variabiliteit in het botregeneratieproces te verminderen, ondersteund door een patiëntspecifieke scaffold.

List of Abbreviations

3D	Three-Dimensional
ALP	Alkaline Phosphatase
AM	Additive Manufacturing
BMP2	Bone Morphogenic Protein 2
BOC	Bone-On-Chip
BRU	Bone Remodeling Unit
BSA	Bovine Serum Albumin
BSP	Bone Sialoprotein
BTE	Bone Tissue Engineering
CD	Cluster of Differentiation
CI	Confidence Interval
CT	Computerized Tomography
DAPI	4',6-Diamidino-2-Phenylindole
DMP	Dental Matrix Protein
DNA	Deoxyribonucleic Acid
ECM	Extracellular Matrix
FE	Finite Element
HOB	Primary Human Osteoblasts
HU	Hounsfield Units
HUVEC	Human Umbilical Vein Endothelial Cell
M-CSF	Macrophage-Colony Stimulating Factor

MSC	Mesenchymal Stem Cell
NaOH	Sodium Hydroxide
OCN	Osteocalcin
OPN	Osteopontin
OSX	Osterix
PDL	Poly-D-lysine
PDMS	Poly(dimethlysiloxane)
PFA	Paraformaldehyde
pNPP	p-Nitrophenyl Phosphate
RANKL	Receptor Activator of Nuclear factor-kB Ligand
rmcorr	Repeated Measure Correlation
RSS	Residual Sum of Squares
SED	Strain Energy Density
TE	Tissue Engineering
TRITC	Tetramethylrhodamine

List of Symbols

α	Fraction of reference daily stimulus
$\bar{\epsilon}$	Effective tissue microstrain
$\dot{\rho}$	Bone mineral density rate
$\dot{V}$	Bone volume deposition rate inside the pores of a bone scaffold
$\dot{V}_{max}$	Maximum bone deposition rate
Ψ	Daily strain stimulus for bone formation
Ψ^*_{local}	Local daily strain stimulus in the peri-implant region
ρ_{max}	Maximum bone mineral density
c	Normalized cell concentration
D	Diffusion constant
E	Young's modulus
k	Constant of bone volume deposition rate
m	Daily strain history parameter
N	Number of different daily load cases
n_i	Average daily cycles
r_{rm}	Repeated measures correlation coefficient
W	Strain energy density

Contents

List of Figures

List of Tables

Chapter 1

Introduction

1.1 Clinical impact of patient-specific scaffolds and the need for bone regeneration

Musculoskeletal disorders and related bone diseases are one of the major causes of pain and disability. Diseases such as osteoarthritis, bone fracture, osteoporosis, bone tumor and intervertebral discs degeneration, affect 1 of 2 adults in United States [1] and more than 100 million Europeans, which induce chronic pain, disabilities and a social and economical burden [2]. Although the great majority of patients undergo non-surgical treatments to limit the disability of musculoskeletal conditions, surgery is the first choice of treatment in extreme cases of pain and mobility impairment, as observed in bone fractures, osteoarthritis and bone tumors [1].

The estimated incidence of bone fractures only is around 3 fractures per 100 people per year in UK [3] and US [4]. Despite the intrinsic repair capacities of bone tissue, 5-10% of fractures do not self-heal (named non-unions) and require expensive operative interventions [5]. Bone traumatic injuries cost $56 billion every year in US alone [4], while fractures associated to osteoporosis cost €37.5 billion in the largest European countries [6]. The current most effective treatments for non-union fractures include bone transplants from a different anatomical site of the same patient (autografts). Unfortunately, autogenic bone transplantation is a painful procedure which is limited to small and single bone defects, thus it is not a valid option for joint replacement operations [7]. When the bone fracture requires a total joint replacement, like in femoral neck fractures, prosthetic implants are the unique solution available [8].

Similarly, osteoarthritis is a chronic joint disease that affects around 10% of men and 18% of women over 60 years of age and it is commonly treated with pharmaceutical agents (mostly anti-inflammatory drugs) [9]. However, end-stage disease is severely debilitating, that is why osteoarthritis is the most common reason for total hip and knee replacements [10]. The total direct cost for joint replacement due to osteoarthritis is around $42 billion in US only and it is set to increase in all westernized countries [11].

In addition, the occurrence of primary malignant bone tumors in young patients, as the osteosarcoma, is associated to the surgical excision of large parts of long bones [12]. Despite innovations in chemotherapeutic drugs have substantially increased the survival rate of osteosarcoma, the implantation of a megaprosthesis is the accepted treatment to restore function and avoid limb amputation [13, 14].

Overall, prosthetic implants are the gold standard for treating severe musculoskeletal disorders, where the joint function is impaired or bone defects are too large for alternative bone grafts (Figure 1.1). However, metals commonly used for load-bearing implants are inert materials and cause the mechanical loosening of the implant over time, requiring complex revision surgeries [15, 16]. Reducing revision rates is an essential objective for the next generation of orthopedic implants, given that the demand for total hip and knee arthroplasties is projected to steadily increase over the next decades [17]. Moreover, western population is aging and the number of joint replacements among younger persons is growing faster than expected [18]. There is the clinical need of implants that remain active for longer period of time.

To address the higher durability of orthopedic implants, three-dimensional (3D) printed or additively manufactured implants have recently emerged as alternative to standard fabrication technologies. With additive manufacturing, tunable porous surfaces can be fabricated at the bone-implant surface, thus enhancing the biological fixation of the implant [19]. 3D printing technology has been innovating the orthopedic field to such an extent that 3D printed implants have been proposed as a new second generation of orthopedic implants [7]. On the one hand, 3D printing offers the production of customized surgical implants, which became essential to treat extreme clinical conditions (e.g. reconstruction after revision surgery or tumour excision). On the other hand, the development of personalized 3D printed implants is a long and expensive procedure compared to regular devices. The higher fabrication cost and regulatory concerns for 3D printed implants are the reasons why they have been applied only to patients identified as needing personalized treatment, even though any patient might benefit for enhanced biological fixation of the implant [20].

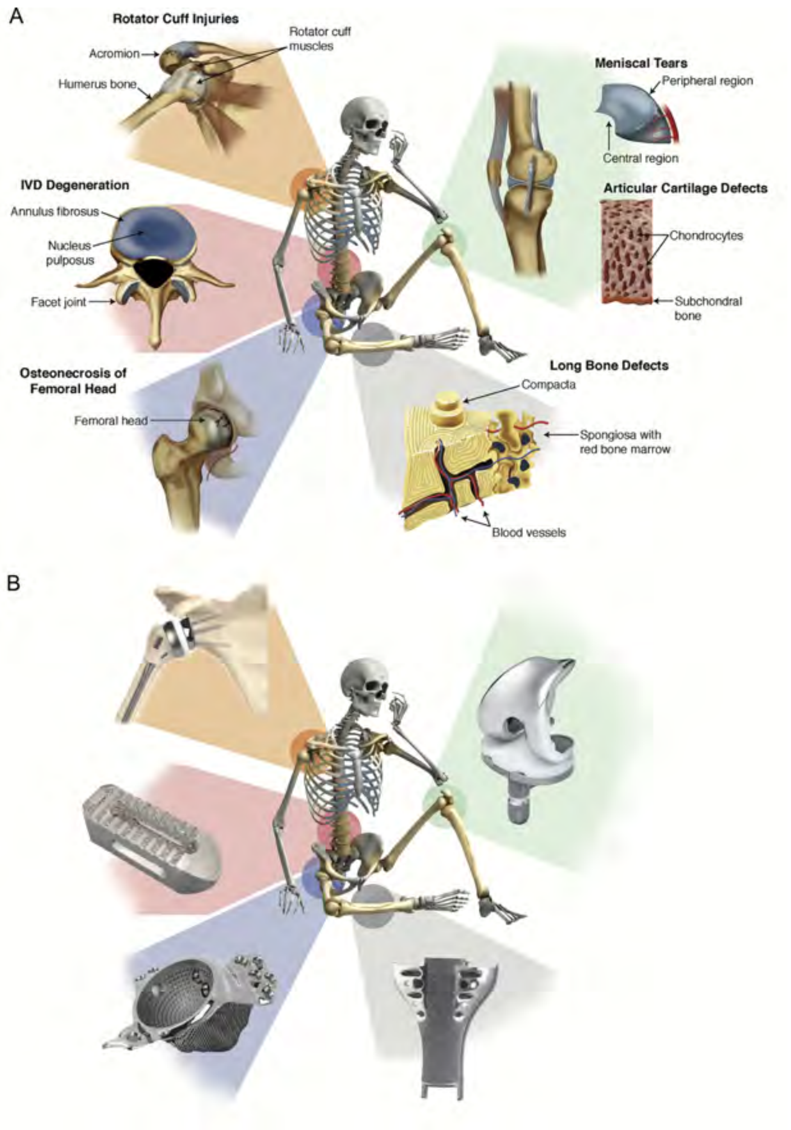

Figure 1.1: **Musculoskeletal disorders are currently treated with prosthetic implants**. (A) Example of musculoskeletal tissues with a high incidence of injuries and degeneration. Image from [21]. (B) Orthopedic solutions to restore the joint and bone mechanical functionality. Starting from the bottom left of the image: *aMace* acetabular implant, Materialise; *Tritanium PL* cage, Stryker; *ReUnion®* shoulder arthroplasty system, Strycker; *Physica* knee implant, Lima Corporate; *GMRS™* proximal tibial component, Strycker.

In search of new beneficial therapies for a wider range of patients, regenerative medicine is constantly growing to offer novel solutions to replace, restore, or regenerate bone [22]. The translation of regenerative medicine principles to orthopedic solutions can define a new, third generation of implants that completes the transition from inert materials to bioactive scaffolds driving the bone regeneration process [7]. In the short-term, regenerative 3D printed orthopedic scaffolds are likely to increase osteointegration, while in the long-term they aim to degrade once the host tissue is fully repaired [23, 24].

Recent developments in regenerative medicine suggest that personalized strategies are an essential condition for regenerative products in a clinical scenario [25]. The biological variability within single patients is intrinsically related to the unpredictability of the regenerative product outcome. As an example, systemic disorders (e.g. diabetes or osteoporosis), comorbidities (e.g. cardiovascular diseases) and medications deeply affect implant osteointegration [26]. Therefore, the development of patient-specific regenerative solutions rely on the concomitant investigation of both (1) the product design based on the environment to regenerate and (2) the patient-specific osteogenic capacity, which is the context of the present thesis.

CLINICAL CHALLENGE

Developing orthopedic implants that facilitate *in situ* bone repair

The translation of regenerative medicine principles to orthopedic solutions can define a new, third generation of implants that completes the transition from inert materials to bioactive scaffolds driving the bone regeneration process once implanted *in vivo*. In the short-term, regenerative 3D printed orthopedic scaffolds are likely to increase osteointegration, while in the long term they aim to degrade once the host tissue is fully repaired.

1.2 Modeling patient-specific regeneration: the role of multiple systems

In view of evaluating and improving the regenerative outcome of patient-specific bone implants, experimental models are continuously evolving to correlate the design of the regenerative scaffold to the patient-specific biological response, thus optimizing osteintegration. Besides human clinical trials, there are different categories of experimental models in regenerative medicine, namely *in vivo*, *in vitro* and *in silico* models. Each modeling approach presents its unique advantages and provides essential information about the regenerative process (Figure 1.2).

Advantages	- Dynamics of biological processes	- Use of human cells	- Complete biological environment
	- Study effects of single mechanism	- Controlled culture environment	- Essential for clinical translation
Disadvantages	- Cost of development	- Not suitable for long-term studies	- Different biological mechanisms than humans
	- Large amount of data for validation	- Lack of all factors of the biological environment	- Ethical concerns

Figure 1.2: **Experimental models for bone tissue engineering**. Main categories of experimental models in bone tissue engineering prior to clinical research. The advantages and disadvantages of each model are listed, suggesting that the synergy of all models might bring regenerative products closer to clinical applications.

In vivo models mimic the complete human biological environment to the greatest extent possible, which is the reason why animal experimentation is an absolute requirement before the clinical translation of tissue engineered medical products [27]. However, biological mechanisms may differ between animal models and humans, which motivates *in vitro* modeling and the culture of human cells in a controlled environment outside of living organisms [28]. Yet, traditional 2D *in vitro* models are not suitable for long-term studies and may fail in recapitulating a clinically relevant environment due to the absence of all factors present *in vivo* [29]. Conversely, *in silico* models can simulate the dynamics of biological processes and quantify the contribution of single mechanisms to the regenerative outcome, even though computational tools have a significant cost of development and require large amount of experimental data for their validation [30, 31]. Once applied to the development of orthopedic scaffolds, different types of experimental models highlight different aspects of the regeneration process. Hence, a tissue engineering strategy based on the synergy of multiple *in vitro*, *in silico* and *in vivo* models brings patient-specific technologies closer to clinical applications.

1.3 Research objectives and hypotheses

Global objective of the thesis

Evaluate the bone regenerative potential associated to 3D printed scaffolds in patient-specific orthopedic applications.

The first objective of this thesis is to determine the role of the patient-specific mechanical environment on the bone regeneration process guided by 3D printed bone scaffolds in load-bearing applications. The second objective is to evaluate the patient-specific osteogenic capacity in a micro-system (organ-on-chip) seeded with human bone cells, isolated from individual subjects. To address these objectives, two hypotheses have been defined and supported by the research presented in chapters 3 and 4 of this thesis:

Research hypothesis 1

A computational strategy incorporating both porous bone scaffolds and the host mechanical environment determines the scaffold regenerative outcome for each specific patient and implantation site.

Research hypothesis 2

Bone-like 3D environments in microengineered systems define personalized devices to induce the differentiation of primary human osteoblasts into osteocytes.

By testing each of these hypotheses, the research objectives outlined above can be addressed. The proposed research will deliver an interdisciplinary methodology to include both the host and the scaffold perspectives during the evaluation of the regenerative outcome of a patient-specific bone scaffold.

1.4 Thesis structure

This thesis comprises the research carried out for the duration of the candidate's doctoral studies (Figure 1.3). **Chapter 2** presents a review of the literature on bone structure, the processes of bone regeneration and healing, as well as their role in tissue engineering. Next, this chapter introduces patient-specific solutions for bone regeneration and advanced modeling techniques. Finally, the chapter ends with a strong focus on the need of modeling the interaction between individual recipients and scaffolds.

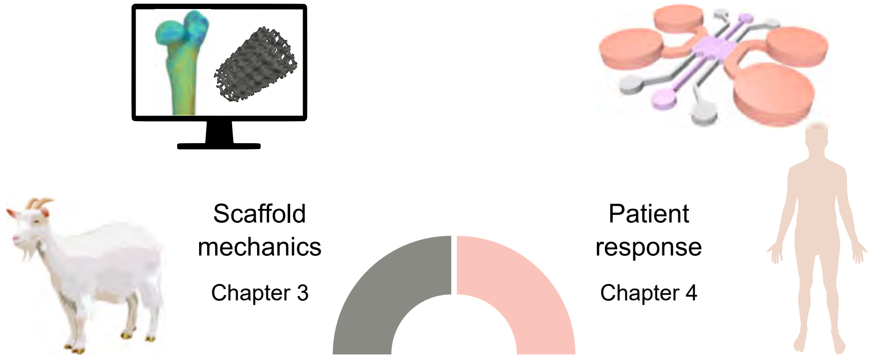

Figure 1.3: **Structure of the doctoral thesis**. The present thesis investigates the regenerative potential of 3D printed bone scaffolds for patient-specific orthopedic applications. Therefore, the thesis comprises the research on scaffold mechanics (chapter 3) and individual patient response (chapter 4).

In **chapter 3**, a computational approach related bone regeneration within scaffold pores to the mechanical state induced by different recipients and anatomical locations. Different implantation sites caused different mechanical conditions and induced distinctive patterns of bone ingrowth distribution in the model, while the mineralization dynamics brought to limited regeneration in the scaffold core. After calibration with *in vivo* data from three recipients, the computational model revealed a stronger responder, testing the research hypothesis 1 of the thesis. **Chapter 4** investigates the development of a patient-specific bone-on-chip system to induce osteogenic differentiation of primary human osteoblasts. A custom image analysis software was first developed to compute cell dendrite elongation. Later, osteogenic differentiation was assessed in terms of changes in cell morphology, proliferation, mineral deposition and protein synthesis. This chapter has a particular focus on the effect of cell seeding density to osteoblast differentiation and tests the research hypothesis 2 of the thesis. The main findings of the thesis are outlined in **chapter 5** and discussed in the context of patient-specific bone regeneration, along with recommendations for future research.

Chapter 2

Literature review [1]

2.1 Bone regeneration process

2.1.1 Bone structure and hierarchical organization

Bones are innervated and highly vascularized organs whose primary functions in the human body involve the support and locomotion of the body, the protection of internal organs, the storage of minerals, the hematopoiesis (formation and turnover of blood cells) as well as the endocrine regulation of energy metabolism [32]. From a structural perspective, bones are natural composites with a hierarchical organization, finely controlled from the nano-(collagen molecules) to the macro-(bone shape) scale (Figure 2.1). Starting from the nanoscale, hydroxyapatite crystals and type I collagen molecules are the principal components of this highly ordered structure, conferring bones their characteristic mechanical properties. Moving up in the hierarchical organization of bone, hydroxyapatite crystals and type I collagen forms mineralized collagen fibrils. Fibrils tend to self-assemble in ordered super-structures: the presence or the absence of net fibrillar orientation in three dimensions led to the distinction between lamellar and woven bone, respectively (sub-microscale) [33]. At higher hierarchical level, two characteristic bone structures consist of concentric layers of lamellae named osteons as well as small beam elements, named trabeculae, where lamellae are aligned to the main direction (microscale) [34]. At the tissue level, densely packed osteons are the units of compact, cortical bone whereas trabeculae are the units of cancellous, trabecular, or spongy bone (mesoscale) (Figure 2.1).

---

[1] Part of the text in this chapter is adapted from the following papers:
- Nasello et al., 2021, submitted to *Applied Sciences*;
- García-Aznar et al., 2021, submitted to *Bone*;
listed in chapter Publications

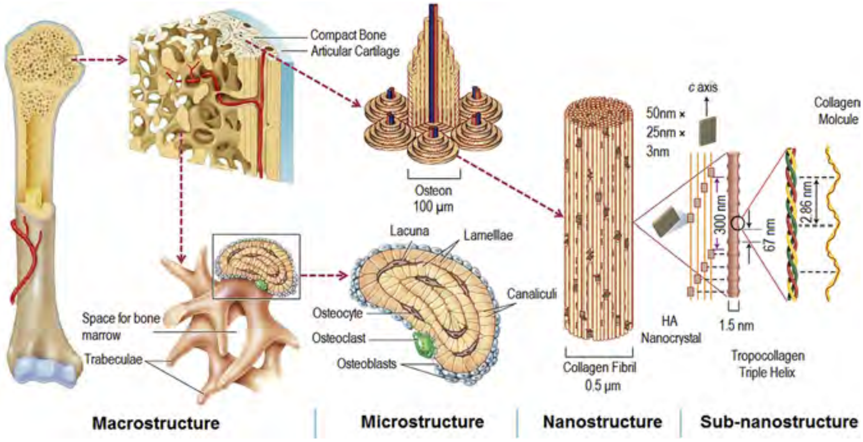

Figure 2.1: **Bone structure and hierarchical organization**. Bone is a natural composite material whose ordered structure is precisely organized from the nano to the macro-scale. Image taken from [35].

Overall, bone cells finely control both processes of formation and maintenance of the bone hierarchical structure. Each cell is responsible of specific tasks, so that their orchestrated action regulates bone growth, remodeling, and repair.

2.1.2 Bone cells

Bone tissue homes cell types deriving from different lineages and whose synergistic action is the basis of bone homeostasis. Cells deriving from the skeletal lineage, such as osteoprogenitor cells, osteoblasts and osteocytes, form new bone matrix and control the bone formation/resorption balance, while cells form the heamatopoietic lineage, such as osteoclasts, resorb the bone matrix [36].

Mesenchymal stem cells

Bone forming cells arise from mesenchymal stem cell progenitors during embryonic and postnatal development, as well as during fracture repair. Their differentiation is associated to the activity of specific transcription factors, such as RUNX2 and osterix (OSX) [37]. Cells isolated from the aspirate bone marrow showed multipotentiality *in vitro*, meaning that they can differentiate into bone, cartilage, muscle, tendon/ligament, fat and other connective tissues. For this reason, those cells were named "mesenchymal stem cells" (MSCs) [38]. According to the International Society of Stem Cell Research, MSCs must be: (1) plastic-adherent; (2) capable of differentiating to osteoblasts, adipocytes and chondrocyte *in vitro*; (3) be positive for the cluster of differentiation 105 (CD105), CD73 and CD90; (4) be negative for CD45, CD34, CD11b, CD14, CD79a and the human leukocyte antigen (HLA) class II (Figure 2.2) [39].

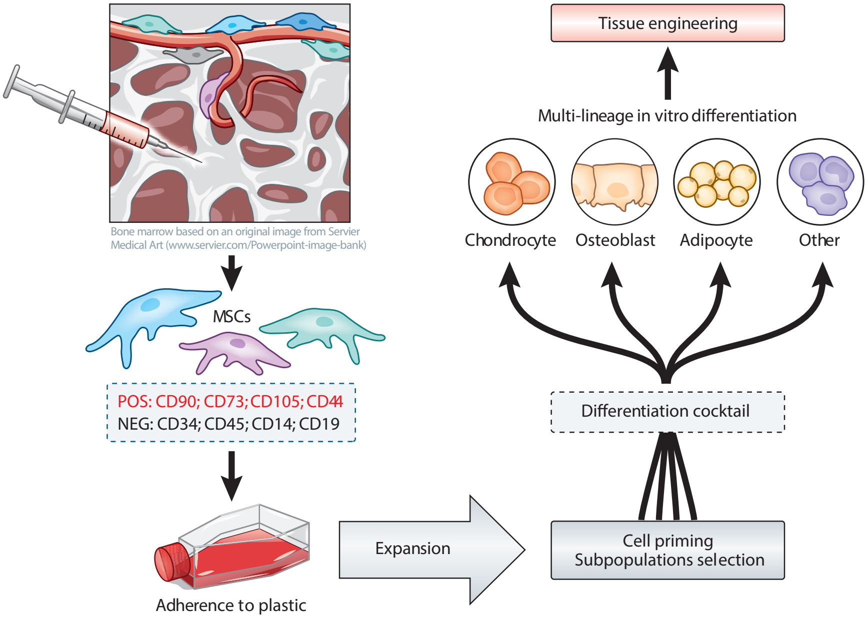

Figure 2.2: **Mesenchymal stem cells are multipotent *in vitro***. Mesenchymal stem cells (MSCs) are isolated from the bone marrow or other vascularized tissues. After isolation, MSCs must be positive (POS) or negative (NEG) to canonical cluster of differentiation (CD). MSCs must also be adherent to plastic and subpopulations might be selected by priming with stimulating solutions. Finally, MSCs can differentiate *in vitro* to chondrocyte, osteoblasts and adipocytes when lineage-specific factors are supplemented. Such *in vitro* multipotentiality has inspired the use of MSCs in tissue engineering applications. Image modified from [40].

MSC minimal criteria have been satisfied by perivascular cells, namely pericytes, isolated in multiple organs including muscle, pancreas, adipose tissue and placenta [41], which motivated the use of adipose-tissue-derived cells in the field of skeletal regenerative medicine [42]. Given their remarkable multipotentiality *in vitro*, MSCs have been investigated in tissue engineering applications, aiming to induce the same differentiation *in vivo*. However, clinical trials showed limited MSC capacity to differentiate and replace damaged tissue *in vivo*, while there are compelling evidences that their immunomodulatory properties facilitate the host regenerative response [38]. As a result, authors suggest to change the name of MSCs to "Medicinal Signaling Cells" due to the beneficial effects of their paracrine activity [43].

Another potential source of osteoprogenitor cells is the periosteum, whose inner layer contains skeletal progenitor cells. Periosteal progenitor cells play a central role in bone formation after fracture, by undergoing expansion and differentiating into osteoblasts and chrondrocytes, and they have been already proposed as cellular source for bone regeneration strategies [44].

Osteoblasts

Osteoblasts are the bone-forming cells and they are usually identified at the bone surface. The differentiation stages of skeletal lineage cells lead to the identification of three different types of osteoblasts, namely preosteoblasts, active osteoblasts and quiescent or bone-lining cells [45]. Preosteoblasts are osteoprogenitor cells who started the differentiation process into mature osteoblasts. Preosteoblasts start producing collagen type I precursor molecules, although they do not deposit bone matrix yet [45].

Differentiation into active osteoblasts is mainly characterized by the bone matrix formation, which is the development and maturation of a calcified extracellular matrix (calcified ECM or bone matrix). Osteoblasts govern the processes of matrix synthesis and mineralization by secreting the major of organic components of the bone matrix and depositing mineral in the form of hydroxyapatite during mineralization [46]. On the surface of existing bone matrix, osteoblasts deposit an organic template with abundant type I collagen named osteoid, which is later mineralized with deposition of hydroxyapatite crystals (Figure 2.3) [47].

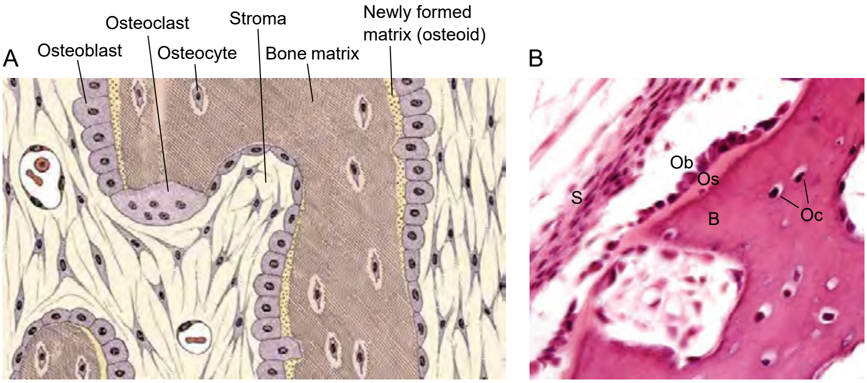

Figure 2.3: **Bone formation mechanism**. (A) Representative diagram of the deposition of newly formed matrix governed by osteoblasts. (B) Photomicrograph of developing bone indicating osteoblasts (Ob), osteocytes (Oc), bone matrix (B), osteoid (Os) and stroma (S). Image adapted from [47].

To accumulate calcium phosphate for matrix mineralization, active osteoblasts synthesize alkaline phosphatase (ALP). Moreover, active osteoblasts synthesize extracellular proteins enriching the matrix, such as bone sialoprotein 2 (BSP2) and osteocalcin [37]. After producing the bone matrix, osteoblasts can undergo three different fates. While a subset of osteoblasts differentiate into osteocytes, others undergo apoptosis or become bone lining cells, which are a quiescent osteoblasts lying on the bone surface [48].

Osteoblast differentiation process is characterized by different developmental signaling pathways, which can be harnessed in TE applications to replicate organogenesis. In particular, the bone morphogenic proteins (BMP2) promote mesenchymal progenitor transition to $\mathrm{RUNX2^{+}OSX^{+}}$ cells and enhance osteoblast function [37]. The direct relationship between BMP2s and postnatal bone formation motivates their use in TE as osteogenic factors [49, 50].

Osteocytes

The bone matrix deposition normally continues until osteoblasts become surrounded by mineralized matrix, when they might experience drastic phenotypical changes and differentiate into terminally differentiated osteocytes [45]. Osteoblast differentation into osteocytes is associated to a characteristic change from cuboidal to dendritic shape, where protrusions create an interconnected cellular network within the mineralized matrix [48]. Moreover, osteocytes cease their osteogenic activity since they are embedded in a mineralized matrix. Osteoblast markers associated to matrix formation are downregulated, such as the Wnt signaling pathway that is inhibited by sclerostin synthesis [48]. The interruption of osteogenic activity corresponds to a new role for osteocytes in the bone tissue, since they become the orchestrators of both processes of bone formation and resorption. Through their dendritic network and their ubiquitous presence within the matrix, osteocytes sense the bone mechanical environment and regulate the activity of both bone forming and resorbing cells [48]. Dendrites are surrounded by fluid made of ECM proteins binding to cell membrane receptors. When fluid flows and causes shear stress, cell membrane receptors, such as integrins, act as mechanoreceptor and transfer mechanical stimulation to the osteocytes [51]. Between all proteins in the fluid surrounding the dendrites, glycocalyx is one of the major components of the pericellular matrix and has a direct impact on integrin attachment and cell stimulation [51, 52]. As for osteocytic markers, E11 and dental matrix protein 1 (DMP1) synthesis characterize young osteocytes that are completing the mineralization of the surrounding matrix, while mature osteocytes synthesize sclerostin as the osteogenic activity is completed [45].

Osteoclasts

As osteoblasts build new bone matrix, osteoclasts resorb the bone matrix. They secrete enzymes to dissolve the damaged tissue and facilitate the deposition of a newly bone matrix [46]. Osteoclasts derive from the heamatopoietic lineage, thus precursor cells in the hematopoietic vascular channel of the bone marrow migrate to the bone matrix and differentiate into osteoclasts when stimulated [53]. *In vitro* experiments have widely demonstrated that osteoclasts differentiation require two factors: macrophage colony stimulating factor (M-CSF) and the receptor activator of nuclear factor-kappa B ligand (RANKL). While M-CSF promotes the adhesion of osteoclast precursors, RANKL guides osteoclast differentiation by activating its membranar receptor, RANK [54]. RANKL depletion induces severe osteopetrosis *in vivo* and it is synthesized in large amount by osteocytes. Therefore, osteocyte regulatory action relies on RANKL expression to finely control bone resorption [55].

2.1.3 Bone tissue adaptation

Bone modeling and remodeling

Bone formation and resorption occur simultaneously throughout the skeleton. When formation and resorption take place on different locations, they are referred to as bone modeling activity. The main function of bone modeling is to control bone shape and eventually increase bone mass [56]. Bone modeling has a prominent role during childhood, governing the skeletal development and growth. In contrast, bone remodeling consists of bone remodeling units (BRUs) where osteoclasts and osteoblasts sequentially resorb and form matrix on the same bone surface (Figure 2.4).

Compared to bone modeling, bone remodeling is a slower process which takes place throughout life, leading to transient or permanent skeletal changes according to the body needs. There are 2-5 million BRUs in the skeletal system of healthy individuals, whose bone resorbing and forming activity is coupled to maintain the bone balance unvaried [57]. Conversely, individuals affected by pathological conditions of bone loss, such as postmenopausal osteoporosis, present higher number of BRUs and their net bone balance is negative [56]. The higher number of BRUs and the net negative bone balance result in a dramatic increase of the bone loss rate [57].

Through remodeling, bone continuously adapts to both systemic and local factors, such as hormones, cytokines, vitamins and mechanical loading [58]. It is important to mention that both bone modeling and remodeling are often referred as "remodeling" when investigating the effects of physical, chemical or biological factors to bone tissue adaptation [59].

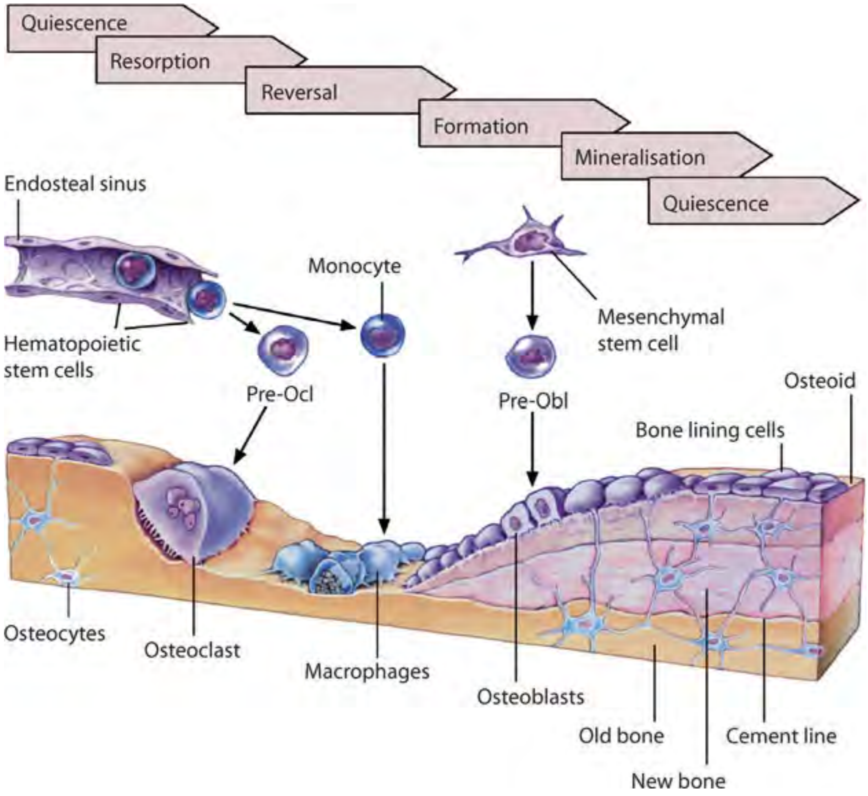

Figure 2.4: **Bone remodeling cycle**. Bone remodeling phases in trabecular bone, when osteoclasts and osteoblasts sequentially resorb and synthesize bone matrix. Image taken from [57].

Mechanical adaptation of bone tissue

The influence of mechanical loading on skeletal architecture, named mechanical adaptation, has been investigated for more than 200 years and can be summarized in the statement of the Wolff's Law (19th century). In brief, the Wolff's law states that "alterations of the internal architecture clearly observed and following mathematical rules, as well as secondary alterations of the external form of the bones following the same mathematical rules, occur as a consequence of primary changes in shape and stressing or in the stress of the bones" [60, 59]. Extreme cases of reduction or increase of skeletal loading show the direct effect of mechanics on both the bone mineral content and shape. The absence of physiological skeletal loading results in rapid bone loss, which is clearly observed in immobilized patients and astronauts.

Although they regularly perform physical exercise, astronauts experience osteocyte apoptosis and 1% loss of bone mass every month due to weightlessness under spaceflight conditions [58]. Conversely, physical activity increases bone strength. For example, bones in the playing arm of tennis players are larger than those in the nonplaying arm [61]. The higher strength of mechanically loaded bones is the result of a concomitant increase in bone mineral content and bone structural reshape [61].

Throughout life, bone adaptation is driven by a fine control of mechanical stimulation, which is not believed to occur only in humans. Comparable peak physiogical strains, around 2000-3000 με, were measured in long bones of various animals, confirming the mechano-based adaptation occurring in the bone tissue [59]. Since Frost's first mathematical model of mechanically regulated bone remodeling [62], tissue-scale mechanobiological parameters have been related to bone adaptation. Macroscopic models of bone remodeling represent bone as homogeneous material and assume a net bone balance equal to zero for tissue-level mechanical stimuli Ψ around a reference value Ψ*. Outside the area of null net bone balance, named dead or equilibrium zone, the difference between Ψ and Ψ* is considered the driving force of bone remodeling, with the simplest models assuming a linear rate of bone formation and resorption (Figure 2.5-A) [63].

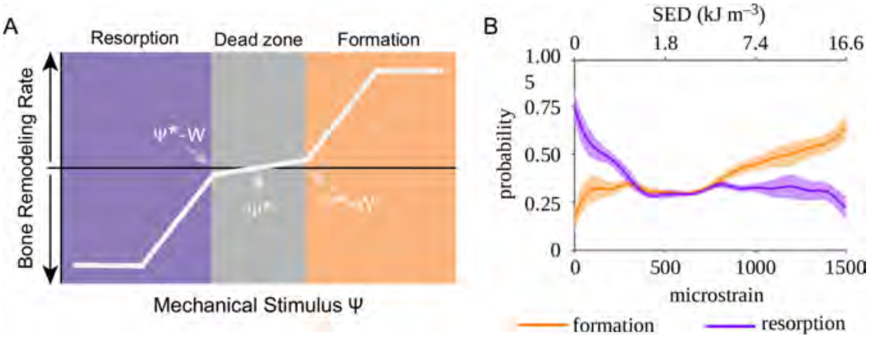

Figure 2.5: **Mechanically regulated bone remodeling**. (A) Macroscopic models of bone remodeling assume a net bone balance equal to zero in the "dead zone", that is for mechanical stimuli Ψ around a reference value Ψ*. Outside the dead zone, the difference between the local Ψ and Ψ* drives the bone remodeling rate. (B) Experimental coupling of mechanical states and microstructural changes in trabecular bone. Results showed that bone resorption and formation correlate with the local values of the strain energy density (SED), providing a local interpretation of macroscopic models of bone remodeling. Image taken from [64].

The assumption of homogeneous bone material makes the mathematical formulations of bone remodeling valid only at the macroscale, where discontinuities in bone composition can be ignored. Indeed, coupling mechanical states and microstructural changes in trabecular bone showed that chances of bone resorption and formation correlate with the local values of the strain energy density (SED) (Figure 2.5-B) [64]. Analyzing the bone structural heterogeneity revealed that bone formation and resorption occurs throughout the tissue, and that the relationships described by macroscale models of bone remodeling consider the overall effect of mechanics on bone adaptation. Low SED values are likely to induce local bone resorption, while high SED values are likely to induce local bone formation. Bone formation and resorption are likely to occur locally with the same frequency, which corresponds to the "dead zone" and a net bone balance equal to zero (Figure 2.5).

2.1.4 Bone healing and large bone defects

A bone fracture is the interruption of bone continuity following a trauma or a disease (e.g. osteoporosis, tumor), while bone healing or bone repair is the subsequent physiological process that restores continuity [47]. Bone healing consists of three characteristic phases leading to the development of a fibrocartilaginous template and the final restoration of the orginal bone structure (Figure 2.6) [65]. Immediately after trauma, the inflammatory phase takes place with the immediate formation of a hematoma (Figure 2.6-1). In the first days after fracture, inflammatory cells remove the necrotic tissue and recruits cells in charge of functional tissue formation that will form a callus. The second reparative phase starts with the recruitment of mesenchymal cells and osteoprogenitor cells, which later produce a fibrocartilaginous matrix named soft callus (Figure 2.6-2). The callus bridges the fracture gap and serves as a template for bone matrix formation [66]. This first mineralized matrix, known as hard callus, is a poorly organized tissue, namely woven bone, that is ready to be converted to lamellar bone (Figure 2.6-3). The final remodeling phase of bone repair follows the bone remodeling dynamics to confer the original shape and strength to the injured bone segment (Figure 2.6-4).

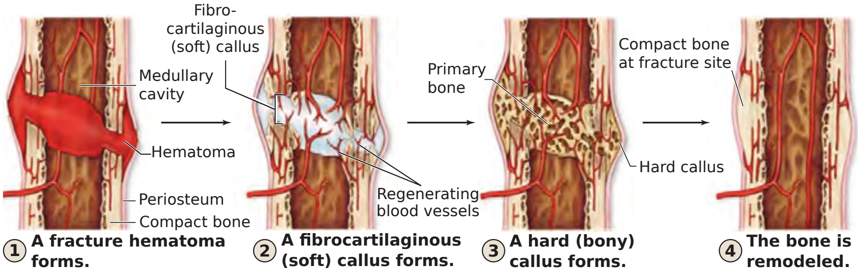

Figure 2.6: **Stages of bone fracture healing**. Three different phases characterizes bone fracture repair. (1) Inflammatory phase with hematoma formation. (2-3) Reparative phase with formation of fibrocartilaginous matrix (soft callus) and subsequent mineralization (hard callus). (4) Remodeling phase to confer the original shape and strength to the injured bone segment. Image adapted from [47].

Bones sometimes fail to bridge the fracture gap and heal. If the healing of the fracture did not occur within 6-9 months after trauma, the fracture is defined as non-union [4]. Non-unions spontaneously occur in critical-size bone defects and might be affected by pathological conditions such as pseudoarthrosis, osteoporosis or bone tumor (Figure 2.7) [67]. In general, non-unions consist of the soft callus failing to turn in a mineralized bone matrix, requiring further medical intervention to heal [68, 69].

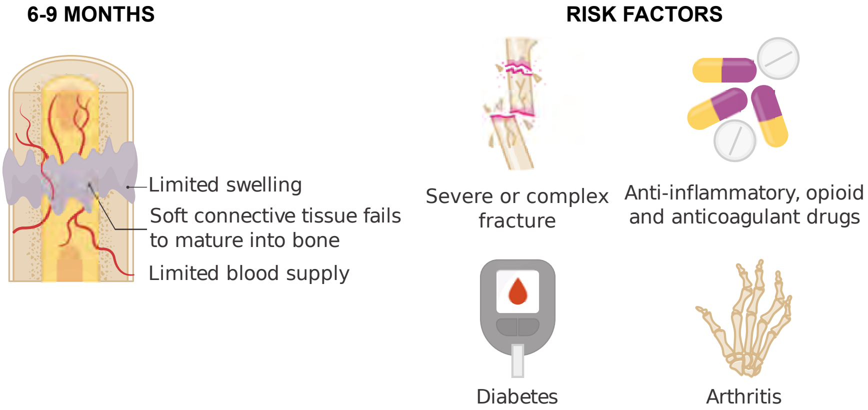

Figure 2.7: **Non-union bone fracture: an unhappy marriage**. Schematic representation of a non-union and risk factors associated. Image adapted from [69].

2.1.5 Bone tissue engineering

Tissue engineering (TE) combines principles of engineering and life science to restore, maintain or improve tissue function [70]. In the context of regenerated tissue, bone tissue engineering (BTE) is a potential solutions to those clinical conditions where bone fails its natural healing response (e.g. non-union, bone tumors and infections) [71]. A standard TE approach involves the development, outside the patient, of a biological substitute combining scaffolds (templates) [72], signals (e.g. growth factors) [73] and (stem) cells [21] which is finally transplanted on the degenerated or injured tissue [74].

Over the past 30 years bone tissue engineered grafts, including a subset or the full triad of scaffolds, signals and cells, were proposed as alternatives to autologous bone grafts. While gold standard autografts have limited availability and are painful to the patient, TE products offer an off-the-shelf solution for clinical conditions where bone repair and regeneration need to be augmented (Figure 2.8) [49]. Yet, few BTE solutions are currently applied in clinical practice and the whole tissue engineering field is moving away from the initial approach of developing fully functional individual tissues outside the patient. Advances in material and stem cell sciences, as well as a deeper understanding of developmental biology, suggest that regenerative medicine should harness the self-healing mechanisms of the body [75].

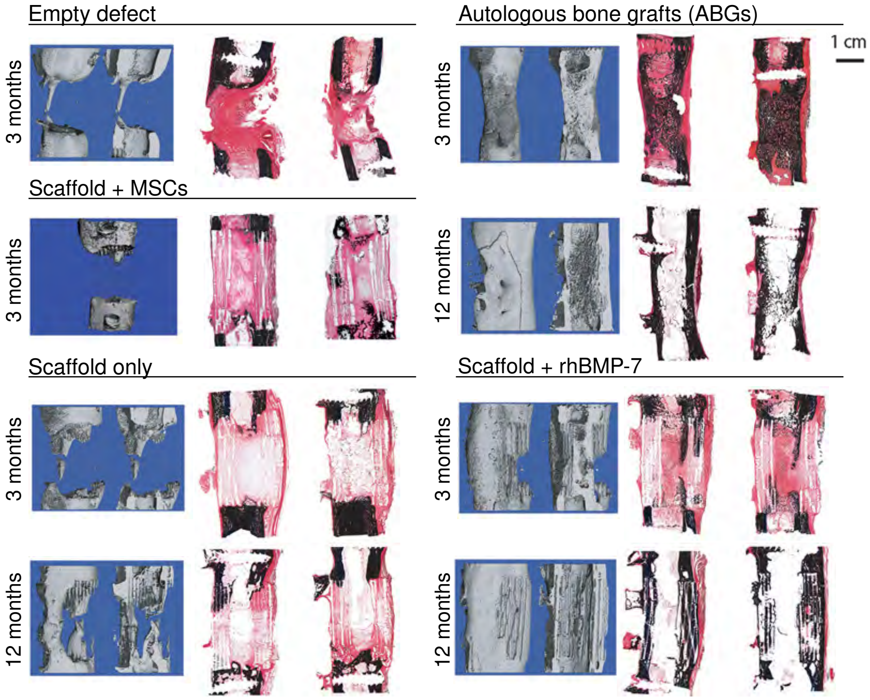

Figure 2.8: **Tissue engineering for segmental defect regeneration**. Histological and imaging analyses of segmental bone defect regeneration in sheep after 3 and 12 months. Comparison between bone regeneration outcomes of different tissue engineering strategies (scaffold, scaffold + cells, scaffold + signal) and the autologous bone graft. Image taken from [49].

There is a growing interest in acellular biomaterials stimulating tissue regeneration, mainly due to the lower technical and regulatory complexities compared to cell-based therapies [76, 77]. The recent definition of *in situ* TE relies on grafts harnessing the endogenous restoration of tissue functionality, orchestrated by the host [78]. Grafts commonly consist of acellular and resorbable scaffolds guiding the recipient in the development of a living autologous tissue (Figure 2.9) [79, 80].

Biomaterials and fabrication technologies for *in situ* TE applications should support endogenous cells in developing and regenerating tissues during all stages following implantation [81]. Both natural and synthetic biomaterials have been proposed as potential scaffolds, the latter ranging from degradable to permanent and from

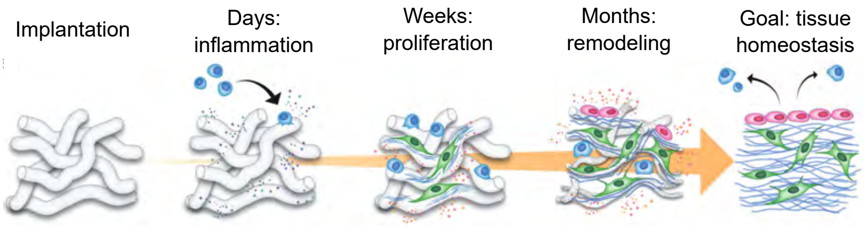

Figure 2.9: **Stages of *in situ* tissue regeneration**. Following the graft implantation, *in situ* tissue engineering relies on guiding the biological processes initiated by the host to develop an autologous living tissue. Image adapted from [78].

metals to ceramics, polymers or hydrogels. Fabrication technologies have been continuously evolving since the initial attempts of bone regeneration, and 3D printing is considered one of the major breakthrough in recent years (Figure 2.10) [82]. By dictating a scaffold's structure and eventually incorporating cells during the fabrication process, 3D printing can mimic the native bone complexity [83].

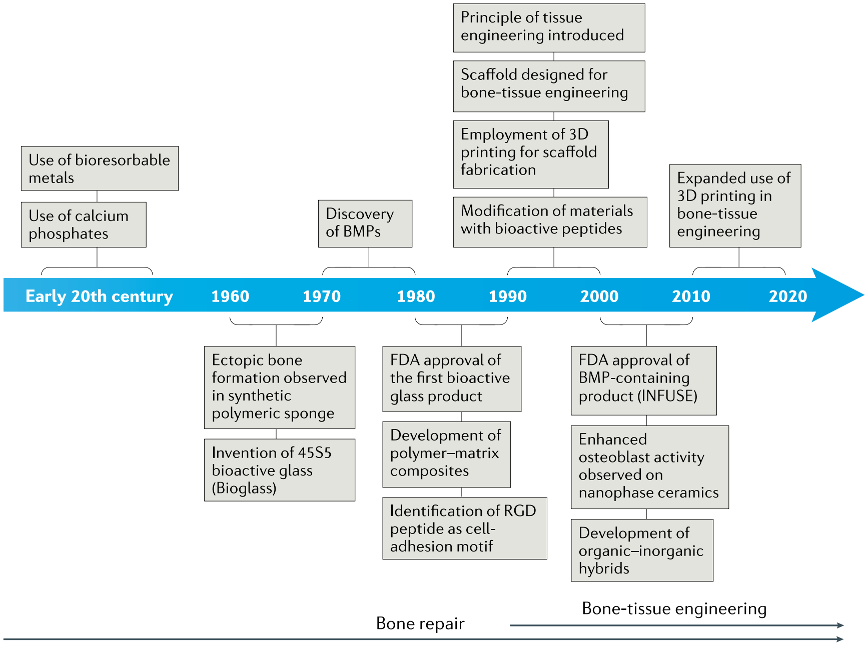

Figure 2.10: **Biomaterials timeline in bone tissue engineering**. Biomaterials have been evolving from the initial attempts of bone repair with bioresorbable metals and calcium phosphate constructs to functionalized scaffolds. Between fabrication technologies, 3D printing is considered one of the major breakthrough to resemble native bone complexity. Image taken from [82].

2.2 Patient-specific strategies for bone tissue engineering

2.2.1 Individual regenerative potential

The intra-subject variability in the outcome of tissue engineering products is one of the main limitations for their clinical translation. Most of the clinical trials based on regenerative medicine therapies relied on adult MSC to stimulate tissue regeneration and were carried out in different medical specialties, ranging from neurology, to orthopedics and nephrology. However, outcomes were often discordant on the efficacy of regenerative therapies, mostly due to uncertainties both in the patient reaction and the reproducibility of the regenerative product (Table 2.1) [84].

Clinical trials	Minimize patient-related modifiers (age, gender, and comorbidities) in phase I/II trials
Preclinical models	Avoid young and healthy animal models to represent clinically relevant scenario
Basic research	Explore the biological response associated to each source of variability

Table 2.1: **Individual regenerative potential in translational research.** Recommendations for the inclusion of individual variability when testing a regenerative product in all stages of translational research.

Sources of variability are systematically underestimated in all stages of translational research. In the clinical stage, the patient selection process should carefully exclude the side effects of comorbidities and aging [85]. In preclinical models, testing small groups made of young and healthy animals might overestimate the clinical potency of a regenerative product [86]. Despite the challenges in modeling a clinically relevant scenario, recent *in vivo* studies illustrated how the bone adaptive response of each subject depends on aging [87] or physical activity [88] and how it leads to drastic changes in bone scaffold design (Figure 2.11) [89].

In basic research, *in vitro* models should explore the underlying biological response in tissue engineering products to reveal the impact of heterogeneous patient responses. Patient-specific models aim to represent individual physiology as well as pathology, thus they require advanced systems whose microenvironments can be tailored to the specific case under investigation. Organ-on-chip systems are advanced solutions to develop culture microenvironments whose mechanical, chemical and physical properties can be finely tuned based on the clinical target that is replicated [90].

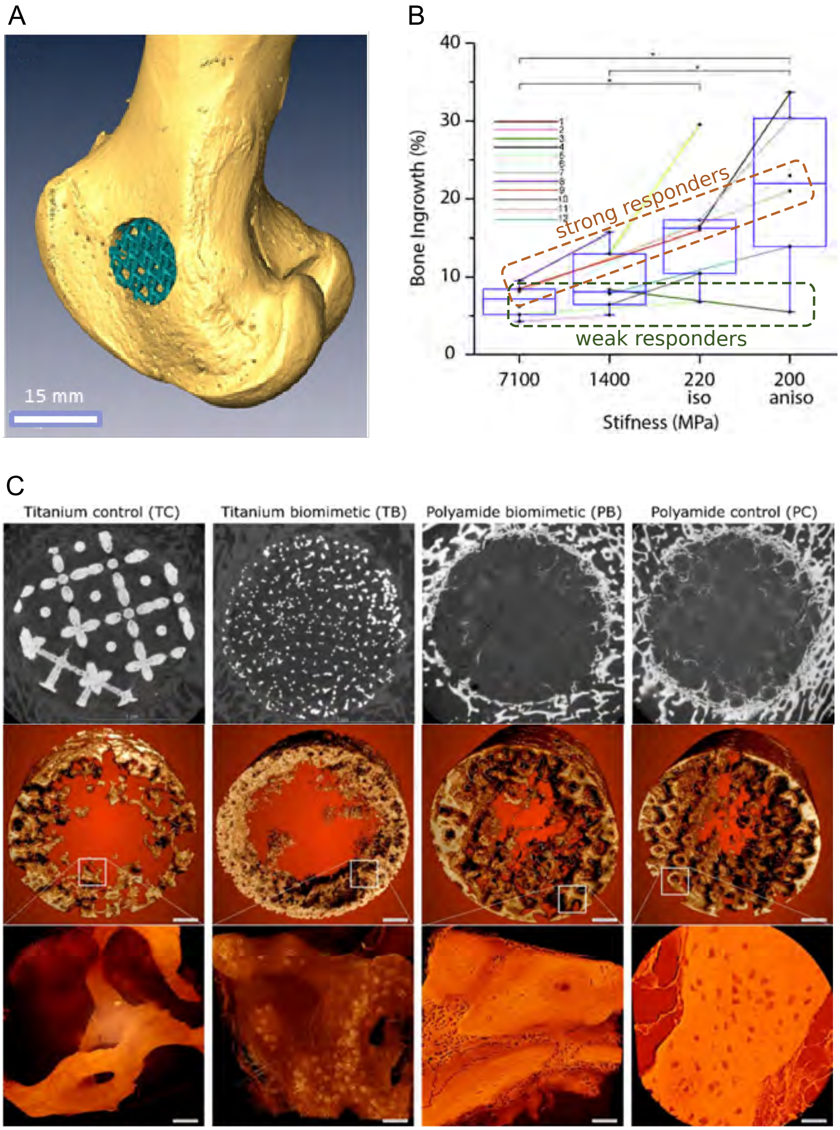

Figure 2.11: **Individual variations in scaffold-guided bone regeneration** (A) Bone scaffold implantation in ovine femur. (B) Regenerative response (bone ingrowth) versus 3D printed scaffold stiffness. Lines connect *in vivo* outcomes from the same animal, identifying two groups of strong and weak mechano-regenerative response. (C) MicroCT images of bone ingrowth and isolation of mineralized tissue within the scaffold pores. Scale bars, 40 µm. Image modified from [89].

Microengineered platforms facilitate the use of primary human cells from single donors, thus the combination of controlled microenvironments and patient cells create personalized testing devices [91]. Moreover, the interconnection between separate culture microenvironments define multi-organ models on-chip with the unique advantage to assess both the local and systemic effects of regenerative therapies [92].

2.2.2 Porous biomaterials and additive manufacturing

Porous biomaterials fabricated via additive manufacturing (AM) were recently proposed to address the lack of osteointegration in orthopedic implants (Figure 2.12) [93]. The rational behind the use of porous structure is that bone ingrowth facilitates the mechanical interlocking of the implant with the surrounding bone.

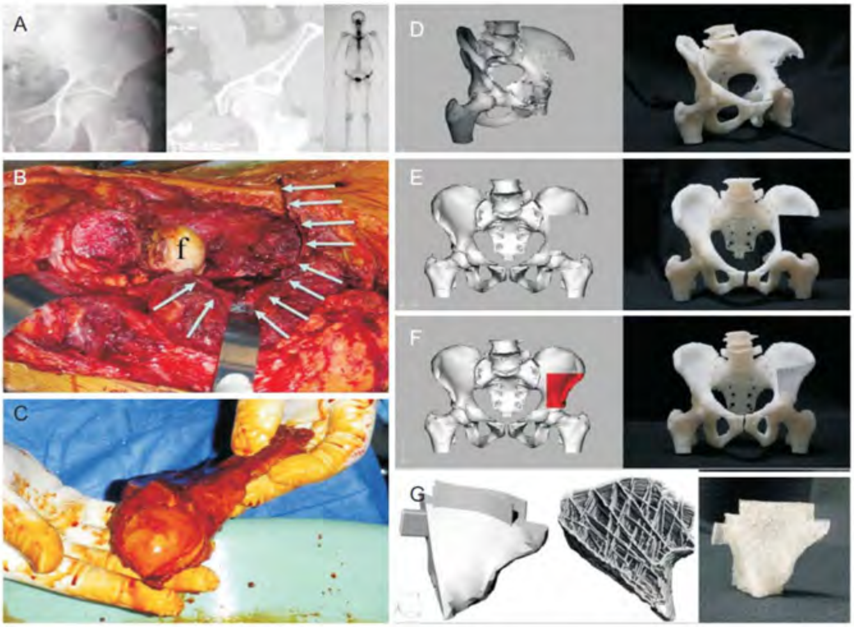

Figure 2.12: **Combined used of CAD and scaffolds as clinical therapy after resection of musculo-skeletal sarcoma.** Clinical case of orthopedic regenerative medicine after resection of malignant bone tumor. Custom scaffold designed from CT data of the patient pelvis and fabricated via additive manufacturing. The implant fits the macro-scale geometries of the specific application, while the porous structure facilitate osteointegration. Image taken from [94].

From a design perspective, AM is moving from the fabrication of patient-specific devices to bio-inspired designs enhancing the biomaterials performance [95]. Not only does an implant fit the macro-scale geometries of individual applications, but it can also boost a regenerative response from the host. Such a challenge is driving three dimensional (3D) printing into the fields of orthopedic regenerative medicine and bone tissue engineering, where the use of open, interconnected and tunable scaffolds are key to elicit bone tissue formation *in vivo* [35, 23, 94]. On the one hand, highly porous structures have a large surface area that improves apatite forming ability and bone ingrowth [96], as well as the deposition of bioactive molecules [97]. On the other hand, the precise control over the final shape makes additively manufactured scaffolds suitable for applying geometrical gradients and influencing the cellular response (Figure 2.13) [98]. Moreover, the regulation of the internal architecture can lower the equivalent Young's modulus of the bulk implant materials, thus matching the mechanical requirements of bone substitutes (Figure 2.14) [99, 35].

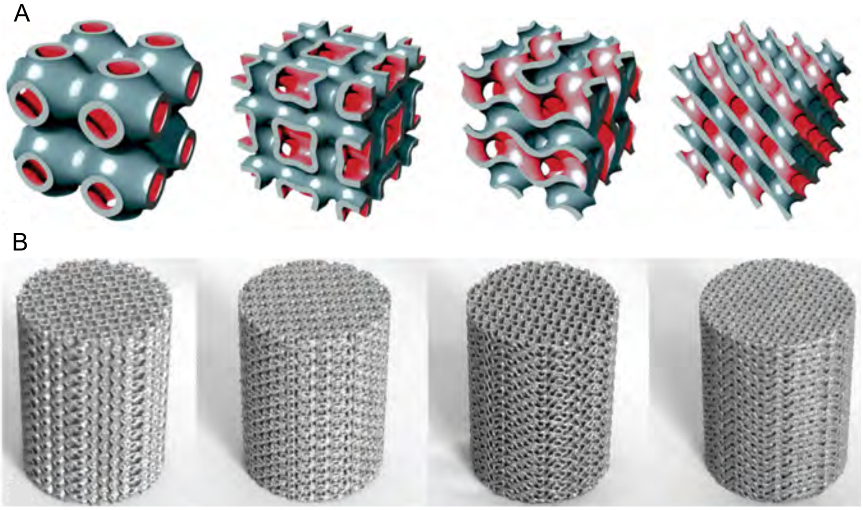

Figure 2.13: **Additively manufactured porous biomaterials.** 3D printing offers precise mechanical and topological control when creating open and interconnected porous structures eliciting bone formation. (A) Topological designs with a class of surfaces, named minimal surfaces, whose mean curvature is comparble to trabecular bone. (B) 3D printed specimens. Image adapted from [93].

Bone regeneration with 3D printed scaffolds might involve the functionalization of the surface, the change of the topological order and the control of mechanical properties. It is clear that computational models provide an optimization framework to guide scaffold design and testing, since they investigate the effect of design parameters on the regenerative performance for each specific application [100].

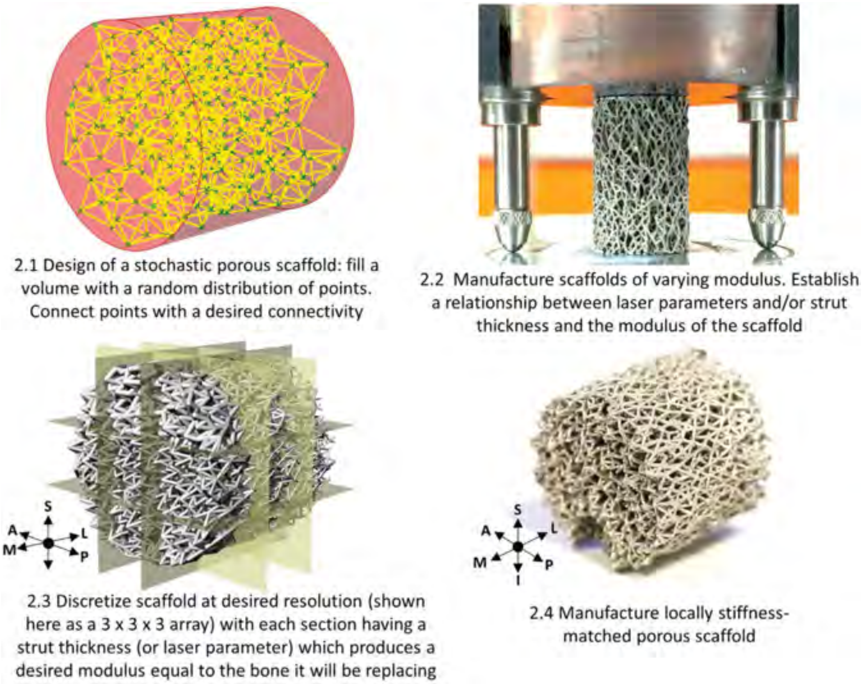
2.1 Design of a stochastic porous scaffold: fill a volume with a random distribution of points. Connect points with a desired connectivity

2.2 Manufacture scaffolds of varying modulus. Establish a relationship between laser parameters and/or strut thickness and the modulus of the scaffold

2.3 Discretize scaffold at desired resolution (shown here as a 3 x 3 x 3 array) with each section having a strut thickness (or laser parameter) which produces a desired modulus equal to the bone it will be replacing

2.4 Manufacture locally stiffness-matched porous scaffold

Figure 2.14: **Locally bone-stiffness-matched porous scaffold.** The stiffness of a 3D printed scaffold can be finely tuned throughout the structure in order to match both the local bone stiffness and the overall compression stress–strain response of the corresponding bone specimen replaced. Image taken from [99].

2.2.3 Microengineered technology for individual response

The organ-on-chip field has recently emerged from the synergy of microfabrication techniques and tissue engineering, with the aim to replicate specific processes of organ functionality in sophisticated *in vitro* microenvironments. The development of organ-on-chips typically starts from a microfabrication technique, such as mask-based photolithography, etching precise microscale pattern into photosensitive materials, thus creating a mold [101]. Later, soft lithography replicates the master pattern in the microengineered device. The soft elastomer poly(dimethylsiloxane) PDMS is the standard material used for the stamp, given its optical transparency, biocompatibility. Moreover, PDMS can restore hydrophobicity after the stamp is bonded to a flat surface, which facilitates the hydrogel filling of the culture chamber [102]. The final device consists of transparent polymeric microchannels where mechanical stimuli and biochemical gradients can be applied, while tissue-tissue interfaces can be replicated [103].

While the use of organ-on-chips for drug screening is steadily increasing [90], the combination of microengineered systems with primary patient cells is inspiring the field of personalized medicine [91] as well as regenerative medicine [104]. Different organ-on-chips were recently developed to predict the variability between individuals associated to specific biological processes, such as the permeability of the blood-brain barrier [105], the inflammation of the human airways [106], the proliferation of multiple myeloma cells [107] and the drug-induced hematotoxicity [108] (Figure 2.15).

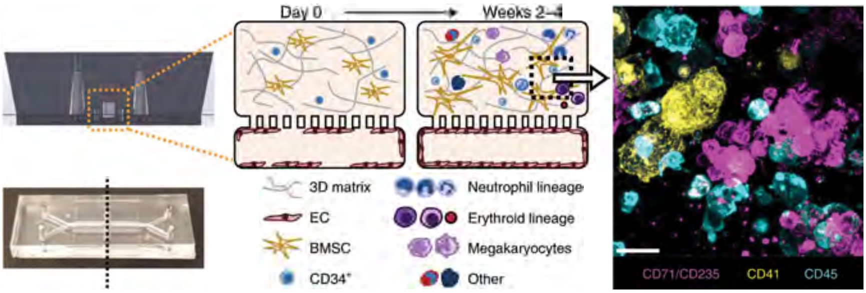

Figure 2.15: **Human bone marrow-on-chip.** A vascularized human bone marrow-on-chip was developed with optically clear poly(dimethylsiloxane) channels. In the top channel, hematopoietic stem cells ($CD34^+$) were seeded, while endothelial cells (EC) created a vascular lumen in the bottom channel. After 2 weeks of *in vitro* culture, hematopoietic stem cells differentiated in multiple blood cell types (magenta: erythroid lineage; yellow: megakaryocyte lineage; blue: neutrophil and other haematopoietic lineages). Scale bar, 20 µm. Image adapted from [108]

.

Compared to other tissues, bone-on-chip platforms have mostly arose only in the last years. The first literature review on the developments and challenges of bone-on-chip systems has been recently published, showing the main technical solutions adopted to study bone cell function, bone regeneration and its interaction with multiple tissues [109]. Starting from a monolayer of mouse osteocyte-like cell line to study mechano-regulation under oscillatory fluid flow [110], bone-on-chips moved to three dimensional (3D) culture systems that investigated the osteocytic network formation [111, 112] or the bone matrix mineralization process [113]. Indeed, 3D culture environments mimicking the extracellular matrix (ECM) provide more representative systems of tissue function and it can be achieved by loading hydrogels. Hydrogel-based bone-on-chip system can potentially answer novel biological questions, but they must always meet the biological requirements of the specific physiological or pathological process modeled (Figure 2.16).

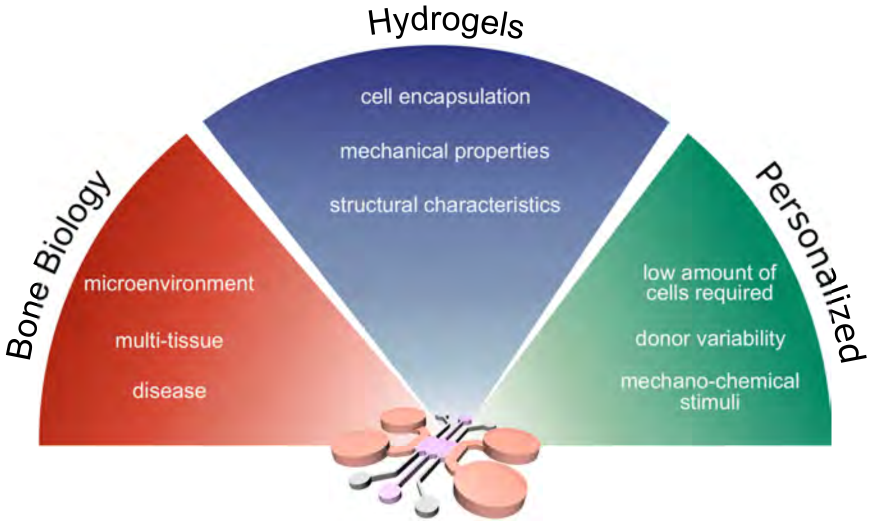

Figure 2.16: **Modeling bone biology with personalized hydrogel-based bone-on-chips.** Bone-on-chips aim at replicating specific functions of the bone tissue in sophisticated *in vitro* microenvironments. From a biological perspective, the variability associated to cell phenotype and bone diseases makes it difficult for traditional models to predict the efficacy of potential therapies. Each physiological or pathological bone process has a specific extracellular environemnt, which can be replicated by using hydrogels and tuning their biomechemical composition, structural and mechanical properties. Therefore, hydrogel-based bone-on-chips offer personalized bone tissue models, where a proper combination of complex 3D microenvironments and primary human cells can answer questions on bone biology and test novel treatments.

Designing hydrogel-based bone-on-chips

Fundamental requirements of any organ-on-chip are one or multiple cell types and a culture micro-chamber. To model biological characteristics of the bone tissue, the selection and the number of different cell types to introduce in a bone-on-chip (BOC) system includes, but it is not limited to, cells normally residing in the bone tissue. The cellular component of the bone matrix is usually represented by MSCs, osteoblasts or osteocytes [108, 114, 115, 116, 117]. Besides including cell types involved in the development, growth and remodeling of bones, a more realistic bone microenvironment requires modeling interactions between tissues made of different cell types. For example, vascular tissue and endothelial cells interact with bone forming cells and affect both bone pathology and physiology. BOC devices can be designed to deposit a layer of human umbilical vein endothelial cells (HUVECs)

[118, 119]. Moreover, organ-on-chips facilitate the interaction between three or four different cells types to model the interaction between tumors, vascular and bone tissue [118, 120, 115, 121] (Figure 2.17). A different approach from the traditional cell seeding consisted of a prior *in vivo* implantation of an hydrogel-based bone microenvironment and subsequent culture in a microfluidic device after explantation [122].

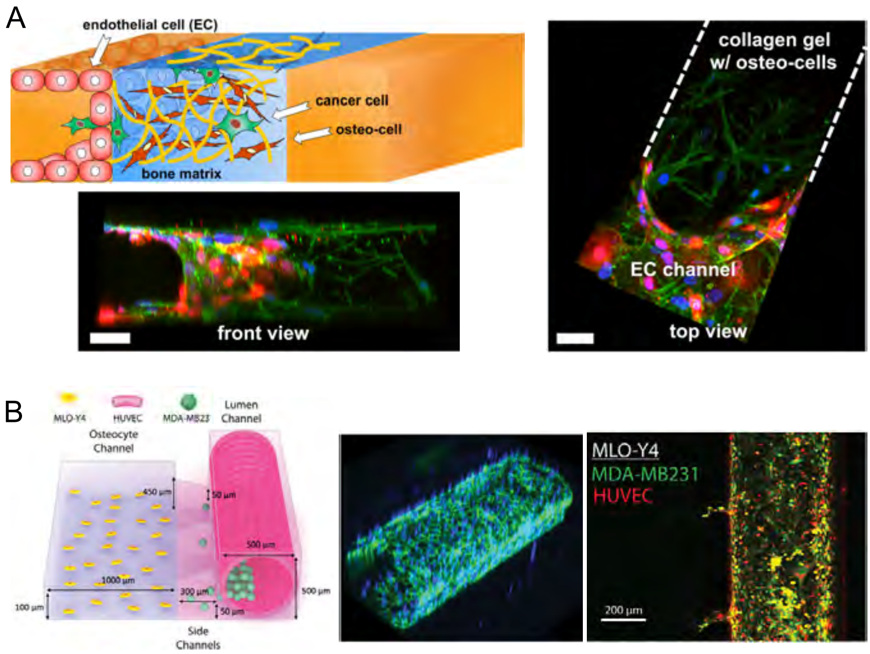

Figure 2.17: **On-chip devices modeling breast cancer metastasis in the bone tissue.** Examples of microfluidic devices modeling breast cancer cell extravasation towards the bone tissue. (A) Tri-culture system where osteo-differentiated mesenchymal stem cells created a bone-like environment by conditioning a collagen hydrogel. After seeding a monolayer of endothelial cells on the edge of the collagen hydrogel, breast cancer cells were introduced and their extravasation ability was assessed. Scale bar, 50 µm. Image adapted from [118]. (B) Tri-culture system where the bone-like compartment was made of an osteocyte monolayer. A lumen seeded with human umbilical vein endothelial cells (HUVECs) represented a blood vessel. Confocal images showed breast cancer cell (MDA-MB231) extravasation through the endothelial cell lumen. Image adapted from [117].

The design of the culture chamber in BOCs is intrinsically related to the complexity of the multi-cellular and multi-tissue interaction modeled with each device (Table 2.2). For example, single channels are normally preferred for cell migration studies

[123, 124, 125]. The definition of compartments in organ-on-chips is one of the most characteristic advantages of microengineered technologies over traditional culture techniques. By means of computer aided design, it is possible to tune the geometry of each single channel and the way multiple channels communicate with each other [126, 117]. Beside using channels as culture chambers, microengineered system might induce chemical gradients within the culture environment, given that microfluidic devices facilitate the application of independent fluid flows for different channels [116].

When a 3D microenvironment is essential to recapitulate the biological process under investigation, cells are mixed with hydrogels prior to loading in the culture chamber. After insertion in the microengineered devices, hydrogels undergo a gelation process and create the 3D matrix where cells are embedded. Due to their remarkable biocompatibility and non-toxicity, natural hydrogels are normally selected to resemble the native ECM in BOC systems (Table 2.2). The hydrogel choice depends on the specific environment to be modeled. For example, the formation of a fibrin matrix immediately after a bone injury makes fibrin gels a suitable model of the bone healing process [114]. In search of a model representing the more developed bone tissue, fibrin can be mixed with collagen type I, whose addition increases the hydrogel stiffness and its mechanical stability [127]. Due to its ubiquitous presence in the bone matrix, hydrogel-based BOC systems normally used collagen I when culturing HOBs. The collagen properties varied for the different applications of the BOCs. In general, collagen concentration was higher when inducing ostegenic differentiation and mineralization [118], while collagen concentration, thus matrix stiffness, was lower for osteoblast migration assays [124, 123]. Hydrogels properties can be enhanced with composite systems. Besides mixing with fibrin, collagen I was also mixed with Matrigel prior to loading in BOC [128]. Moreover, hydroxyapatite nanoparticles were incorporated in fibrin hydrogels and loaded into BOC systems [121, 129]. Instead of incorporating inorganic phases, hydrogel-based BOCs recreated mineralized environments by combining a collagen I hydrogel with osteogenic factors [122] or by culturing osteo-differentiated MSCs depositing mineralized matrix [118].

Goal	Cells	Chamber	Hydrogel	Main findings	Ref
Cancer metastasis	MDA-MB-231 hBM-MSC HUVEC	4 independent gel chambers	Osteo-cell conditioned collagen (6.0)	Extravasation of breast cancer cells is influenced by cell receptor CXCR2	[118]
	MDA-MB-231 MLO-Y4 HUVEC	Lumen and osteocyte channel	Mix of collagen I (5.5) and Matrigel (2.5)	Mechanically stimulated osteocytes reduced breast cancer cell migration	[117]
	hBM-MSC-OD hBM-MSC HUVEC MDA-MB-231	1 gel channel	Fibrin (5.0)	Bone-mimicking microenvironment induced the highest breast cancer extravasation rates	[114]
	OD MSC HUVEC LF MDA-MB-231	1 channel and endothelial monolayer	Mix of fibrin (2.5) and collagen I (0.2)	3D vascularized spheroids-on-chip enhances breast cancer cell migration	[115]
	Cancer cell (SW620 or MKN74) HUVEC LF	Separate channels for tumor and fibroblast co-culture	HA (0.2-0.4%)/ fibrin (2.5) composite	Inhibitory effect of HA in cancer cell migration and angiogenic sprout formation	[121]
Osteochondrogenesis	ADMSC	2 serpentine and 1 linear channel	Agarose (2.5%)	Simultaneous osteogenic and chondrogenic differentiation of stem cells	[116]
Vascularized bone	HUVEC LF	4 channels	HA (0.05-0.5%)/ fibrin (-) composite	HA enhances sprouting speed and increased lumen size, sprout length and number	[129]
Bone marrow physiology	Subcutaneous implantation prior to *in vitro* culture	Chamber for the explant and perfusion channels	Collagen I (3.0) with DBP, BMP2, BMP4	Reconstitution of hematopoietic niche physiology and response to radiation toxicity	[122]

Table 2.2: **Recent studies using hydrogel-based bone-on-chips.** Selection of recent studies using hydrogel-based bone-on-chips to model physiological or pathological bone microenvironments. Hydrogel concentrations are between brackets and expressed in mg/ml or weight/volume %. (Continue next page)

Goal	Cells	Chamber	Hydrogel	Main findings	Ref
Bone marrow pathology	$CD34^+$ cell BMSC HUVEC	Apical and basal channels	Mix of fibrin (5.0) and collagen I (0.2)	Prediction of clinically observed haemato-toxicities and representation of Shwachman–Diamond syndrome	[108]
	SUP-B15 BMSC HOB	4 channels	Collagen I (2.0 and 4.0)	Bone marrow microenvironment enhances leukemia cell survival during drug treatment	[120]
	leukemic cell (U937, HL60 or K562) HUVEC HS5	Gel channel, leukemic channel and endothelial channel	Collagen I (2.5 and 5.0)	Angiogenesis in bone marrow promotes leukemia cell proliferation and survival	[119]
Cell migration	HOB	1 channel	Collagen I (4.0)	Interstitial fluid flow alters hydrogel microstructure and cell migration	[123]
	HOB	1 channel	Collagen I (4.0)	The inhibition of ECM degradation reduces cell motility	[124]
	hBM-MSC	1 channel	Mix (1:1) of collagen (2.0) and Matrigel	Dose-dependent chemoattractant ability of different chemokines	[125]

Table 2.2: (Previous page). Abbreviations: *hBM* human bone marrow derived, *MSC* mesenchymal stem cell, *MDA-MB-231* human mammary adenocarcinoma cell (high invasion capacity), *HUVEC* human umbilical vein endothelial cell, *MLO-Y4* murine osteocyte-like cell Line, *OD* osteoblast-differentiated, *BMSC* bone marrow stromal cell, *SUP-B15* acute lymphoblastic leukemia cell line , *HOB* primary human osteoblasts, *HS5* human bone marrow stromal cell line, *DBP* bone-inducing demineralized bone powder, *BMP* bone morphogenetic protein, *HA* hydroxyapatite, *SW620* human colon cancer, *MKN74* human gastric cancer, *LF* human lung fibroblast, *ADMSC* adipose-derived mesenchymal stem cell, *ECM* extracellular matrix.

2.2.4 Computational models of scaffold-driven bone tissue regeneration

The optimization of design-oriented porous structures relies on the assistance of predictive computational algorithms to test the efficacy of different topological designs for each specific use [130]. Computational models are often based on either a bioregulatory or a mechanoregulatory process governing the bone regeneration dynamics [131]. On the one hand, bioregulatory models describe interactions in the biological microenvironment and might include a description of cellular behavior based on growth factor concentration and oxygen tension. As an example, bioregulatory models were already applied to identify culturing conditions that maximize bone formation in cell seeded scaffolds [132]. On the other hand, mechanoregulatory models relate a mathematical definition of the mechanical stimulus to tissue formation and differentiation [133].

Mechanical variables and regenerative response can be correlated at multiple length scales. At the tissue level, where the newly formed bone tissue is considered as homogeneous continuum, the SED, octahedral shear strain and interstitial fluid flow are used to derive mechanical stimuli triggering bone formation (Figure 2.18). The mathematical formulation associated to the SED is derived from the bone remodeling theory, thus bone regeneration is represented as newly mineralized tissue induced by a mechanical gradient [134]. The mathematical formulation associated to the octahedral shear strain and interstitial fluid flow leads to a biophysical stimulus driving the differentiation of mesenchymal stem cells into fibroblasts, chondrocytes and osteoblasts. The biological output of such mechanoregulatory theory is the amount of fibrous, cartilaginous and osseus tissue formed [135, 136]. At the cellular level, the mechanical stimulation on individual cells seeded into a bone scaffold can be compared to the strains that bone cells experience *in vivo*, thus identifying the optimal perfusion and compression inducing osteogenic differentiation [137].

Besides implementing a mechanoregulatory theory, computational models of bone regeneration have a cellular component migrating within the scaffold pores and depositing new ECM [138]. For a more complete mechanobiological perspective, novel approaches include the effect of chemical factors on cell proliferation, apoptosis and differentiation, defining mechano-chemical models of scaffold-driven bone regeneration [100, 139, 140]. The majority of the bone regeneration theories assume that MSCs differentiation to osteoblasts, chondrocytes or fibroblasts depends on the intensity of mechanical cues, thus the dynamic processes of cell differentiation and tissue formation update the mechanical cues and regulate the regeneration process. When applied to cell-seeded porous scaffolds, modeling the evolution of differentiated cell and tissue phenotypes identified the combination of compression and pore pressure inducing osteogenic differentiation and higher stiffness of the newly formed matrix [136].

Another mechanoregulatory approach adapts the mathematical formulation of the bone remodeling theory (Section 2.1.4) to the bone reparative phase after injury. Briefly, the driving force for the mineralization process is the difference between the mechanical stimulus and a reference value, so that the bone apposition rate is reduced as tissue gets mineralized and stiffer [63]. While models adapting the bone remodeling theory strongly focuses on the influence of porous scaffold mechanics in the regeneration process, they also consider the contribution of variable loads and physical activity [141].

Mechanobiological opitmization of bone scaffolds

The validation of computational models, thus the correspondence between numerical predictions and *in vivo* outcomes, is an crucial requirement for their use in an optimization workflow of the scaffold design. When applied to *in vivo* studies, computational results revealed that scaffold mechanobiology can contribute to the regenerative outcome. A mechanobiological model simulated the bone healing process supported by titanium scaffolds loaded with a bone graft. The computational analysis decoupled the individual effects on bone regeneration of the scaffold and the bone graft implanted. Results showed that the osteoconduction was the most determinant stimulatory effect of the bone graft, more than the progenitor cells embedded [138]. The authors reported that the model predicted the bone formation dynamics and patterning for one of the two scaffold designs tested, suggesting that additional effects should be included to explain the *in vivo* differences [138]. Although the entire bone regeneration process cannot only depend on the scaffold properties, modeling the mechanobiological interaction between the scaffold and the host environment can identify the best design for each specific application.

Computational models evaluating the bone regeneration guided by bone scaffolds can be introduced in an optimization workflow where scaffold designs are finely tuned until optimal criteria are satisfied. In addition, FE analysis can test different loading conditions, thus identifying whether the same optimal design performs best in different applications. For example, optimizing the porosity distribution in functionally graded scaffold showed significant variations in bone formation only for a pure shear loading, while the regenerative outcome was almost unchanged under compression loading [142]. Given the dynamic interaction between scaffold, host environment and newly formed tissue, computational analyzes should consider the temporal variation of the mechanobiological environment when evaluating the scaffold performance. For this reason, optimization frameworks targeting the initial mechanical stimulus as optimal criteria might fail in the identification of the most effective scaffold during the whole regeneration process (Figure 2.18) [143].

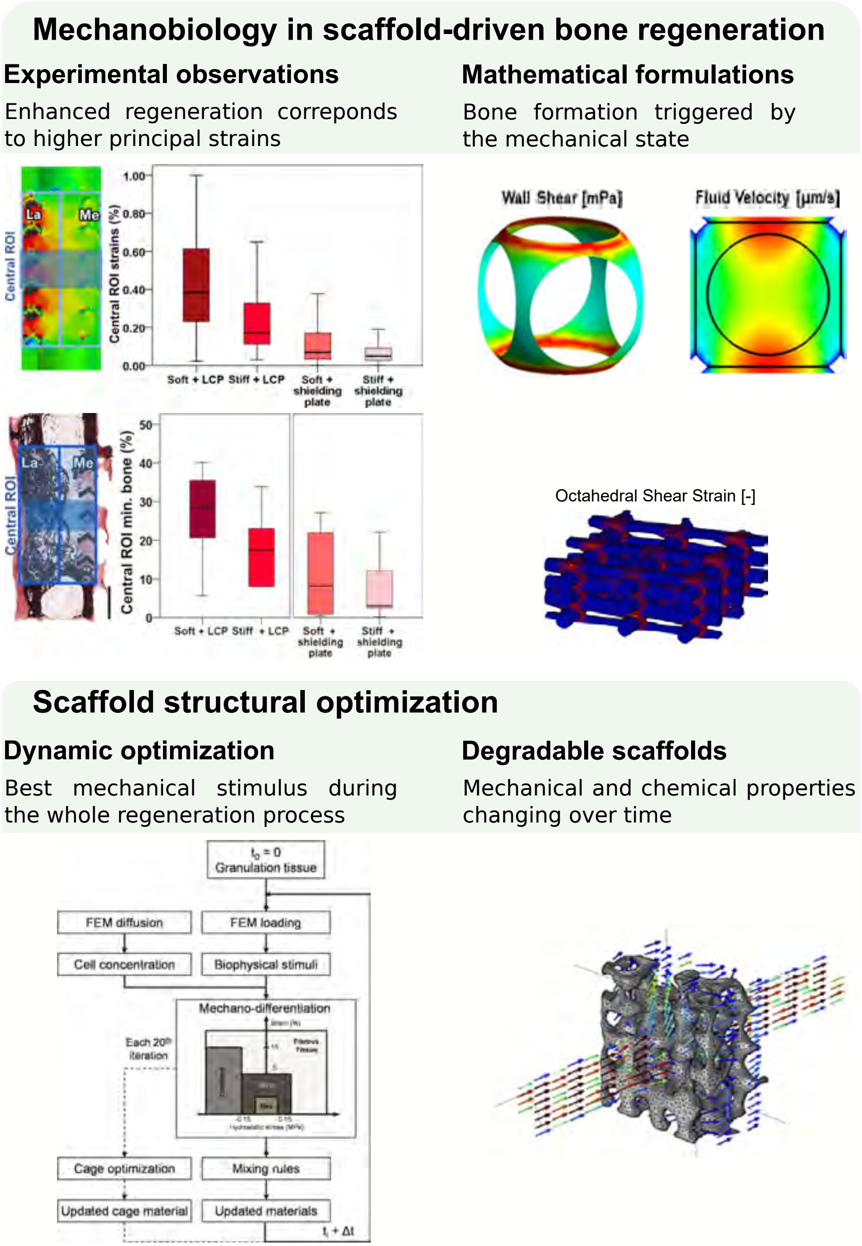

Mechanobiology in scaffold-driven bone regeneration

Experimental observations

Enhanced regeneration correponds to higher principal strains

Mathematical formulations

Bone formation triggered by the mechanical state

Scaffold structural optimization

Dynamic optimization

Best mechanical stimulus during the whole regeneration process

Degradable scaffolds

Mechanical and chemical properties changing over time

Figure 2.18: **Computer-based methods to evaluate the mechanobiogical performance of bone scaffolds.** Finite element-based methods support the experimental observations that reducing the stiffness of a (Continue next page)

Figure 2.18: (Previous page.) porous scaffold increases bone formation within the scaffold pores (image from [144]). Mechanoregulatory models of bone regeneration directly relates bone formation to mechanical variables, such as the wall shear stress, fluid velocity or octahedral shear strain (images from [135, 145]). Computational models could therefore be implemented in optimization frameworks to maximize scaffold-driven bone formation (image from [143]). However, computational models should include the dynamic change of mechanobiological environment, which can be achieved with biodegradable scaffolds (image from [146]).

To actively influence the mechanobiological response throughout the bone regeneration process, degradable materials have the unique advantage of gradually transfer mechanical loads, and thus stimuli, to the newly formed tissue. Numerical tools evaluate the mechanical state within scaffolds undergoing degradation, which might be related to experimental observation of weight loss and reduced mechanical properties (Figure 2.18) [146]. As a result, computer-based methods can simultaneously model the degradation of bone scaffolds and their mechanobiological role in bone regeneration [147, 141]. Scaffold optimizations based on combined degradative and regenerative models identify the initial designs and degradation kinetics that maximize bone formation during the entire regenerative response. Overall, computational models have the unique advantage of capturing the dynamics of the bone regeneration process. The biological environment, loading conditions and the mechanical properties of both the scaffold and the newly formed tissue are continuously changing over time, thus scaffold designs should provide effective support throughout the regenerative period (Figure 2.19). Current trends consider computational models an essential support to mechano-biologically optimize 3D printed bone scaffolds [148].

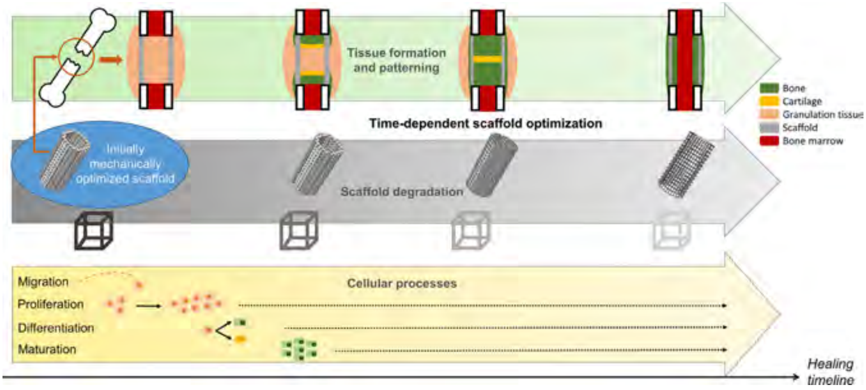

Figure 2.19: **Mechanobiologically-optimized porous bone scaffolds** Computational models simulate the temporal dependency of the mechanical and biological requirements for scaffolds during bone regeneration. Image adapted from [148].

2.3 Interaction between individual recipient and bone scaffolds

Given the effect of the host characteristics on functional tissue formation, it is clear that the natural regenerative potential of the recipient is an essential factor to consider in the design of a TE product. The host response is extremely relevant for *in situ* TE applications, even though the TE product might consist only of a scaffold. On the one hand, scaffold optimization involves tuning properties such as mechanical response, surface topography or functionalization. On the other hand, the *in vivo* outcome of the scaffold relies on patient characteristics such as age or comorbidities (Figure 2.20) [78].

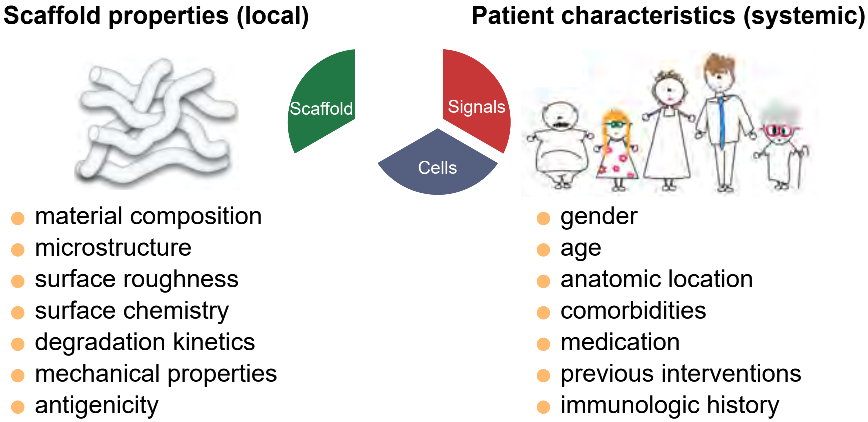

Figure 2.20: **Factors affecting *in situ* tissue regeneration**. The regenerative outcome of an *in situ* tissue engineering product depends on the properties of the scaffold implanted as well as the patient characteristic affecting its ability to restore tissue functionality. Image adapted from [78].

Scaffolds have been considered as temporary replacements until tissue regeneration occurs. They are now evolving to regenerative products that guide the endogenous restoration, even though this transition is one of the greatest challenges for current biomaterials [24]. The design of an *in situ* TE product cannot leave the analysis of the patient-specific response out of consideration, and herein lies one of the limitations of current TE treatments. As a consequence, the scaffold and the patient define a unit that should be analyzed and modeled as a whole.

2.4 Summary

This chapter has presented a detailed overview of bone architecture, healing and regeneration with a particular focus on patient-specific solutions for bone regeneration. In summary, bones sometimes fail to heal fractures despite their excellent regenerative capacities, as observed in critical-size bone defects. Autologous bone grafts are the current gold standard for large bone defects, even though their limited availability and the associated pain for the patient call for novel clinical treatments. In search of off-the-shelf and painless therapeutic solutions, TE is on of the most promising strategies to augment bone repair and regeneration. However, the clinical translation of TE products was delayed due to the limited knowledge on the effects of the recipient and the design parameters to the regenerative outcome. One way of overcoming the challenge of functional bone formation is the fabrication of customized 3D printed constructs, which relies on interconnected and tunable scaffolds to induce endogenous tissue regeneration. Although bio-inspired designs, tuning of mechanical properties and surface functionalizations have been shown to enhance bone regeneration of 3D printed porous biomaterials, to date no optimization approach consider both the scaffold and the patient characteristics as determinant factor of the final *in vivo* outcome.

To address the deficit in knowledge regarding patient-specific strategies for bone regeneration, chapter 3 examines the host mechanical contribution to the scaffold-driven bone regeneration by means of computational modeling, while chapter 4 of this doctoral thesis investigates the use of microengineered systems for patient-specific models of osteogenic differentiation.

Chapter 3

Scaffold regenerative potential depends on the host and the location-specific mechanical environment [1]

3.1 Abstract

It is well founded that the mechanical environment may regulate bone regeneration in orthopedic applications. The purpose of this study is to investigate the mechanical contributions of the scaffold and the host to bone regeneration, in terms of subject specificity, implantation site and sensitivity to the mechanical environment. Using a computational approach to model mechano-driven regeneration, bone ingrowth in porous titanium scaffolds was simulated in the distal femur and proximal tibia of three goats and compared to experimental results. The results showed that bone ingrowth shifted from a homogeneous distribution pattern, when scaffolds were in contact with trabecular bone (max local ingrowth 12.47%), to a localized bone ingrowth when scaffolds were implanted in a diaphyseal location (max local ingrowth 20.64%). The bone formation dynamics revealed an apposition rate of 0.37±0.28 %/day in the first three weeks after implantation, followed by limited increase in bone ingrowth until the end of the experiment (12 weeks). According to *in vivo* data, we identified one animal whose sensitivity to mechanical stimulation

---

[1] This chapter is a modified version of [149] published open access in *Bone*.

was higher than the other two. Moreover, we found that the stimulus initiating bone formation was consistently higher in the femur than in the tibia for all the individuals. Overall, the dependence of the osteogenic response on the host biomechanics means that, from a mechanical perspective, the regenerative potential depends on both the scaffold and the host environment. Therefore, this work provides insights on how the mechanical conditions of both the recipient and the scaffold contribute to meet patient and location-specific characteristics.

3.2 Introduction

Despite the intrinsic healing capacities of bone tissue, revision arthroplasty caused by extensive bone loss and implant mechanical loosening is a major clinical burden [16]. The demand for total hip and knee arthroplasties is projected to reach 4 million procedures per year in the U.S. only for 2030 [17]. Improving implant longevity is therefore important to reduce the number of revision procedures and limit the cost for healthcare systems. The next generation of orthopedic implants aims to guide the bone healing process and inspires innovative solutions in the field of orthopedic regenerative medicine. In the short term, these solutions are mainly aimed at increasing the implant lifespan by improving biological fixation, while in the long term they are aimed at providing temporary implants that will degrade and be fully replaced by functional host tissue [7].

Porous metallic biomaterials, fabricated via additive manufacturing (AM), were recently proposed to address the lack of osteointegration in orthopedic implants [93, 150]. With AM, orthopedic implants are fabricated with porous surfaces at the bone-implant interface, acting as scaffolds that enhance the biological engraft of the implant with the surrounding bone tissue [19, 151, 95]. Not only does a AM-fabricated implant fit the macro-scale geometries of individual applications, but it can also boost a regenerative response from the host [35, 23, 94]. In order to achieve functional integration with the host tissue, the optimization of 3D printed bone substitutes relies on, among others, the control of their mechanical properties to bear the weight of patients and the daily loading the bone is subjected to [93]. A fine tuning of the apparent stiffness is appropriate for encouraging bone ingrowth into porous materials, given the intrinsic relationship between mechanical stimulation and bone adaptation [152]. AM is commonly associated to the development of porous scaffolds matching the local bone stiffness [99, 153], although matching bone mechanical properties leaves out relevant aspects of the relation between mechanical stimulus and bone formation.

Firstly, the host sensitivity to mechanical stimulation has a critical impact on bone regeneration. The impact can be severe, such that weak responders, those with limited regenerative potential, may require permanent scaffolds for load-bearing applications [89]. A possible reason is the drastic alteration of the mechano-regulated processes of bone formation and resorption that takes place with aging [154, 87]. As a consequence, the design of porous substitutes should take into account the variability in the host response. Secondly, the cellular response is site-specific and within a single subject may therefore vary from bone to bone and within the same bone. Indeed, the different parts of the skeleton experience mechanical stimulations that varies in intensity and type, causing specific adaptations by bone cells. Moreover, multiple biomechanical requirements are associated with specific histomorphometrical indicators and load transfer behaviors within the same bone. This is clearly visible in the differences in shape and proportions of trabecular bone of a single structure, such as in the femoral neck [155] and the fibula [156]. Depending on the local history of mechanical loading, it has been proposed that bone cells accommodate and respond differently to the same mechanical stimulation [157]. Thus, a macroscopic mechanical analysis of the performance of a bone substitute design needs to consider the dependence on the local biomechanical demand. It is well established thereby that control over the mechanical requirements of additively manufactured bone scaffolds can be potentially addressed with *in silico* modeling. By testing the efficacy of topological designs for each specific use and patient, computational algorithms are the most adequate approach to inspect the mechanobiological potential of 3D printed scaffolds [148, 130]. An optimization framework implementing the finite element (FE) method already verified that the local stiffness of mechanobiologically optimized titanium scaffolds enhances endogenous bone regeneration, but did not consider how the formation of novel bone tissue alters the mechanical environment [144].

The implementation of phenomenological models *in silico* describes the influence of mechanical forces on the adaptation or the regeneration of bone tissue [158, 133]. The simulation of bone mechano-regulation or regeneration processes can model their dynamics, in terms of continuous variation of bone mechanical properties [159, 148]. When applied to porous scaffolds, regeneration algorithms elucidated the relationship between the tissue being formed within the pores and the loading environment, as well as the mechanical benefits of a degrading scaffold during bone formation [141, 160]. However, no previous model of mechano-driven bone ingrowth has estimated the effect of local biomechanical demand and individual response variability on scaffold regenerative performance. There is a need for a wider evaluation of the mechanical interplay between scaffold and host subject.

Following the need of modeling the scaffold regenerative potential for patient-specific applications, the purpose of this study is to evaluate the scaffold performance based on the biomechanical contributions of both the host and the scaffold itself. It was hypothesized that (1) local mechanical stimuli determine the distribution of bone ingrowth inside a scaffold and that (2) inter and intra-animal variations require subject-specific parameters to describe the local biomechanical demand

and individual sensitivity to mechanical stimulus. Therefore, it was developed a computational model of mechano-driven bone regeneration in porous scaffolds where the local mechanical environment and the regenerative potential of an individual host regulate the bone ingrowth within the scaffold pores. Mechanical properties were constantly updated during each analysis and model parameters represented the host reaction. The model predictions were validated by means of *in vivo* animal data (goat) of bone ingrowth in 3D printed porous titanium scaffolds, where scaffolds were inserted in distinctive implantation sites and in different recipients. This computational model presents a subject-specific applicability on the evaluation of the scaffold regenerative potential. From a mechanical perspective, it evaluates the scaffold regenerative performance for each specific patient and in each implantation site.

3.3 Materials and methods

3.3.1 Mechano-driven bone regeneration model

Mathematical formulation

Computational methods of mechano-regulation relate bone formation and/or resorption directly to a mechanical stimulus. We define bone formation as the process by which new bone tissue is formed by osteoblasts that differentiate from osteoprogenitor cells. When translated to macroscopic models where bone is a continuous material without a hierarchical structure, the mathematical formulation of bone mechano-regulation reduced to a relation between local strain levels and bone mineral density [141, 161, 162]. Here, we assumed that a simultaneous process of cell invasion and a bone formation phase regulated by the mechanical stimulus could simulate the bone regeneration process [134].

Cell invasion in the granulation domain (Figure 3.1-A) was modeled as a diffusion process, where cell concentration c in the scaffold pores was normalized to the maximum cell concentration (Figure 3.1-B). It had a constant value of 1 at the bone-granulation interface and initial zero value in the scaffold pores [141]. From the mechanical perspective, the daily strain stimulus Ψ was based on the effective tissue microstrain $\bar{\epsilon}$, calculated from the strain energy density W and the Young's modulus E [163] (Figure 3.1-B). Together with the daily strain history, the strain level described the importance of each load cycle in the mechanical stimulus [164].

Earlier studies have implemented relations between mechanical stimulus and bone remodeling [63] to predict tissue regeneration in bone scaffolds [141]. These studies imply that bone formation occurs for values of the mechanical stimulus above a reference value, which could be identified with the local stimulus Ψ^*_{local} in the neighboring area [165].

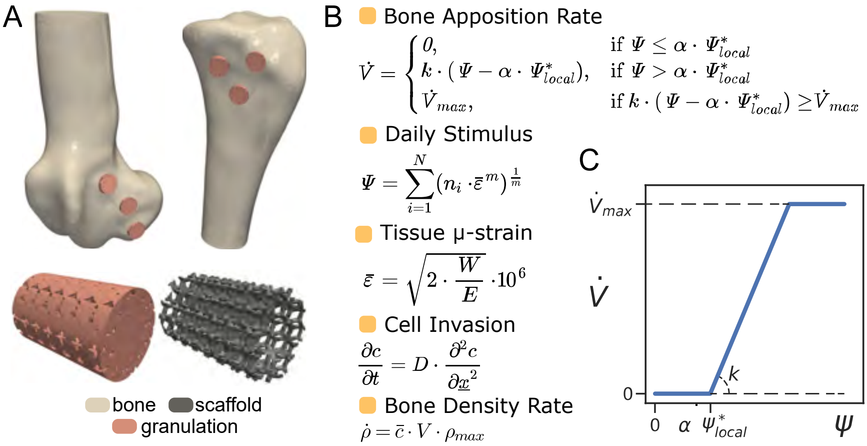

Figure 3.1: **Overview of the mechano-driven bone regeneration model.** (A) Representative femoral and tibial *in silico* models of mechano-driven bone regeneration and detail of a scaffold-granulation unit, where the granulation tissue filled the scaffold pores. (B) Mathematical formulation of the mechano-driven model of bone ingrowth. The model consisted of a simultaneous process of cell invasion and a bone formation phase regulated by the mechanical stimulus (effective tissue microstrain), the daily load history and the mechanosensitivity of the host (*k* constant). (C) Graphical display of the bone volume deposition rate proposed in the model. It was assumed that: bone formation is proportional to mechanical stimulus Ψ up to a maximum bone deposition rate $\dot{V}_{max}$, no bone resorption took place for low Ψ and bone formation initiated for mechanical stimuli higher than a fraction α of the local mechanical stimulus Ψ^*_{local}.

In the present model, the mathematical formulation of the bone apposition rate $\dot{V}$ assumed that (1) bone formation is proportional to mechanical stimulus Ψ up to a maximum bone deposition rate $\dot{V}_{max}$ [166], (2) no bone resorption took place for low Ψ [134] and (3) bone formation initiated for mechanical stimuli higher than a fraction α of the local mechanical stimulus Ψ^*_{local} (Figure 3.1-C). Ψ^*_{local} was calculated as the volume-averaged daily strain stimulus in the bone at the location where the scaffold was placed and the immediate surrounding area, thus covering the implant region and also the peri-implant region that is mechanically altered after insertion of the implant [64]. The linear relationship between bone formation and mechanical stimulus was represented by subject-specific constant of bone volume deposition rate k. This constant represented the capacity for mechanosensation of the single organism, thus it was a patient-specific parameter. On the other hand, the biomechanical demand was considered to be location-based, thus Ψ^*_{local} and α varied within the same organism for different implantation sites. The detailed mathematical description of the bone regeneration model is given in Appendix A.

Numerical implementation

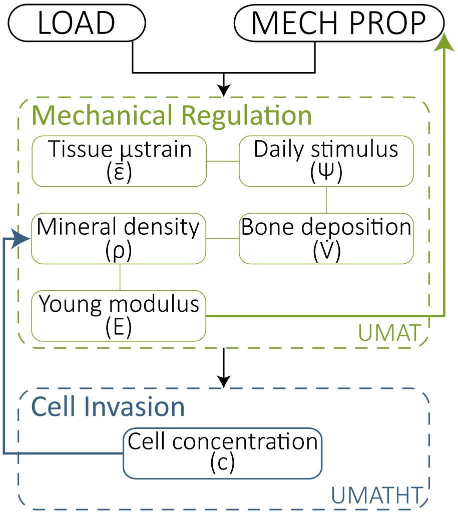

Figure 3.2: **Block diagram of the bone regeneration algorithm**. Using a coupled thermal-stress analysis, the algorithm sequentially implemented the concurrent processes of mechanical regulation and cell invasion described in the bone regeneration model. By means of Abaqus UMAT and UMATHT subroutines, cell concentration was extracted at each time step and used in the following step to compute the bone deposition rate due to mechanical regulation. Tissue mechanical properties were updated at the end of each step, thus changing the mechanical stimulus at each iteration.

The mathematical model of mechano-driven bone regeneration was solved with FE methods implemented in ABAQUS 6.14 (Dassault Systèmes, Suresnes, France). The concurrent events of mechanical regulation and cell invasion required a sequential solution and update during the FE analysis. The mechanical behavior of the system was simulated with a linear stress analysis, where the material properties of the newly formed bone were updated with a UMAT subroutine [167]. Cell invasion was simulated by means of a heat transfer problem, where temperature represented the non-dimensional cell concentration *c* and was updated with a UMATHT subroutine. The use of a coupled thermal-stress analysis allowed the sequential implementation of the two processes, while the user subroutines continuously updated the bone formation process and the tissue mechanical properties (Figure 3.2). To facilitate the model convergence in the first iterations, the initial time increment was set to 0.05 day. After, the software automatically increased the size of the subsequent increments up to 1 day.

3.3.2 Model application to an *in vivo* goat study

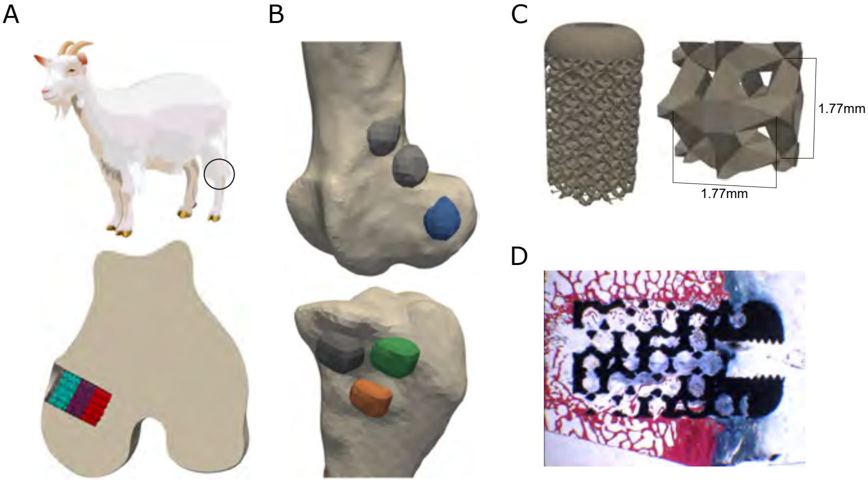

Figure 3.3: **Overview of the *in vivo* goat study**. (A) Detail of the insertion of a 3D printed titanium scaffold in the epiphyseal location of a goat femur. Bone ingrowth was quantified with microCT imaging in the medullary (red), middle (purple) and periosteal (light blue) subregions of the scaffold. (B) Representative femur and tibia showing the locations where the titanium scaffolds were implanted within the bone. Bone ingrowth was assessed only for two scaffolds (blue, green) in epiphyseal and one (orange) in diaphyseal location. (C) Design of the cylindrical porous titanium scaffold fabricated by additive manufacturing as repetition of a dodecahedron unit cell with thick struts (shown in the detail). (D) Histological analysis confirmed the novel formation of bone tissue within the scaffold pores after 12 weeks from surgery. Samples were stained with Stevenel's blue (connective tissues) and Von Gieson's picro-fuchsin (staining bone in red).

The experimental data used to calibrate the proposed model were taken from an unpublished animal study conducted by Materialise NV (Leuven, Belgium). Briefly, cylindrical porous titanium scaffolds were additively manufactured and three of them were inserted in each left femur and tibia of six goat models (Figure 3.3-A,B). A regular porous structure (diameter 8 mm, length 12 mm, porosity 71%) was built up of dodecahedron unit cell with thick struts (strut thickness 0.50 mm and mean pore size 1.77 mm) and covered with a solid cap to facilitate press-fit insertion into the bone (Figure 3.3-C). The apparent stiffness of the scaffold was 2 GPa (Materialise data). Empty scaffolds were implanted, not pre-seeded with cells or filled with bone graft. Three animals were euthanized at 6 weeks post-operatively, while the other three were euthanized at 12 weeks. Computerized tomography (CT) scanning of the goats was performed only for those euthanized 12 weeks after implantation, thus computational models were based on their bone geometries

Case	Week	Imaging		Bone ingrowth quantification				Pull-out
		CT	microCT	Femoral epiphysis	Femoral diaphysis	Tibial epiphysis	Tibial diaphysis	
1	12	×	×	●			●	● ● ● ●
2	12	×	×	●		●		● ● ● ●
3	12	×	×	●			●	● ● ● ●
4	6		×	●	●			● ● ● ●
5	6		×	●		●		● ● ● ●
6	6		×	●		●		● ● ● ●

Table 3.1: **Detailed data of the *in vivo* test system.** Summary of the *in vivo* data used to build and calibrate the computational model of bone ingrowth. 6 porous titanium scaffolds were implanted in the distal femur (3 scaffolds) and the proximal tibia (3 scaffolds) of 6 goats (cases), euthanized 6 or 12 weeks after implantation. Animals euthanized at week 12 received CT scanning, which were used to build the numerical simulations. For each animal, 2 samples were imaged by microCT scanning to quantify bone ingrowth withing the scaffold pores in different locations of the femur and the tibia. The shear strength of the bone-scaffold interface was measured for 4 samples by means of a pull-out test.

(cases 1, 2 and 3 in (Table 3.1). For each animal euthanized at week 6 and 12, four scaffolds were used to evaluate the shear strength of the bone-scaffold interface (pull-out test), while two scaffolds were imaged ex-vivo using microCT to quantify bone ingrowth (Table 3.1). Bone ingrowth was defined as the mineralized bone tissue detected by the microCT scans. MicroCT scans were performed on a Phoenix NanoTom S (GE Measurement and Control Solution, Wunstorf, Germany) at the Department of Materials Engineering of the KU Leuven (Leuven, Belgium). The scanner was equipped with a 180 kV/15 W high-performance nanofocus X-ray tube and a 2304x2304 pixel Hamamatsu detector. A tungesten target was used, and the applied voltage and current were 90 kV and 240 µA, respectively. A 0.3 mm cupper filter was installed. Beam hardening correction was applied during reconstruction of the cross-sectional images with Phoenix Datos|x 2.0 reconstruction software (GE Measurement and Control Solutions). The reconstructed micro-CT dataset had an isotropic voxel size of 6.0 µm. Later, a multi-level Otsu segmentation distinguished between the scaffold, bone and non-mineralized tissue [168]. Finally, bone tissue formation within the scaffold pores was studied by histological analysis and Von Gieson's picro-fuchsin staining (Figure 3.3-D).

Overall, bone ingrowth after 12 weeks was assessed for the scaffolds inserted in the femoral condyle of all three goats, thus in contact with trabecular bone (Figure 3.3-B). As for the tibiae, the scaffold in contact with more cortical bone was analyzed in two goats. For the remaining goat, bone ingrowth was quantified in a scaffold inserted in the tibial epiphysis (Figure 3.3-B).

3.3.3 Implementation of the finite element model

A FE model was built for modeling the *in vivo* goat study, simulating the femurs and the tibiae of the three goats euthanized at 12 weeks post-operatively. The FE model simplified host reaction immediately after scaffold implantation [169] by filling scaffold pores with granulation tissue, thus creating a "scaffold-granulation units". These scaffold-granulation units were inserted in the tibia or in the femur at the specific locations extracted from CT images (Figure 3.3-B). The scaffold-granulation units consisted of the titanium scaffolds and the granulation tissue.

FE discretization and material properties

All parts were computationally modeled with linear unstructured meshes (4-node tetrahedral elements, C3D4 for bone and scaffold, C3D4T for granulation) generated using automatic algorithms (Materialise 3-matic™14.0, Materialise, Leuven, Belgium). The scaffold-granulation unit was meshed once and later inserted in the femur or in the tibia for each simulated case.

Femur and tibia Firstly, CT images were segmented with a livewire technique (Materialise Mimics™22.0, Materialise) to extract the femur and the tibia geometries. Each bone model was trimmed 10 cm from the condyles and meshed with target edge length of 1.4 mm, resulting in approximately 400.000 elements. Hounsfield units (HU) from CT images were mapped onto the FE models [170] and a custom algorithm was developed in the Python programming language to adjust for the partial volume effect at the edge between cortical bone and soft tissue. The algorithm redefined the HU at any node of the bone surface to the one of the nearest internal node, only if the inner HU value was higher than the outer [171].

Mapping material properties on FE models means transforming HU from CT images to mineral density values in the FE model. The empirical density–elasticity relationship was expressed in terms of the apparent density (ρ_{app}, which is just ρ in this document) [172], although CT scans provide only information about the bone mineral content, i.e. radiological density (ρ_{QCT}). Therefore, the workflow used to map material properties consisted of two main assumptions [173]:

- ρ_{QCT} (radiological density) was assumed equal to ash density (ρ_{ash});
- the ρ_{ash} / ρ_{app} ratio of 0.6 was used to calculate ρ_{app} from ρ_{ash} [174].

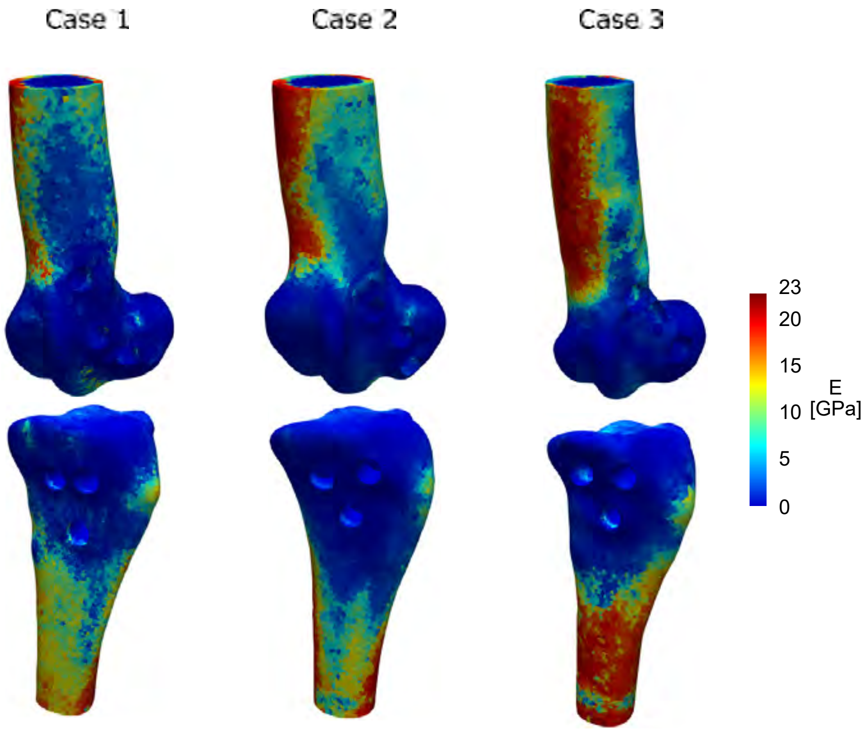

$$E\ (MPa) = \begin{cases} 521.22 \cdot \rho^{0.43}, & \text{if } \rho < 0.9g/cm^3 \\ 65006.86 \cdot \rho - 58008.23, & \text{if } 0.9g/cm^3 \leq \rho \leq 1.2g/cm^3 \\ 17275.04 \cdot \rho^{0.80}, & \text{if } \rho > 1.2g/cm^3 \end{cases}$$

Figure 3.4: **Bone material mapping**. CT images Hounsfield units (HU) were mapped onto the FE models, which were later pseudo-calibrated to transform HU into apparent density. Finally, bone material properties were assigned based on a continuous relationship between apparent density and modulus for ovine bone taken from the literature [99].

Consequently, the procedure to extract material properties was adapted as follows:

- HU were sampled from CT-scans of the goat;
- HU were converted to ρ_{QCT}, assumed equal to ρ_{ash}, using a linear pseudo-calibration;
- $\rho_{QCT} = \rho_{ash}$ was converted to ρ_{app} using the 0.6 ratio;
- $\rho_{app} = \rho$ was ultimately converted to Young's modulus using a referenced relationships [99].

In summary, after transforming HU into apparent density [175], bone material properties were assigned based on a continuous relationship between apparent density and Young's modulus for ovine bone taken from the literature [99] (Figure 3.4). In the FE analysis, femur and tibia were modeled as a linear elastic material, where Young's modulus was determined from the density-modulus relationship and Poisson's ratio was set to 0.3 [175].

Scaffold-granulation unit The cylindrical titanium scaffold was uniformly meshed, with a maximum edge length of 0.55 mm. The porous domain within the scaffold was considered the granulation tissue of the model. Starting from a cylinder matching the titanium scaffold size, the granulation tissue domain was determined as a non-manifold assembly, with the titanium scaffold as intersecting entity. In this way, the two parts shared nodes and element surfaces at their interface. Each pair of nodes was constrained to have identical displacement (tie-constraint), ensuring matching scaffold and tissue displacements at their interface.

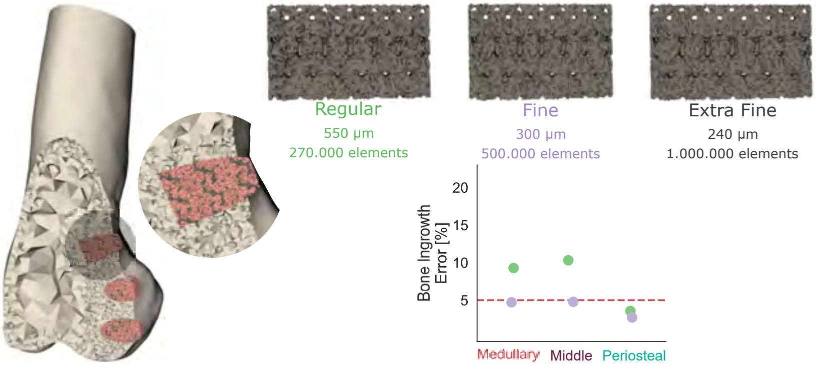

Figure 3.5: **Influence of mesh size on numerical predictions**. (A) Representative mesh of femoral *in silico* model and section detail of the scaffold-granulation unit. (B) The maximum edge length and the final number of elements are indicated below each mesh tested for the granulation domain. Prediction errors of bone ingrowth were computed with respect to the outcome of the extra fine mesh. The fine mesh was the only one with prediction errors lower than 5% in all subregions.

After investigating three different mesh sizes, the granulation volume was meshed with a maximum edge length of 0.3 mm, so that the titanium-granulation unit constituted a cylindrical part of approximately 630.000 elements to subtract from the bone (Figure 3.5). Both the scaffold and the granulation tissue parts were modeled as linear elastic materials. For the titanium alloy, a Young's modulus of 104 GPa (Materialise data) and Poisson's ratio of 0.3 were used. For the granulation tissue, the mechanical properties followed the continuous relationship between apparent density and Young's modulus used for the femur and the tibia, with initial bone density $\rho_{initial}$ set to 0.001 g/cm^3, and Poisson's ratio set to 0.3.

Boundary conditions

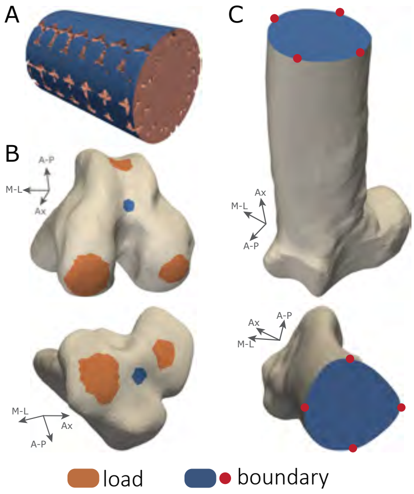

Figure 3.6: **Boundary and loading conditions of the finite element model of bone regeneration**. Boundary conditions were applied to the blue surfaces, while loading conditions to the orange regions. (A) Granulation tissue. The boundary condition of the thermal analysis was applied at the granulation-bone interface, assuming a constant and maximum normalized cell concentration. (B) Knee joint. The displacement of a 5 mm radius area around the knee center was set to zero along the antero-posterior (A-P) and the axial directions (Ax). The total forces are distributed over the contact areas of the patella and the condyles. (C) Boundary conditions on the distal femur and proximal tibia.

Cell invasion Cell invasion of the scaffold pores was implemented as a thermal diffusion process from the surrounding bone tissue, where the normalized cell concentration was maximum. Thus, the temperature of the surface nodes at the bone-granulation interface was set to 1 during the analysis. The bone-granulation interface comprised the cylindrical surface of the scaffold (Figure 3.6-A) as well as the flat surface on the medullary side of the scaffold (Figure 3.3). Conversely, cell diffusion was obstructed from the flat surface on the periosteal side of the scaffold, where the scaffold had a solid cap used for the press-fit insertion.

Mechanical loading The anatomical landmarks of the hip, ankle and knee centers, as well as the centers of the condyles and the tibial plateaus, were identified in each femur and tibia [176]. Boundary and loading conditions were applied in a new co-ordinate system based on the femur [177] or the tibia [178] landmarks (Figure 3.6-B,C). In the model, loads were applied to the condylar surfaces (Figure 3.6-B), while

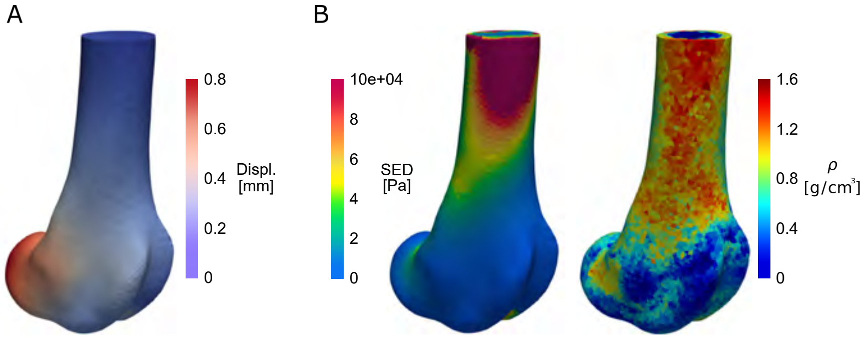

Figure 3.7: **Effects of displacement constraints in the finite element model.** (A) Representative femoral *in silico* model showing that absolute displacements were below 1 mm throughout the model. (B) Strain energy density (SED) output of a finite element model with uniform mechanical properties of the femur (Young's modulus of 1 GPa, Poisson ratio of 0.3) and comparison with bone mineral density mapping extracted from CT images.

boundary conditions were applied to both the trimmed diaphyses and the knee centers of the femur and tibia (Figure 3.6-C). The application of displacement constraints at both ends of a long bone produces physiological deformation and minimizes reaction forces at the constrained nodes [179]. For this reason, displacements along the axial and the antero-posterior directions of a 5 mm radius area around the knee center were set to zero, similarly to the physiological boundary conditions applied in a previous femur model [179]. Moreover, displacements were fully constrained to zero in four nodes of the trimmed surfaces, while all other nodes of the trimmed surface had only their axial displacement constrained to zero (Figure 3.6-C). In this way, all absolute displacements throughout the model were below 1mm (Figure 3.7).

Contact forces were based on experimental studies in ovine models quantifying the total force at the knee joint during a gait cycle [180, 181]. Forces were scaled to the animal body weights (Table 3.2). The distribution of the total knee contact force over the contact areas was based on the force distribution as determined by a validated musculoskeletal model of a human knee while squatting [182]. According to the musculoskeletal model, forces were divided over the contact areas of the patella and the condyles, while in the tibia they were divided over the tibial plateaus (Table 3.2) [182]. Bone remodeling and regeneration algorithms commonly use peak loadings during walking to quantify mechanical stimulation [63, 183, 134], which corresponds to 60° of knee flexion in the ovine gait cycle [180]. Therefore, total knee joint forces were distributed based on the proportions between medial and lateral contact forces measured in the musculoskeletal model at the position of 60° of flexion [182].

Femur			PATELLA			MEDIAL COND.			LATERAL COND.		
Case	Age	BW	Axial	A-P	M-L	Axial	A-P	M-L	Axial	A-P	M-L
1	2.8	72	554	-680	25	605	815	3	367	369	-66
2	3.7	65	500	-614	22	547	736	3	332	333	-60
3	2.8	58.5	450	-553	20	492	662	2	298	300	-54

Tibia			MEDIAL PLAT.			LATERAL PLAT.		
Case	Age	BW	Axial	A-P	M-L	Axial	A-P	M-L
1	2.8	72	-1009	-91	73	-511	-118	14
2	3.7	65	-911	-82	-66	-461	-107	13
3	2.8	58.5	-820	-74	59	-415	96	12

Table 3.2: **Summary of the loading conditions applied on the femur and the tibia.** Knee joint forces were scaled to the body weight and distributed over the different contact areas of the femur and the tibia. Forces were distributed over the patella and the condyles for the femurs and over the tibial plateaus for the tibiae. All forces were applied along the axial, the antero-posterior (A-P) and the medio-lateral (M-L) directions. Body weights (BW) are in kg, age is expressed as years at the beginning of the *in vivo* experiment, while all forces are in N.

3.3.4 Post-processing finite element output

Local daily strain stimulus The local daily strain stimulus Ψ_{local}^* was calculated first in the neighboring area of the bone scaffold. Before each remodeling analysis, the daily strain stimulus Ψ was measured for all femur elements within a cylinder of 8 mm radius and 16 mm length centered on the scaffold-granulation unit. Ψ_{local}^* was then computed as a weighted average, with the element volumes as weights.

In silico microCT and bone ingrowth assessment The computational model included all scaffolds implanted in each animal to properly account for each scaffold's effect on the local mechanical environment. However, only the numerical predictions of the microCT imaged scaffolds were analyzed and used to calibrate the computational model. In order to quantitively compare numerical predictions with *in vivo* experimental measurements, the simulation outputs were processed similarly to *in vivo* data [99], thus an Otsu thresholding algorithm separated the non-mineralized tissue from the newly formed bone in the granulation tissue. The identification of a medullary, middle and periosteal subregion within the granulation tissue (length 3.5 mm each) led to the bone ingrowth assessment, as performed in the *in vivo* procedure. The periosteal subregion was the closest to the external surface of the bone, while the medullary subregion was the furthest (Figure 3.3).

3.3.5 Parameter estimation

The constant of bone volume deposition rate k and the reduction factor α, introduced in the mathematical model of bone regeneration, are directly associated with physiological quantities. They represent the mechano-sensitivity of the organism and the reduction of the reference stimulus initiating bone formation in the peri-implant region, respectively. Therefore, model calibration comprised identifying a subject-specific k and a location-specific α that minimized the difference between computational and *in vivo* experimental results. The factor α was investigated in the range (1, 100) [%], since it was a reducing factor of the local reference strain stimulus. The constant k was investigated in the range ($1{\cdot}10^{-5}$, $9{\cdot}10^{-4}$) [% · μstrains^{-1} · day^{-1}], which included the values of similar parameters used for bone regeneration [141] and remodeling [184] models (Table 3.3). When calibrating the model, the residual sum of squares (RSS) were first calculated for all numerical outcomes. When calibrating the model, the residual sum of squares (RSS) were first calculated for all numerical outcomes. Since α was a location-specific parameter, we determined the values of α that minimized the RSS for each value of k. Next, samples were grouped by recipient and we determined the value of k that minimized the RSS for the whole recipient. Therefore, both α and k were determined by minimizing of the RSS. On the one hand, the determination of α allowed intra-subject variation. On the other hand, the determination of k required that it was the same for samples within the same subject.

The diffusion constant D indicates the migration at which the host cells invade the granulation domain. Given that D represented the whole cell population, the mechano-driven model of bone regeneration was calibrated with D set to 0.01 mm^2/day, representing the midpoint of the range of diffusion constants used in a previous bioregulatory model of bone healing [185]. By way of sensitivity analysis, the computation was then repeated with D set to 0.1 and 0.001 mm^2/day. Table 3.4 shows the remaining model parameters used in the FE analysis.

Bone volume deposition rate $k \quad \dfrac{\% \left[\frac{mm^3_{bone}}{mm^3_{tissue}}\right]}{\mu strains \cdot day}$								
$1 \cdot 10^{-5}$	$1.25 \cdot 10^{-5}$	$1.50 \cdot 10^{-5}$	$1.75 \cdot 10^{-5}$	$2 \cdot 10^{-5}$	$2.25 \cdot 10^{-5}$	$2.5 \cdot 10^{-5}$	$2.75 \cdot 10^{-5}$	$3 \cdot 10^{-5}$
$3.25 \cdot 10^{-5}$	$3.50 \cdot 10^{-5}$	$3.75 \cdot 10^{-5}$	$4 \cdot 10^{-5}$	$4.25 \cdot 10^{-5}$	$4.5 \cdot 10^{-5}$	$4.75 \cdot 10^{-5}$	$5 \cdot 10^{-5}$	$5.25 \cdot 10^{-5}$
$5.50 \cdot 10^{-5}$	$5.75 \cdot 10^{-5}$	$6 \cdot 10^{-5}$	$6.25 \cdot 10^{-5}$	$6.5 \cdot 10^{-5}$	$6.75 \cdot 10^{-5}$	$7 \cdot 10^{-5}$	$7.25 \cdot 10^{-5}$	$7.50 \cdot 10^{-5}$
$7.75 \cdot 10^{-5}$	$8 \cdot 10^{-5}$	$8.25 \cdot 10^{-5}$	$8.5 \cdot 10^{-5}$	$8.75 \cdot 10^{-5}$	$9 \cdot 10^{-5}$	$9.25 \cdot 10^{-5}$	$9.5 \cdot 10^{-5}$	$9.75 \cdot 10^{-5}$
$1 \cdot 10^{-4}$	$1.25 \cdot 10^{-4}$	$1.50 \cdot 10^{-4}$	$1.75 \cdot 10^{-4}$	$2 \cdot 10^{-4}$	$2.25 \cdot 10^{-4}$	$2.5 \cdot 10^{-4}$	$2.75 \cdot 10^{-4}$	$3 \cdot 10^{-4}$
$3.25 \cdot 10^{-4}$	$3.50 \cdot 10^{-4}$	$3.75 \cdot 10^{-4}$	$4 \cdot 10^{-4}$	$4.25 \cdot 10^{-4}$	$4.5 \cdot 10^{-4}$	$4.75 \cdot 10^{-4}$	$5 \cdot 10^{-4}$	$5.25 \cdot 10^{-4}$
$5.50 \cdot 10^{-4}$	$5.75 \cdot 10^{-4}$	$6 \cdot 10^{-4}$	$6.25 \cdot 10^{-4}$	$6.5 \cdot 10^{-4}$	$6.75 \cdot 10^{-4}$	$7 \cdot 10^{-4}$	$7.25 \cdot 10^{-4}$	$7.50 \cdot 10^{-4}$
$7.75 \cdot 10^{-4}$	$8 \cdot 10^{-4}$	$8.25 \cdot 10^{-4}$	$8.5 \cdot 10^{-4}$	$8.75 \cdot 10^{-4}$	$9 \cdot 10^{-4}$	$9.25 \cdot 10^{-4}$	$9.5 \cdot 10^{-4}$	$9.75 \cdot 10^{-4}$

Reduction factor α [%]											
1	2.5	5	7.5	10	12.5	15	17.5	20	25	30	35
40	45	50	55	60	65	70	75	80	90	95	100

Table 3.3: **Range of parameters tested for fitting the *in vivo* bone ingrowth results**. The constant of bone volume deposition rate k and the reduction factor α represent the mechano-sensitivity of the organism and the reduction of the reference stimulus initiating bone formation, respectively.

Parameter	Description	Value	Unit	Ref
$\rho_{initial}$	Initial bone mineral density	0.001	$\frac{g}{cm^3}$	-
D	Diffusion constant	0.01	$\frac{mm^2}{day}$	range in [185]
m	Daily strain history parameter	4	$adim$	[63]
N	Number of loading cycles	10'000	$\frac{cycles}{day}$	[186]
$\dot{V}_{max}$	Maximum bone deposition rate	4	$\frac{\%}{day}$	adapted from [166]
ρ_{max}	Maximum bone mineral density	1.6	$\frac{g}{cm^3}$	[99]

Table 3.4: **Finite element parameters of the bone regeneration algorithm.**

3.3.6 Temporal evolution of bone ingrowth

Bone ingrowth predictions were computed at each time increment of the numerical analysis and the temporal evolution was defined for the whole period simulated (12 weeks). As for the *in vivo* data, bone ingrowth was assessed for samples located in the femoral epiphysis of all goats, while in the tibiae two scaffold were in contact with compact bone and another one was in contact with trabecular bone (3.3-B,C)). In the *in vivo* data, bone ingrowth was quantified in both groups euthanized at different timepoints (6 and 12 weeks). Numerical predictions were computed for the experimental group euthanized at week 12, and the temporal evolution of the bone ingrowth was compared to experimental data at 6 and 12 weeks.

3.3.7 Statistics

The Python programming language was used to run all the statistical analyses. Repeated measures correlation (rmcorr) was used to compare numerical predictions of bone ingrowth in each subregion to the experimental data, since the assumption of error independence between observations was violated for predictions within the same recipient [187]. The repeated measures correlation coefficient r_{rm} and its 95% confidence interval (CI) were used as measure of goodness of fit of the computational model.

3.4 Results

3.4.1 *In vivo* bone ingrowth in distal femur and proximal tibia

After 12 weeks from surgery, bone formation mostly occurred in the outer pores of the scaffold for all samples, with limited ingrowth in the core (Figure 3.8) and different distribution depending on the anatomical location. When implanted *in vivo*, scaffolds in contact with trabecular bone (Figure 3.10, green and blue scaffolds) had a homogeneous bone ingrowth distribution throughout the medullary, the middle and the periosteal subregions. Conversely, close to the tibial diaphysis bone ingrowth was substantially shifted in the periosteal subregion (Figure 3.10, orange scaffolds). Moreover, a single animal (case 1) had both the highest periosteal bone ingrowth for the scaffold in contact with compact bone and the highest mean bone ingrowth for the scaffold in contact with trabecular bone (Figure 3.10-B, left column). Bone ingrowth was also quantified in the femoral epiphysis for a different group of recipients euthanized 6 weeks after surgery. Bone ingrowths did not markedly differ at weeks 6 and 12 in any subregion (Figure 3.14).

3.4.2 *In silico* computerized tomography

Based on the normalized tissue density histogram at the end of the computational analysis, the Otsu's segmentation determined an optimal density threshold of 0.251 ± 0.068 g/cm^3 to separate two tissue types, leading to the identification of the newly formed bone in the scaffold pores (Figure 3.8-B). In addition, the apparent density of the newly formed bone after the last iteration covered the ranges of both trabecular bone ($\rho < 0.8$ g/cm^3) and the one separating trabecular from cortical bone ($0.8 < \rho < 1.2$ g/cm^3) (Figure 3.8-B) Similarly to the analysis of the *in vivo* data, medullary, middle and periosteal subregions were defined in the granulation tissue to assess bone ingrowth distribution (Figure 3.8-C,D).

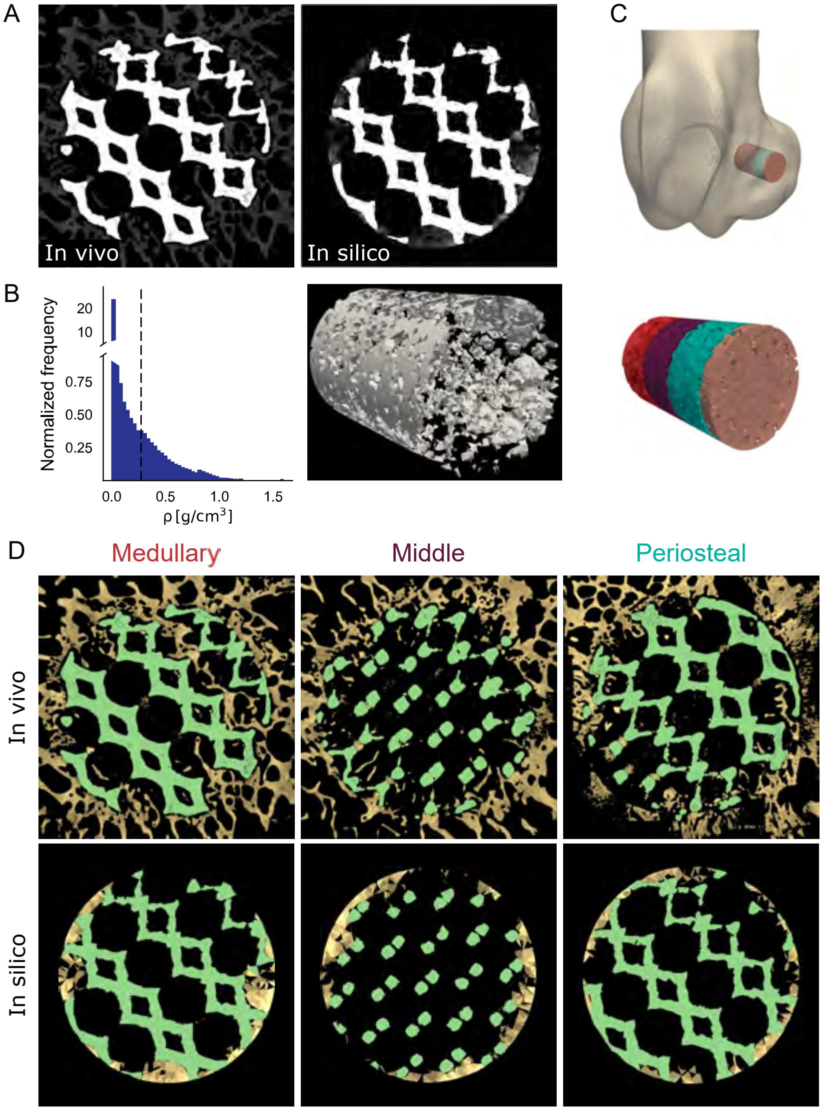

Figure 3.8: ***In silico* microCT**. (A) Representative microCT image of bone forming within the defect located in the goat femoral epiphysis (case 1) at the end of the *in vivo* experiment (12 weeks) and *in silico* microCT image of the comparable location in the computational model of bone regeneration. (B) Left - Normalized count of elements in the granulation tissue of the *in silico* model at the end of the simulation. Dash line represents the Otsu's threshold used to separated the mineralized part of the granulation domain from the not-mineralized one. (Continue next page)

Figure 3.8: (Previous page.) Right - *in silico* CT rendering of the bone ingrowth into the porous scaffold. (C) Location of the defect in the goat femoral epiphysis simulated in the *in silico* model and detail of the granulation domain (pink) with the medullary (red), middle (purple) and periosteal (light blue) subregions highlighted. (D) Representative *In vivo* and *in silico* microCT slices of the medullary, middle and periosteal subregions where bone is labeled in yellow and metal is labeled in green.

3.4.3 *In silico* predictions of bone ingrowth in distal femur and proximal tibia

The distribution of simulated mechano-driven bone ingrowth inside each scaffold correlated closely to the experimental data (r_{rm} = 0.90, 95% CI [0.72, 0.96], Supplementary Material - Figure S5). Experimental and simulated ingrowth both showed a clear dependence on the anatomical location (Figure 3.10-B), which corresponded to different distributions of the mechanical stimulus within the scaffold pores at implantation time (Figure 3.11). Compared to experimental results, the model slightly overestimated the ingrowth in the medullary region for scaffolds in contact with trabecular bone (mean ingrowth 8.74±5.74 % vs. 7.43±3.87 %, Figure 3.10-B, green and blue scaffolds).

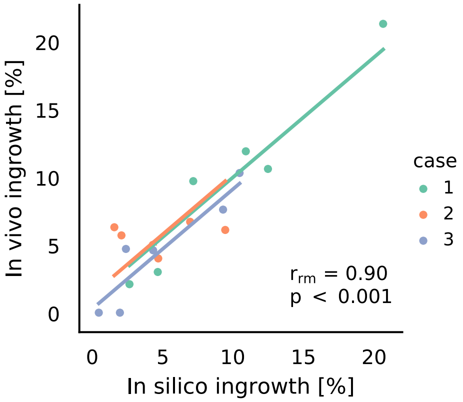

Figure 3.9: **Repeated measure correlation (rmcorr)**. Results for predicted (*in silico*) and experimental (*in vivo*) bone ingrowth data. Each dot represents bone ingrowth data in one of the medullary, middle and periosteal subregion of the scaffolds implanted in the left femurs and the tibiae of three different goats (cases). Observation from the same animal are given the same color, with lines showing the individual rmcorr.

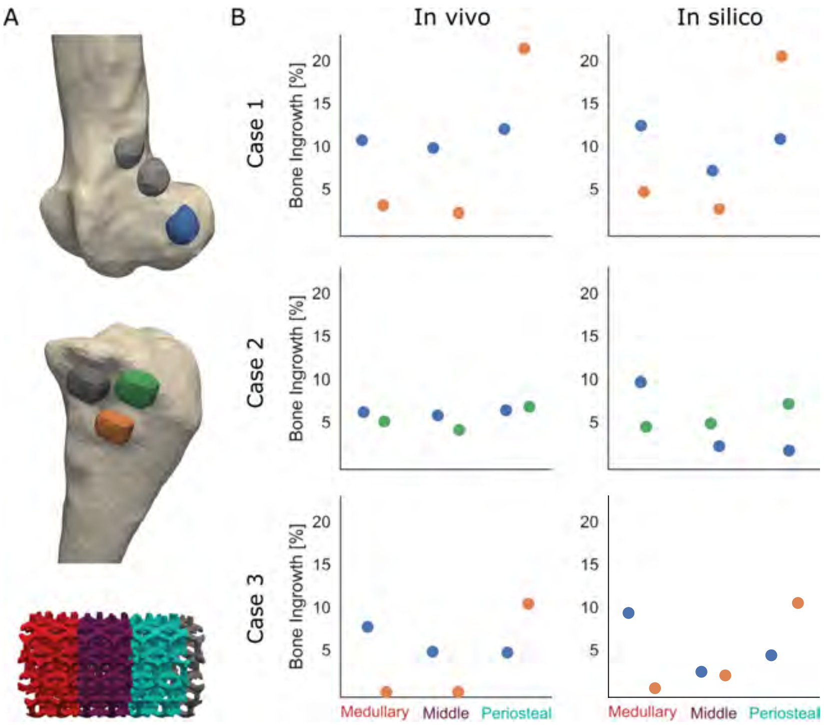

Figure 3.10: **Mechano-driven regeneration predicted bone ingrowth distribution in different scaffold locations**. Bone ingrowth was assessed in six different scaffolds inserted into the left femurs and the tibiae of three different goats (cases) after 12 weeks from implantation. (A) Representative femur and tibia models showing the epiphyseal (blue, green) and diaphyseal (orange) locations of the titanium bone scaffolds. The scaffolds were simulated with the finite element model of mechano-driven bone regeneration. Three-dimensional view of the porous titanium scaffolds (gray) with the medullary (red), middle (purple) and periosteal (light blue) subregions highlighted. (B) Bone ingrowth comparison between *in vivo* and *in silico* models.

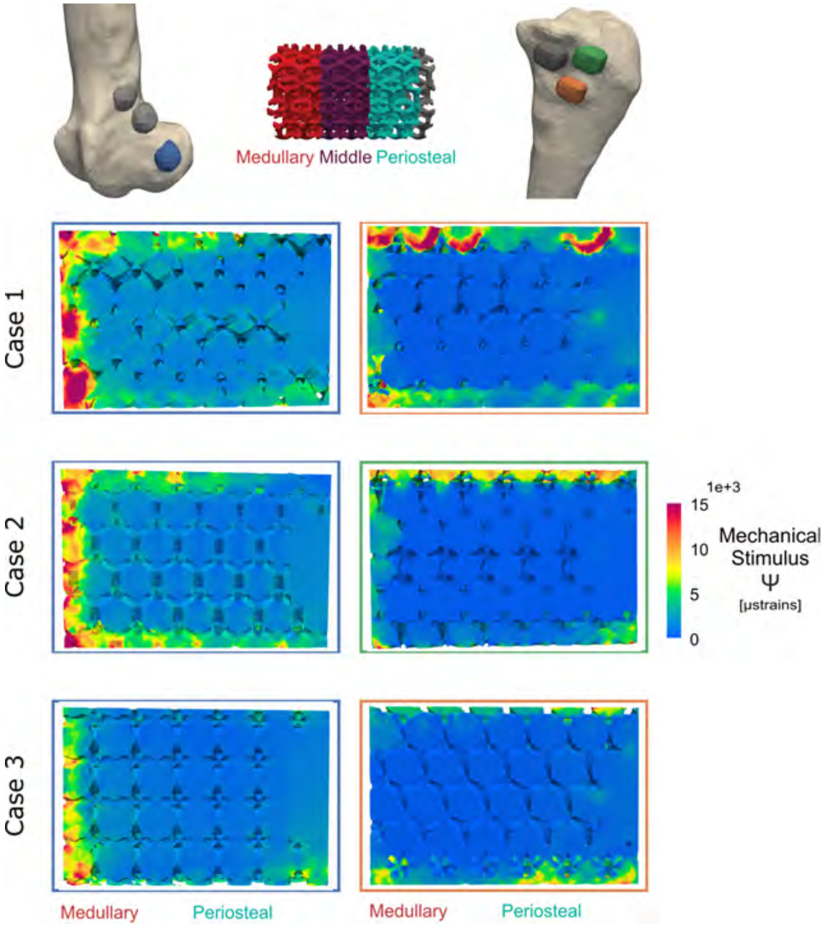

Figure 3.11: **Local mechanical environment within the bone scaffolds at implantation time.** Representative sections of the granulation domains at implantation time. Sections show the spatial distribution of the mechanical stimulus variable used in the mechano-driven model of bone regeneration (daily strain stimulus Ψ).

Scaffolds inserted close to the diaphysis consistently showed higher bone ingrowth in the periosteal subregion when tuning the individual parameters k and α (Figure 3.12) and when changing the diffusion constant D (Figure 3.13).

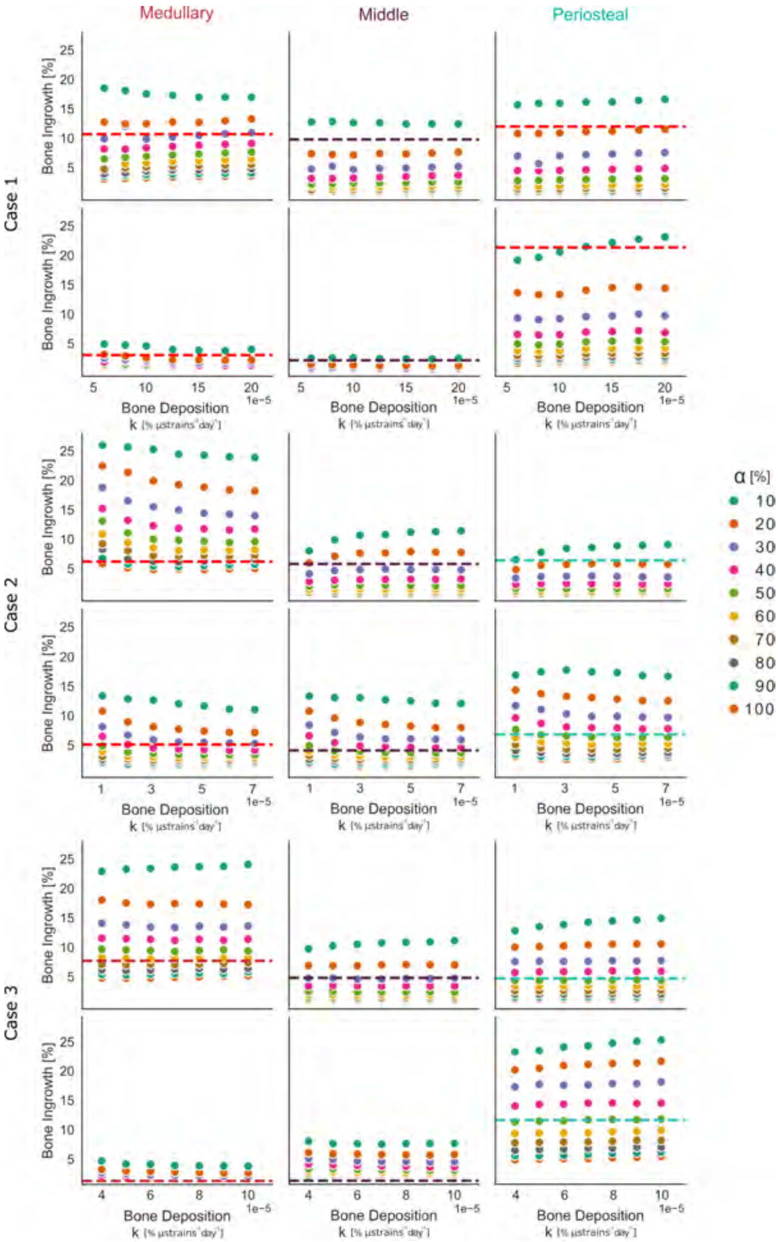

Figure 3.12: **Effect of tuning the constant of bone volume deposition *k* and the reduction factor α in the mechano-driven model of bone regeneration.** Each row shows the variability in the bone ingrowth outcome (Continue next page)

Figure 3.12: (Previous page) predicted in the medullary, middle and periosteal subregions of a porous titanium bone scaffold when tuning *k* and α within a predefined range. Six scaffolds were analyzed, two per goat (case). *In vivo* data of bone ingrowth in each subregion (dashed line in the plot) was used to estimate both *k* and α for each specific case and implantantion site. Parameters were selected based on the minimization of the residual sum of squares (RSS).

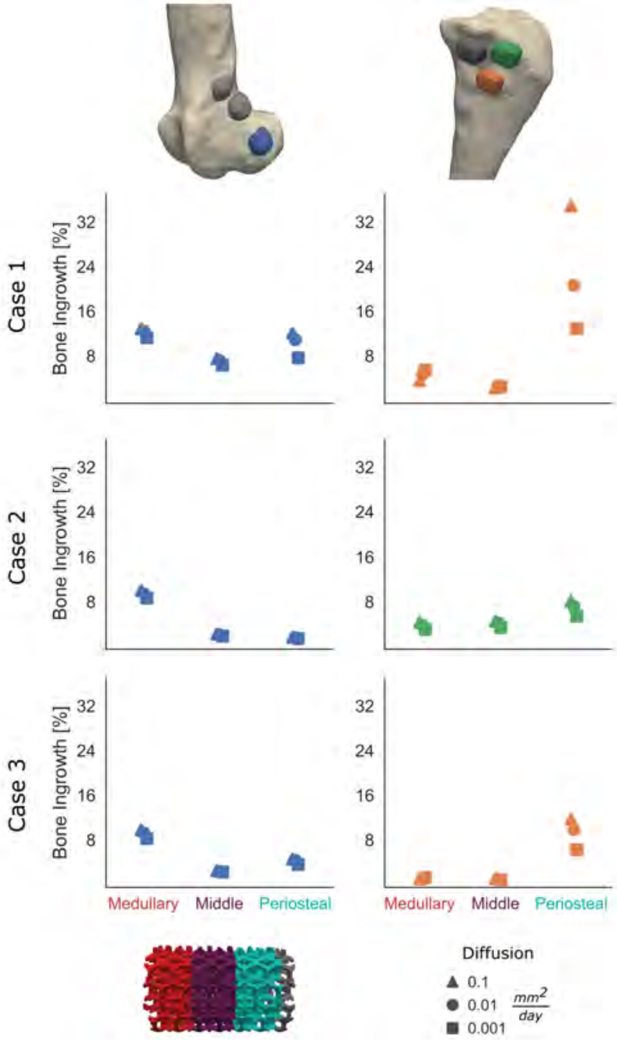

Figure 3.13: **Effect of changing the diffusion constant *D* in the mechano-driven model of bone regeneration.** Bone ingrowth was assessed in six different scaffolds inserted on the left femurs and the tibiae (Continue next page)

Figure 3.13: (Previous page) of three different goats (cases) after 12 weeks from implantation. Scaffolds were implanted in the epiphyseal (blue, green) and diaphyseal (orange) locations and bone ingrowth was quantified in the medullary (red), middle (purple) and periosteal (light blue) subregions. The mechano-driven model of bone regeneration was first calibrated while setting a cell diffusion constant D of 0.01 mm^2/day. Later, the computational analysis was repeated using a higher and a lower value of D, to covered the whole range of diffusion constants [185].

The temporal evolution of predicted bone ingrowth highlighted a sharp increase in the first 3 weeks after implantation, during which the mean apposition rate for all scaffolds was 0.37±0.28 %/day (Figure 3.14). After that, bone ingrowth in all samples exhibited a plateau in all scaffold subregions, with a slight underestimation compared to the experimental data in the middle and periosteal subregions. Bone ingrowth was mostly observed in the outer pores of the scaffolds, while it was limited in the scaffold core (Figure 3.15).

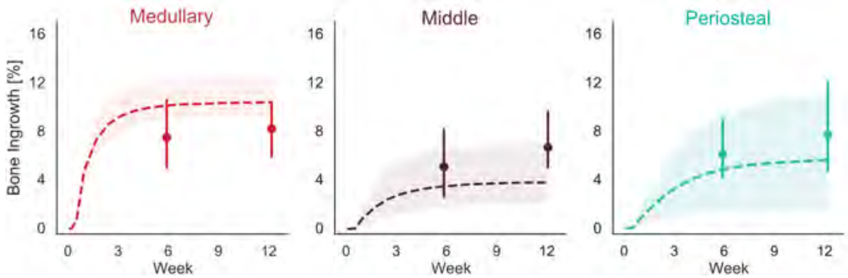

Figure 3.14: **The temporal evolution of bone ingrowth in porous titanium scaffolds revealed limited increase in bone ingrowth after 3 weeks from implantation**. Temporal evolution of the bone ingrowth in the medullary, middle and periosteal regions of titanium porous scaffolds inserted in the femoral epiphysis of goat animal models. Comparison between *in silico* (dashes) and *in vivo* (points) results. Point plots and dashed lines denote the mean of n=3 samples, with error bars and error bands representing 95% of confidence interval.

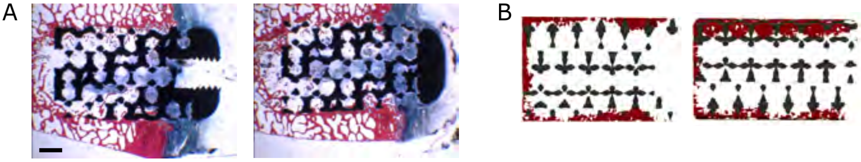

Figure 3.15: **Novel formation of bone tissue in the outer scaffold pores**. (A) Representative histological images and (B) numerical predictions showed bone tissue formation within the scaffold pores after 12 weeks from surgery. Both *in vivo* and *in silico* data reported limited bone ingrowth in the scaffold core. Scale bar, 20mm.

3.4.4 Individual and local biomechanical demands

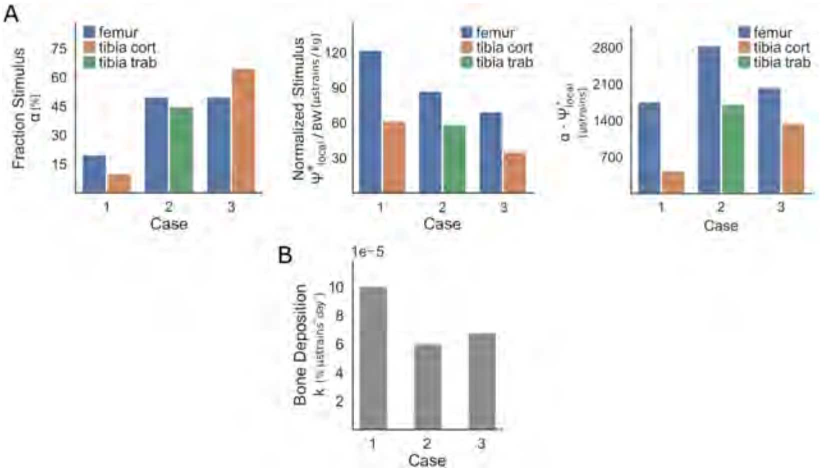

Figure 3.16: **Individual model parameters identified a stronger responder to mechanical stimulation and a mechanical stimulus initiating bone formation that varied among different implantation sites**. Individual parameters of the mechano-driven model of bone regeneration applied to the three case studied. (A) Location-specific parameters. The local reference stimulus Ψ^*_{local} was normalized by the body weight (BW) of each animal. Together with the reduction factor α, they were location-dependent and denoted the biomechanical demand of the peri-implant environment, while $\alpha \cdot \Psi^*_{local}$ defined the mechanical stimulus triggering bone formation. (B) Subject-specific parameter. The constant of bone volume deposition *k* denoted the subject's mechano-regulatory potential.

By fitting experimental results, the *in silico* model estimated a constant of bone volume deposition rate k in the range of [6, 10] 10^{-5} %· μstrains^{-1} ·day^{-1}, where the highest constant corresponded to the recipient reporting the highest bone ingrowths in both the femoral epiphysis and the tibial diaphysis (case 1, Figure 3.16-B). Moreover, the local reference stimulus Ψ^*_{local} ranged from 35 to 120 μstrains/kg, depending on the implantation site and the animal. It was consistently higher in the femur than in the tibia for all three cases simulated, with higher magnitudes corresponding to higher body weights (Figure 3.16). As for the reduction factor α, the model identified comparable values for different scaffold locations within each recipient. It ranged from 45 % to 65 % for both femoral and tibial locations of cases 2 and 3, while it was 20 % and 10 % for the femoral and tibial location of case 1, respectively (Figure 3.16-A). As a result, the mechanical stimulus triggering bone formation, which was the product of Ψ^*_{local} and α, had the opposite trend of the constant of bone ingrowth k: bone formation was triggered at lower values of mechanical stimulus in recipients with higher k (Figure 3.16-A).

3.5 Discussion

3.5.1 Mechano-driven regeneration predicts bone ingrowth distribution

The *in silico* model presented here revealed that a regenerative process purely based on mechanical stimulation predicts the bone ingrowth distributions, penetration depths as well as the bone formation dynamics observed *in vivo* when porous titanium bone scaffolds were implanted in different recipients and implantation sites. The model outcome indicated different mechanical states when the same scaffold architecture was implanted in the diaphyseal or in the epiphyseal location (Figure 3.11).

Compared to *in vivo* data, medullary bone formation in the epiphyseal subregion was slightly higher whereas middle and periosteal bone formation in the same location were lower, which might be related to a wider surface in direct contact with bone tissue and aspirate bone marrow for the medullary subregion. The higher (but not significant) mean bone ingrowth was also observed *in vivo* both at 6 and 12 weeks in the medullary region (Figure 3.14). Therefore, the computational model predicted both the *in vivo* trends of slightly higher bone ingrowth in the medullary subregion for the epiphyseal location and the significantly higher bone ingrowth in the periosteal subregion for the diaphyseal location.

The two different mechanical environments of the epiphyseal and diaphyseal implantation sites are the result of the adaptation of long bones. Indeed, on the one hand diaphysis adapted to bending and some torsional loadings [188]. On the other hand, the presence of cancellous bone confers epiphyses a shock absorbing function, homogeneously distributing their load throughout their volume [155].

These results suggest that different biomechanical demands on the epiphyseal and the diaphyseal locations of a long bone induce distinctive bone ingrowth distributions for the same scaffold microarchitecture. The use of the *in silico* approach revealed the regulatory role of the mechanical environment on the scaffold performance.

3.5.2 Mechanics limits complete bone formation within the scaffold pores

The use of an automatic algorithm to segment the bone tissue in the granulation domain resembled the common procedure applied with *in vivo* samples (Figure 3.8). Bone density thresholds in the *in silico* results were around 0.25 g/cm^3, which is comparable to the lower range of apparent density in trabecular bone specimens

[99]. By applying the same automatic thresholding technique, the computational model reached threshold values similar to the *in vivo* cases, strengthening the use of such mechano-regulatory theory to capture the dynamics of bone formation within the scaffold pores. Moreover, the mean bone volume deposition rate in the first three weeks after implantation was 0.37 %/day, corresponding to a bone apposition rate of 3.7 µm/day for a bone surface of 1 mm^2. Such a bone apposition rate is comparable to the one of 1-2 µm/day observed in osteoids [189].

The analysis of the temporal evolution of bone ingrowth suggested that further deposition was not expected within the scaffolds pores. As bone started forming, the increase in the material properties led to a steady decrease of the mechanical stimulus, thus a reduction in the bone apposition rate. Mechanical stimulation in the scaffold core never reached the threshold value initiating bone formation, which suggests that the scaffold core was mechanically shielded by the newly forming bone in the outer pores. Thus, bone ingrowth was limited to the outer pores of the scaffold (Figure 3.15). Once mechanical stimulation was also lower than the reference value in the outer pores, new bone tissue formation stopped entirely. *In silico* predictions estimated that the bone ingrowth plateau started 3 weeks after implantation, which might explain the similar values of *in vivo* bone ingrowth at 6 and 12 weeks (Figure 3.14). Similarly, Chen et al. reported increasing mean bone ingrowth for porous titanium in ovine model up to 4 weeks. After 4 weeks, bone ingrowth did not increase until the last timepoint of the study (12 weeks) [190].

In general, the use of computational modeling in this study was essential for revealing information about the dynamic interaction between scaffold and host. Investigating the temporal evolution of bone ingrowth *in vivo* is expensive and has ethical concerns since it requires different animals for each timepoint, while the *in silico* model has no such concerns. Moreover, it provided a mechanical explanation of the limited bone penetration depth and the plateauing of bone ingrowth. Even though the model was only fit to results from the end of each experiment, it was still able to predict the limited bone ingrowth gain from the earlier timepoint.

3.5.3 Subject- and location-specific parameters model host mechano-response

Fitting experimental results is not only a successful strategy to calibrate an *in silico* model but, more importantly, it is decisive in extracting physiologically relevant information from the numerical analysis.

The parameter of bone volume deposition rate k represents the host capacity to form novel bone tissue based on mechanical stimulation. In the present model the identification of the optimal parameters for each simulation led to similar values of k for cases 2 and 3, while a higher value of k was found for case 1 (Figure 3.16-B). Correspondingly, case 1 reported the highest absolute bone ingrowths in both the femur and the tibia (Figure 3.10-B). The higher regenerative potential of this subject was captured by the *in silico* model, both in terms of total bone ingrowth and mechanosensitivity.

The model consistently showed higher local surrounding stimulus Ψ^*_{local} for the femoral location in all cases studied, suggesting that the stimulus triggering bone ingrowth in the femur was higher compared to the tibia. Bone adaptation to a local mechanical state might take into account that bone cells adapt to each characteristic state. Results presented here are consistent with the finding that instead of a single value throughout the skeleton, the minimum effective strain threshold is expected to vary locally depending on the loading environment, which defines the local biomechanical demand [157].

Best fits of the *in silico* model were obtained for values of the reduction factor of the reference stimulus α around 50 % for cases 2 and 3, while its value was below 20% for case 1 (Figure 3.10-B). From a biological perspective, the model suggested that bone formation within the scaffold pores was triggered by a fraction of the mechanical stimulus in the surrounding tissue. An earlier study combining *in vivo* experimental data with a FE analysis of the local tissue mechanics, confirmed the alteration of the remodeling rules around a titanium implant. The authors reported bone started to form for mechanical stimuli 66% lower than those observed far from the implant [64].

Variability in the mechano-regulatory capacity of each subject depends on multiple factors, such as aging [87] or physical exercise [191]. More in general, the inherent variation between patients deeply affects the clinical outcome of regenerative products [86]. This source of variability is normally underestimated in preclinical models, where typically a small number of young, healthy animals are studied. The same issue arises with *in silico* models, which are commonly calibrated on single or ideal subjects [192].

The present study provides a mechanical interpretation of the response variability between individual recipients. By modeling the host mechanical response with a subject and a location specific parameter, bone formation within porous scaffolds was predicted, showing that the scaffold osteointegration cannot depend on its mechanical properties alone.

3.5.4 The mechanobiological potential of the host-scaffold unit

Taken together, results indicate the essential role of host mechanical environment and mechano-sensitivity in the process of bone ingrowth into a porous bone scaffold. Scaffolds with the same microarchitecture exhibited different bone ingrowth patterns when inserted in a diaphyseal or in epiphyseal location, which was associated with a diverse mechanical demand of the local environment. Interestingly, the *in silico* model facilitated determining a host-specific mechano-sensitivity, whose effects led to different bone ingrowth outcomes between recipients even though the scaffold was implanted at identical locations. The use of a mechano-based model also revealed specific aspects of the bone ingrowth dynamics, showing for instance that most of the increase in bone ingrowth occurred within the first 6 weeks after implantation. Similarly to the concept of the bone-healing unit, which produces a dynamic physiological response based on its biological and mechanical environment [193], the mechanical factor in the bone regeneration process depends on the dynamic interaction between the scaffold and the host mechanical environment, which combines the local tissue strain with anatomical location-dependent habitual strain levels and host-dependent strain sensitivity. Therefore, from a mechanical perspective, the combination of host and scaffold defines a mechanobiological unit contributing to the final scaffold regenerative potential.

Modeling the host response to the implantation of an additively manufactured porous material has direct implications on its design. Current patient-specific implants mainly aim to provide a tailored geometry and often include a porous metallic surface to improve their osteointegration, but they do not vary the mechanical properties of the porous surface depending on the specific implant location or the host regenerative potential. Scaffolds with lower apparent modulus enhance bone regeneration, although they must be stiff enough to ensure strength against mechanical failure [144]. Translated to the *in vivo* study analyzed, it is likely that a scaffold with a lower apparent modulus in the core would have improved bone formation (Figure 3.15). In search of an optimal apparent modulus, degradable biomaterials or scaffolds with stiffness gradients are two potential approaches to reduce the scaffold apparent modulus and improve its mechanobiological performance. On the one hand, degradable scaffolds reduce mechanical properties over time [194], thus they gradually increase the strain throughout the scaffold pores. On the other hand, scaffold architecture can be finely tuned [195] to maximize both bone regeneration and scaffold stability, for example by designing lower apparent modulus where the bone tissue is likely to be formed while keeping the apparent modulus higher where bone formation is unlikely to happen. However, patients with lower response to mechanical stimulation might be insensitive to stiffness gradients and would probably need nondegradable scaffolds [89]. Therefore, a subject-specific model of mechano-driven bone regeneration could identify which patients benefit from a degradable scaffold or from a scaffold with a stiffness gradient or from a combination of both.

From a pragmatic perspective, the definition of the local biomechanical demand could rely on patient-specifc models comprising bone mechanical properties, kinematic data and musculoskeletal load [196], while the clinical assessment of the individual mechano-sensitivity still requires further investigation. For example, the influence of the genome on bone mechano-responsiveness, already reported for inbred strains of mice [197], suggests that genetic diversity among patients might be associated to their individual mechano-sensitivity [198]. In addition, estrogen deficiency is another factor that impairs the bone cell mechano-sensation [199, 200]. Therefore, mechano-sensitivity in computational models of mechano-driven bone regeneration might be correlated to the circulating estrogen levels, which are lower for female postmenopausal patients. Overall, the definition of a mechanobiologically-based approach, including individual estimates of the local biomechanical demand and mechano-sensitivity, would get closer to the specific needs of each recipient and facilitate endogenous bone formation.

3.5.5 Limitations

The use of FE methods is a well established procedure to define the bone mechanical state in different applications [201, 174, 202]. However, the mechano-driven model of bone regeneration used some assumptions that should be justified in line with the final conclusions here obtained.

Firstly, although the total forces applied on both the femurs and the tibiae were measured at the knee joint of ovine models, the distribution of mechanical loads over the femoral or tibial surfaces relied on a musculoskeletal model of a human knee while squatting. This chioce was motivated by the absence of studies reporting the distribution of loading over the medial and lateral condyles in the knee joint for ovine animals during a gait analysis, and a model of the human knee was used because of its similarity to the ovine knee joint. Moreover, the present study considered mechanical loads proportional to the recipient body weight, while the loading history was assumed to be the same for all individuals. Nonetheless, activity levels following experimental interventions may vary between individuals [88]. Thus, future mechano-driven models of bone regeneration should include experimental *in vivo* studies tracking movement and activity for each subject.

Secondly, the regeneration model assumes that bone is the only tissue that could form within the scaffold pores. When micromotion occurs at the bone-scaffold interface, fibrous tissue could form and impair osteointegration [203]. However, at the start of the animal experiment, scaffolds were inserted through press-fitting, limiting micromotion at the bone-scaffold interface. Therefore, fibrous tissue formation was neglected in this study, although micromotion and eventual fibrous tissue formation should be modeled when the mechanical stability of the bone-scaffold interface is not guaranteed [204]. As for the properties of the newly formed bone tissue, the hierarchical structure of the tissue was replaced by a homogeneous material with equivalent linear elastic properties [63]. In addition, the model assumed that fully developed bone tissue is formed after deposition [63]. As a result, the model did not include any analysis of the bone histomorphometry, although the efficacy of bone scaffolds is directly related to the quality of the newly formed bone. Differences in the apposition of mature lamellar bone have been recently reported for compliant and stiffer scaffolds, but variations in the final bone quality (e.g. woven-to-lamellar bone transition) corresponded to differences in the mechanical properties and final bone ingrowth [89]. Therefore, the model presented here cannot predict the histomorphometry of the regenerated bone tissue, but it can compare the global regenerative performance of different bone scaffolds for a patient-specific application, as well as the global performance of the same scaffold for different implantation sites.

Thirdly, the present model neither includes the initial cascade of immune events following implantation [169] nor the effect of precise bioregulatory factors on bone regeneration. Factors as the level of oxygen tension and angiogenesis can be more determinant to the osteogenic or chondrogenic differentiation of mesenchymal stem cells (MSCs) than mechanical stimulation [205]. In view of predicting progenitor cell fate, *in silico* models implementing bioregulatory factors have been extensively applied in the field of bone regeneration, with a strong focus on bone fracture healing processes [206, 131]. However, the objective of this study was to isolate the mechanobiological problem of bone ingrowth into a porous scaffold and evaluate the influence of both the scaffold and the recipient. By reducing the cellular invasion process to a diffusion process coupled to mechano-driven regeneration, it was defined a simplified system compared to the real conditions, but with the unique advantage of revealing the importance of mechanical stimuli in bone regeneration, which provided a biophysical interpretation of the results presented here.

Furthermore, one additional limitation regards the *in vivo* data used to calibrate the model. The animal study was not designed to address the objectives of this work, thus relevant data that could strengthen the model calibration was never collected, such as CT scans of animals euthanized 6 weeks after surgery or a larger number of samples and locations where bone ingrowth was assessed. On the one hand, to demonstrate an absolute relationship between mechanical stimulus and bone ingrowth distribution, scaffolds should have been tested in the same implantation site while undergoing different loading conditions. On the other hand, only recent *in vivo* studies highlighted the importance of the local biomechanical demand and the individual response for bone regeneration [89], as well as the role of bone mechanobiology in the maximization of bone ingrowth. The different bone ingrowth patterns observed *in vivo* for the same scaffold architecture suggest that mechanics plays a key role in determining the final outcome, and the different magnitudes reported for each recipient support the hypothesis of inter-subject variability. Thus, these results call for new investigations on the *in vivo* impact of mechanobiologically-optimized scaffolds. Designing concomitant *in vivo* and *in silico* studies is the most successful strategy to maximise the clinical impact of such an optimization process.

3.6 Conclusions

Mechanical stimulus is intrinsically associated with the regenerative response to bone scaffolds in terms of bone formation. Successful application of a specific graft therefore requires a better understanding of the local mechanical microenvironment. The mechanical interaction between the scaffold and the subject relies on the local environment and the host response, in terms of both the distribution and the amount of newly formed bone within the scaffold. Using computational methods, it was demonstrated that different implantation sites cause different mechanical conditions and induce distinctive patterns of bone ingrowth distribution, while the dynamics of mechanical stimulus limited bone penetration depth within the scaffold. The model calibration against *in vivo* data revealed a stronger responder between the recipients as well as different mechanical stimuli initiating bone formation in the femur and in the tibia. The scaffold and the host defined a mechanobiological unit, whose dynamic state controlled the bone ingrowth process and the scaffold regeneration potential. From a clinical perspective, modeling the host mechanical response provides a mechanobiologically-based approach to meet both subject- and location-specific needs by tuning scaffold mechanical properties.

Code availability

The Python modules developed to pre- and post-process ABAQUS simulations are available under github.com/gabnasello/fempy and github.com/gabnasello/odbhelper.

Chapter 4

Bone-on-chip systems model the individual osteogenic potential [1]

4.1 Abstract

Microengineered systems provide an *in vitro* strategy to explore the variability of individual patient response to tissue engineering products, since they prefer the use of primary cell sources representing the phenotype variability. Traditional *in vitro* systems already showed that primary human osteoblasts embedded in a 3D fibrous collagen matrix differentiate into osteocytes under specific conditions. Here, it was hypothesized that translating this environment to the organ-on-a-chip scale creates a minimal functional unit to recapitulate osteoblast maturation towards osteocytes and matrix mineralization. Primary human osteoblasts were seeded in a type I collagen hydrogel, to establish the role of lower ($2.5 \cdot 10^5$ cells/ml) and higher ($1 \cdot 10^6$ cells/ml) cell density on their differentiation into osteocytes. A custom semi-automatic image analysis software was used to extract quantitative data on cellular morphology from brightfield images. The results are showing that cells cultured at a high density increase dendrite length over time, stop proliferating, exhibit dendritic morphology, upregulate ALP activity and express the osteocyte marker DMP1. On the contrary, cells cultured at lower density proliferate over time, do not upregulate ALP and express the osteoblast marker BSP2 at all timepoints.

---

[1] This chapter is a modified version of [207] published open access in *Frontiers in Bionengineering and Biotechnology*.

This work reveals that microengineered systems create unique conditions to capture the major aspects of osteoblast differentiation into osteocytes with a limited number of cells. It is propose that the microengineered approach is a functional strategy to create a patient-specific bone tissue model and investigate the individual osteogenic potential of the patient bone cells.

4.2 Introduction

Osteoblasts experience marked transitional stages during bone formation, involving changes in cell morphology and gene expression. Osteoblasts express ALP to provide phosphate ions and initiate the mineralization process [208]. They also secrete osteocalcin (OCN), bone sialoprotein 2 (BSP2) and osteopontin (OPN) until the end of the mineralization phase [45]. When osteoblasts turn to a more mature phenotype, they reduce ALP expression, become embedded in a mineralized matrix and form an interconnected network of osteocytes [209]. During this transition, osteoblasts upregulate characteristic proteins as E11 and dentin matrix protein 1 (DMP1) [210]. The expression of sclerostin (Sost gene) is associated with the final stage of osteocyte differentiation [48, 211].

However, osteoblasts can have three other possible fates but the mechanism regulating this transition is not clearly understood yet: they can become bone-lining cells (inactive osteoblasts), undergo apoptosis, or transdifferentiate into chondroid-depositing cells [212]. Gene expression profiles [209, 111] and immunohistochemistry stainings [213, 214, 215] in traditional 3D culture systems showed that the expression of osteoblast and osteocyte markers *in vitro* corresponded to the *in vivo* expression at the same differentiation stages [45]. In this context, *in vitro* bone tissue models are a prerequisite tool for answering specific questions of cell biology, where minimal platforms are mandatory for effective research on human tissue function [216, 217, 218].

While traditional tissue engineering aims to recapitulate whole organs *in vitro*, organ-on-chip systems "combines the key features of specific tissue microenvironments and architecture within a microfabricated device, facilitating the creation of 3D models that exhibit functional hallmarks of native tissues" [90]. They provide minimal units mimicking specific features of living organs and human physiology, as the tissue barrier properties of the human gut and lung, the parenchymal function of cardiac and hepatic tissue, the multiorgan interactions between the lymph node and the skin [90, 219, 101, 220].

Bone models on a chip were developed in recent years to reveal different elements of bone biology, each one based on a critical advantage of microengineered devices over traditional 2D or 3D macroscale *in vitro* systems. For example, the use of optically transparent materials allowed the monitoring of osteoblast motility in a confined 3D environment [124]. The results of this study elucidated the effect of ECM degradation and its architecture on osteoblast migration, by applying growth factor gradients or interstitial fluid flow [123]. Moreover, the culture chamber geometries facilitate the reproduction of 3D organ-level structures. Microengineered devices highlighted how a 3D microvasculature integrates with the mineralized bone tissue microenvironment and enhances osteogenic differentiation of cells in the surrounding tissue construct [129, 221]. Organ function relies on the presence of biomechanical and biochemical stimuli. Mechanical, electrical and chemical stimuli can simultaneously stimulate cells cultured in organ-on-chip systems [90]. The use of compartmentalized culture environments promotes the selective application of those stimuli to different cell types. A 2D microfluidic platform with osteoclasts and osteocytes cultured in separate compartments was key to observe the cross-talk between mechanically stimulated osteocytes, osteoclast precursors and unstimulated osteocytes [222, 110].

Microfabrication techniques applied to cell biology aims to develop advanced human disease models by the inclusion of pathological factors. For example, organ-on-a-chip systems with an *ex vivo* decellularized bone matrix or an osteo-cell conditioned extracellular matrix (ECM) have recreated the interplay between cancer and endothelial cells with the bone matrix in metastatic colonization [223, 118]. Such systems consisted of a bone-like microenvironment including a monolayer of endothelial cells, which provided the capacity to obtain quantitative data on the extravasation of breast cancer cells. They were proposed as an advanced model to screen novel organ-specific therapeutics, since the osteo-cell conditioned microenvironment secreted specific chemokines affecting the extravasation process [118].

Osteocytes are the central regulators of bone homeostasis *in vivo*. Their regulatory activity on both processes of bone formation and resorption relies on the secretion of specific proteins to interact with osteoblasts and osteoclasts [48]. Mature osteocytes are the only bone cells expressing sclerostin after matrix mineralization, which suppresses osteoblast activity and inhibits further bone formation [224]. On the other hand, RANKL is a cytokine that controls osteoclastogenesis and has an fundamental role in bone remodelling. The expression of RANKL by osteocytes is ten times higher than by osteoblasts in normal mice and its specific deletion in osteocytes induces osteopetrosis [55]. The effect of osteocyte activities to other bone cells is a vital function that requires advanced *in vitro* models to be investigated.

Traditional *in vitro* cultures replicated essential features of the interaction between osteoblasts and osteocytes, such as osteoblast maturation and matrix mineralization. These systems consisted of 3D collagen hydrogels/sponges and human osteoblast-like cells [225, 226, 227] or mouse clonal cell-lines (MC3T3-E1 and IDG-SW3)

[214, 228], with the last ones usually preferred due to the excessive number of cells required. On a micro-scale, a 2D layer of MC3T3-E1 cells spontaneously formed a mineralized collagenous matrix in long-term cultures (up to 1 month) [113]. Cells were mainly present in the apical and basal layers of the matrix, possibly due to excessive proliferation of the mouse cell-line. No previous bone-on-a-chip device has differentiated primary human osteoblasts into osteocytes while embedded in a 3D extracellular matrix. There is a need for a novel microengineered model to explore the interaction between the two cell types.

Microfabricated platforms facilitate the use of cells derived from patients, thus creating models of human physiology with higher clinical impact. Primary and mature human cells are difficult to extract in large amounts, proliferate slowly and tend to dedifferentiate rapidly. Those systems require a limited amount of cells and aim to recreate the native microenvironment: they provide an approach to culture cells representing the variability of the cell phenotype [90]. This is a key advantage of the organ-on-a-chip over traditional technologies, considering the growing concern about the use of immortalized cell-lines for reliable human models [229]. Cell-lines could lead to different results with respect to primary cells from the same species. For example, murine early osteocyte cell-line MLO-A5 created an interconnected 3D network in a microfluidic perfusion device [230] but produced a highly mineralized and dense tissue compared to primary murine bone cells [215].

A bone-on-a-chip device was developed to translate the findings of traditional macro-models on differentiated osteocyte networks to the scale of micro-devices. It was hypothesized that the combination of primary human cells and a 3D fibrous collagen matrix in a microengineered platform creates a more robust model to recapitulate osteoblast maturation towards osteocytes and matrix mineralization. Such 3D cell culture system consisted of the structural and the biochemical microenvironment to induce 1) the mineralization of a collagen matrix and 2) the differentiation of primary human osteoblasts into osteocytes. The specific aims were to determine the osteogenic behavior of osteoblasts embedded in a collagen type I hydrogel in terms of: 1) cellular morphology, 2) dendrite tracking, 3) cell proliferation, 4) ALP activity, 5) calcium deposition and 6) synthesis of specific osteoblasts and osteocytes markers, respectively, BSP2 and DMP1, as well as the role of cell density in the formation of a bone tissue model.

4.3 Materials and methods

4.3.1 Cell culture

The low quantity needed for bone-on-a-chip experiments and the stability in the expression of the most critical genes during *in vitro* culture [111] favoured the choice of primary human osteoblasts (HOBs) for the bone tissue model presented in this study. HOBs were purchased from PromoCell (C-12720, Germany). These cells are fully differentiated osteoblasts isolated from femoral trabecular bone tissue from the knee or the hip joint region of healthy single donor. HOBs from two different donors were used (donor 1: caucasian female 86 years, donor 2: caucasian male 74 years). Cells were cultured under standard conditions (5% CO_2, 37°C), in cell expansion medium containing standard DMEM low glucose (Thermo Fisher Scientific, MA) supplemented with 10% FBS (Thermo Fisher Scientific), 100 U/mL penicillin, 100 µg/mL streptomycin and 2 mM L-glutamine (all Lonza, Switzerland). At each passage, cells were washed with PBS (Lonza), detached with TrypLE^{TM} Express (Invitrogen, CA) and plated in T25 cell culture flasks (Thermo Fisher Scientific) at a density of 15,000 cells/cm^2. Cells were used at passage 4-7 and mixed to the collagen gel solution. Final cell densities of $2.5\cdot10^5$ (low) and $1\cdot10^6$ cells/ml (high) were based on recent findings on osteocyte differentiation in traditional *in vitro* systems [214].

Once loaded to the organ-on-a-chip devices, HOBs were cultured under static conditions in cell osteogenic medium, containing cell expansion medium supplemented with 50 µM ascorbic acid and 10 mM β-glycerol phosphate (both Sigma-Aldrich). Those supplements are widely accepted to induce osteogenic differentiation of stem cells *in vitro* and deposition of mineralized extracellular matrix [231].

4.3.2 Bone-on-a-chip system

Bone-on-a-chip devices were fabricated in poly(dimethlysiloxane) (PDMS) by soft lithography, following the methodology described by Shin et al. [102]. A commercial product was used to produce the silicone elastomer (Sylgard 184 Silicone Elastomer Kit, Dow Chemical, Germany), which comprises a polymeric base and a silicone resin solution as curing agent. The two liquid parts were mixed in a 10 (base) :1 (curing agent) ratio and poured in a master made of SU-8 where the microengineered geometry was patterned with a photolithography technique. The masters were then placed in a vacuum desiccator for one hour, to remove air bubbles in the PDMS solution, and kept in a dry oven overnight to cure the mixture. Later, dermal biopsy punches were used to create the reservoirs for cell culture media and the hydrogel

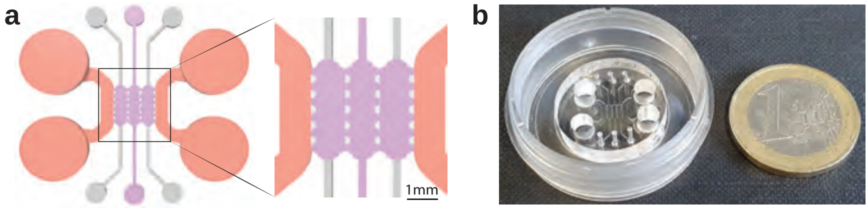

Figure 4.1: **Geometry of the bone-on-a-chip system.** (A) 2D top view of the bone-on-a-chip system and detail of the culture chamber divided into three compartments by trapezoidal columns. The cell laden collagen hydrogels (purple) were loaded through the central compartment, while cell culture media (pink) was provided through the lateral channels. The height of the culture chamber is 290 ± 20 µm. (B) Picture of the bone-on-a-chip system bonded to a 35 mm glass.

inlets to the culture chamber (Figure 4.1-A). PDMS devices followed a wet and a dry autoclave cycle before being bonded to a 35 mm glass (Ibidi, Germany) by plasma treatment (PDC-32G Basic Plasma Cleaner, Harrick Plasma, NY, USA) under vacuum conditions. They were then coated with PDL (poly-D-lysine; 1 mg/ml in phosphate buffered saline; Sigma-Aldrich, Germany) and washed after 4 hours to enhance matrix adhesion. Before use, the devices were left in a dry oven at 80ºC for 48 hours to restore the hydrophobicity of the bonded surfaces [102].

A previously developed geometry that consists of a central culture chamber divided into three compartments was selected for this study [232]. Briefly, the length of a single compartment was 2.5 mm, the width was 1.145 mm and the average height was 290 µm (Figure 4.1-A). The chip uses equally spaced (175 µm) trapezoidal columns to separate the compartments and support the hydrogel via surface tension: gel contraction occurs only on the lateral channels while the 3D culture environment is maintained in the central channel during the whole experiment.

Cell laden collagen hydrogels, with a final collagen concentration of 6 mg/ml, were prepared by mixing in an ice bath collagen type I solution (Rat Tail; 8.9 mg/ml; Corning, NY), 10x Dulbecco's phosphate buffered saline (DPBS; Sigma-Aldrich), 0.5 M NaOH (Sigma-Aldrich) to adjust the pH to 7.4-7.6 and human osteoblasts suspended in cell expansion medium. After gently pipetting the solution into the culture chamber, it polymerized for 20 minutes in a humid chamber at 37°C. This temperature and the pH conditions induced a self-assembled gelation process of the collagen hydrogels, where collagen fibers are physically crosslinked [233]. During the polymerization process, collagen fibers create an interpenetrating polymer network in presence of living cells [234]. The microarchitecture and the mechanical properties of the collagen fibrous hydrogels used in this study were characterized in previous studies [235, 123]. In the present work, it was selected the 6 mg/ml gel because its Young modulus ($\sim$0.72 kPa, from [236]) was comparable to the one ($\sim$0.58 kPa) that allowed a homogeneous cell distribution in a 3D matrix and enhanced osteocytic differentiation of MC3T3-E1 cells [214].

4.3.3 Fluorescence staining

Morphological analysis of cell phenotype is commonly used to assess osteoblast-osteocyte differentiation [237]. Cells were fixed after 21 days of culture using 4% (w/v) paraformaldehyde (PFA, Thermo Fisher Scientific) for 30 min, blocked overnight in PBS with 5% bovine serum albumin (BSA) and incubated overnight with Phalloidin-Tetramethylrhodamine (Phalloidin-TRITC, 0.1 mg/ml in PBS, Sigma Aldrich) and DAPI (4',6-Diamidino-2-Phenylindole, 0.01 mg/ml in PBS, Invitrogen). Samples were observed with a confocal microscope (Zeiss LSM880, Zeiss, Germany). Maximum intensity and 3D volumetric images were generated from z-stacks using ImageJ software (v 1.49, NIH).

4.3.4 Cell dendrite tracking

Brightfield images of the same samples were taken to track changes in dendrite morphology. Devices were observed at 10x and 20x magnification over the 21 days of culture with an inverted brightfield microscope (Nikon D-Eclipse C1, Japan) and focused in the middle of the culture chamber. Z-stacks were obtained with a distance of 5 µm between each slice and for a maximum thickness of 100 µm. A minimum number of 3 stacks were taken for each cell density at each timepoint. A custom semi-automatic image analysis software was developed with Python programming language to track cell dendrite length over time. Original z-stacks images were opened with the Bio-format software tool [238] and processed with the scikit-image library [239]. After cells were manually contoured, an automatic algorithm computed the medial axis transform of the binary cell mask. An Otsu's thresholding algorithm later separated the cell body primary and secondary dendrites from the cell body. The software quantified the length of cell primary protrusions, defined as the longest branches starting from the cell body, and detected cell-cell connections if cell boundaries were in the same image of the z-stack. Osteocytes exhibit exploratory dendrites that extend and retract from the surrounding extracellular matrix before forming a fully developed osteocyte network [214]. Cell primary protrusions longer than 10 µm were defined as dendrites, as previously described [237].

4.3.5 Cell proliferation assay

Osteoblasts move from a proliferative to a quiescent phase during differentiation [45]. Thus, DNA (deoxyribonucleic acid) content was measured using the Hoechst 33258 DNA assay to monitor cell proliferation over time. Cells were isolated by digesting the collagen matrix overnight in a solution of collagenase from *Clostridium histolyticum* (Sigma-Aldrich, 2 mg/ml, $\geq$ 125 CDU/mg) and centrifugating cell suspension at 13,000 rpm for 15 min. 100 µl of Hoechst buffer (1 mM ethlenediaminetetraacetic acid, or EDTA, 10 mM Tris (hydroxymethyl) aminomethane and 0.1 M Sodium Chloride at pH 7.4, all reagents from Sigma-Aldrich) was added to the pellet. Cells were lysed by applying 3 cycles of freezing (-80°C)-thawing procedure before running the biochemical assay. Later, 20 µl of cells lysate or DNA standards were suspended in 200 µl of Hoechst dye solution (0.1% v/v, Sigma-Aldrich) and added in a 96-well plate in triplicate. Fluorescence was then measured (excitation: 380 nm; emission: 440 nm) using a fluorescence spectrophotometer (Synergy HT Multi-mode microplate reader, BioTek Instruments, VT, USA). Readings were converted to DNA content using a standard curve with samples containing no cells subtracted as background.

4.3.6 Extracellular alkaline phosphatase activity

The metalloenzyme ALP initiates the calcification process by providing inorganic phosphates [240, 241]. It is used as a marker for osteoblast activity, since ALP expression changes over time when osteoblast differentiation occurs [225]. Extracellular ALP activity was measured using a colorimetric assay of enzyme activity (SIGMAFAST p-NPP Kit, Sigma Aldrich). It uses p-nitrophenyl phosphate (pNPP) as colorimetric substrate that changes absorbance when dephosphorylated by ALP. Cell culture media was changed and sampled after 2 hours at days 3, 7, 14, 21 and stored at -80°C. After thawing, 40 µl of medium were added to a 96-well plate in triplicate with 50 µl of pNPP solution [242]. Samples were incubated at room temperature in the dark for one hour, and absorbance was read at 405 nm with a spectrophotometer. Readings were converted to ALP production using a standard curve, with samples containing no ALP subtracted as background. ALP production was normalized by the DNA content of each sample in order to get comparable estimations of ALP activity between samples with different initial cell seeding density.

4.3.7 Mineralization

Calcein green staining (Sigma Aldrich) was performed to analyze calcium deposition without affecting cell viability after 7, 14 and 21 days [243]. Calcein was dissolved in 0.5 M NaOH solution (sodium hydroxide, Sigma Aldrich) at 2.5 mg/ml. After mixing, the solution was sterilized with a 0.2 µm Nylon filter, wrapped with aluminium foil and stored at 4°C. Cells were incubated with calcein (25 µg/ml in osteogenic media) (Sigma) for 5 days, washed 3 times in PBS and fixed using 4% (w/v) PFA. Samples were imaged with a confocal microscope (λ_{ex} = 470-509 nm) and maximum intensity images were generated from z-stacks using ImageJ software.

4.3.8 Immunofluorescent staining

BSP2 is a non-collagenous protein upregulated by osteoblasts during the tissue mineralization and downregulated when osteocyte differentiation occurs. DMP1 is an extracellular matrix protein associated with osteocytes. BSP2 and DMP1 immunofluorescent stainings indicate whether cells cultured in the bone-on-a-chip samples synthetized osteoblast or osteocyte markers, respectively [225, 212]. Cells were fixed after 7, 14, 21 days of culture using 4% (w/v) PFA for 30 min and blocked overnight with 5% BSA. Later, samples were incubated at 4°C overnight with mouse monoclonal BSP2 (Santa Cruz Biotechnology, sc-73630, Texas) or DMP1 (Santa Cruz, sc-73633) antibody at a dilution of 1:100 in PBS with 0.5% BSA. After washing 3 times for 5 minutes with PBS, samples were incubated at 4°C for 6 hours with the relevant secondary antibody (for BSP2, goat anti-mouse Alexa Fluor® 555, Molecular Probes, Oregon, A21424; for DMP1, goat anti-mouse Alexa Fluor® 633, Molecular Probes, A21052) at a dilution of 1:50 in PBS with 0.5% BSA. Cell nuclei were then counterstained with DAPI and samples were observed with a confocal microscope. Maximum intensity images were generated from z-stacks using ImageJ software.

4.3.9 Statistics

All experiments were conducted in technical triplicates (n=3) with two independent experiments, by using different donors. Python programming language was used to run all the statistical analyses. A one-way analysis of variance (ANOVA) was used for all the biochemical analyses to assess significant differences between timepoints, followed by pair-wise multiple comparison procedure (Tukey's HSD test). Linear regression models described the variation of dendrite length over time. Experimental data are presented as mean ± 95% of CI if not otherwise specified. P value < 0.05 was considered significant.

4.4 Results

4.4.1 Cell morphology

In order to observe changes in osteoblast morphology, actin filaments were stained at the latest timepoint (21 days), when cells at high density exhibited a dendritic morphology as well as initial interconnections. On the other hand, cells at low density kept an aligned morphology with a limited amount of dendrites (Figure 4.2).

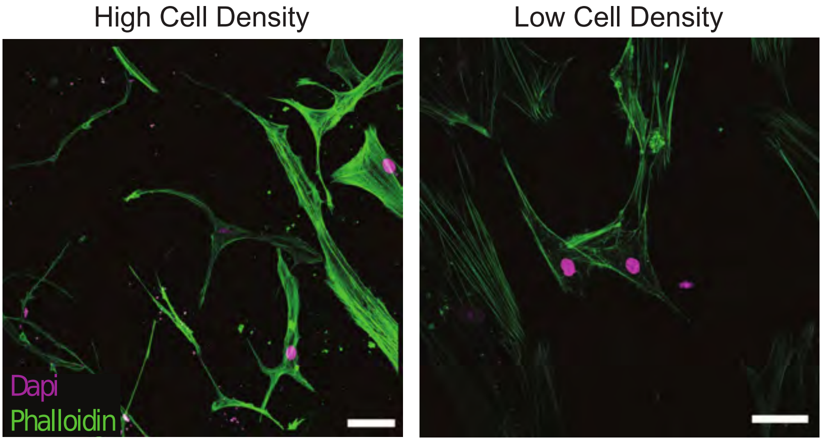

Figure 4.2: **Cells cultured at high density show dendritic morphology.** Representative confocal images of cell nuclei (DAPI) and actin filaments (phalloidin) after 21 days of culture in bone-on-a-chip samples at high and low cell density. Scale bar, 50 µm.

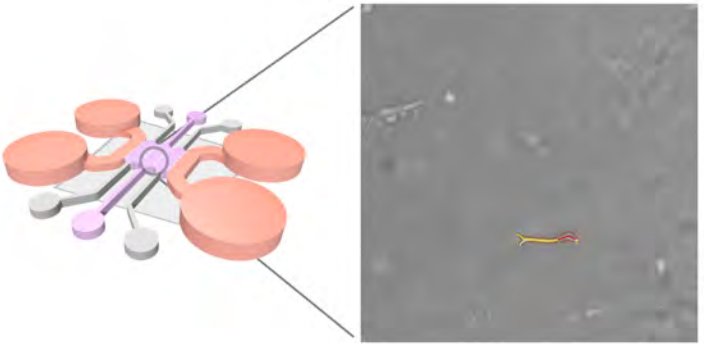

Figure 4.3: **Cell protrusion tracker software.** Cell protrusion tracking of an image stack of primary human osteoblasts cultured in the bone-on-a-chip device. Link to the animation and software source code available with the QR code and at the end of the chapter.

To demonstrate a consistent change in cellular morphology, a customed image analysis software was developed to quantify the cell dendrite length and detect cell-cell connections of cells in the same image of the z-stack (Figure 4.3 and Figure 4.4). The software automatically separated cell body from dendrites, after a manual selection of the cell boundary (Figure 4.5-b). Cells cultured at high density experienced a significant dendrite growth of 1.01±0.25 µm/day over the whole period of culture ,whereas cells cultured at low density did not increase dendrite length over time (Figure 4.5-c).

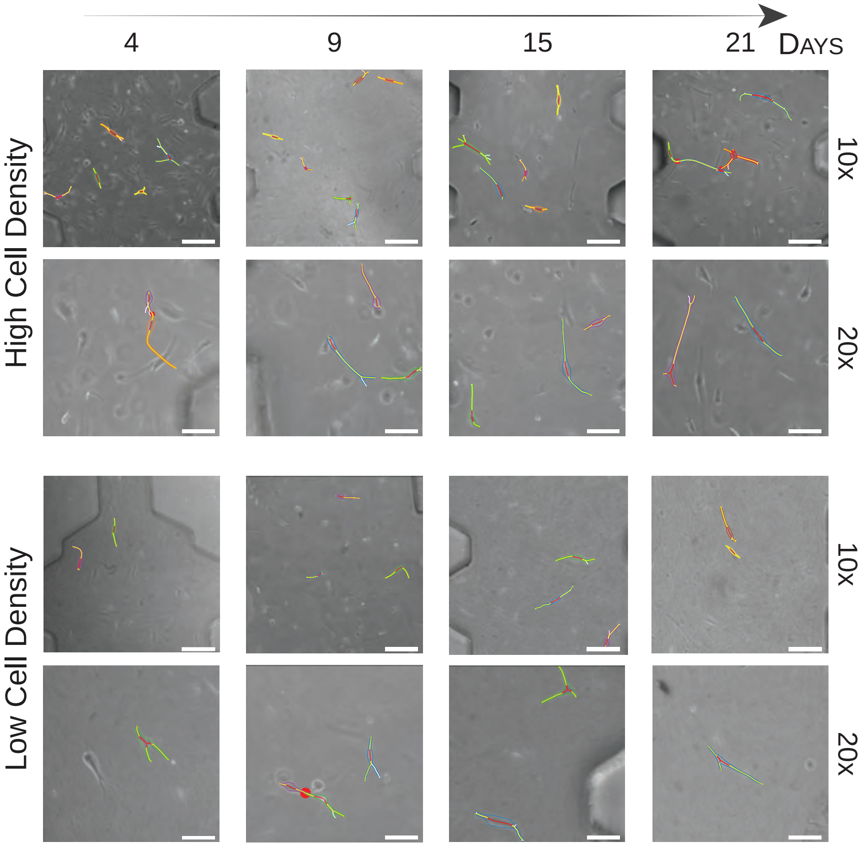

Figure 4.4: **Live image of primary human osteoblasts.** Cells cultured at low ($2.5{\cdot}10^5$ cells/ml) and high ($1{\cdot}10^6$ cells/ml) cell density. Scale bar for images magnified at 10x = 150 µm. Scale bar for images magnified at 20x = 75 µm

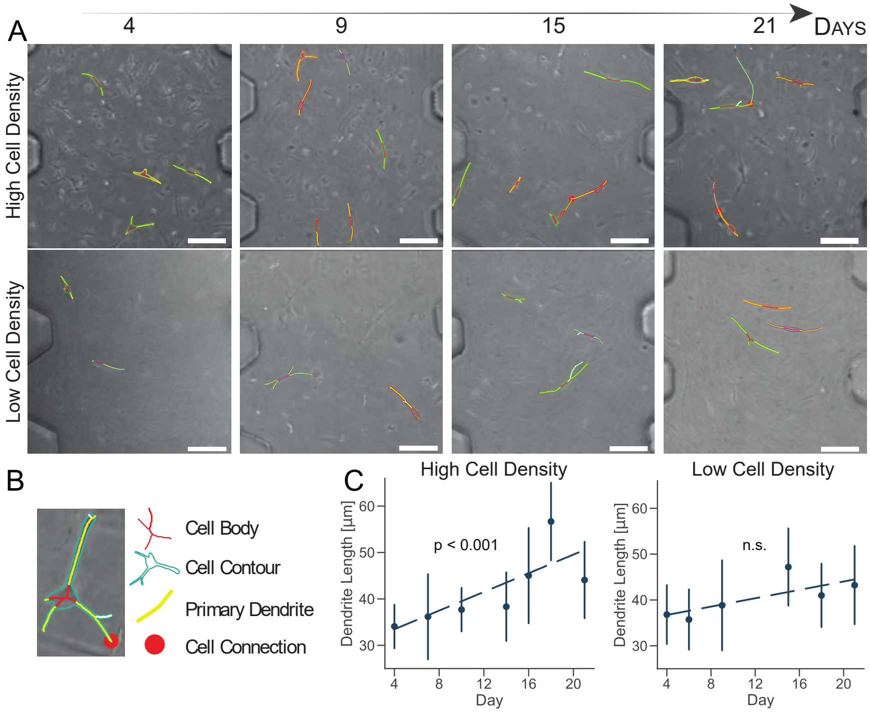

Figure 4.5: **Cells cultured at high density increase primary dendrite length over time.** (A) Brightfield images of cultured human osteoblasts with superimposed tracking. Scale bar = 150 µm. (B) Cell image detail. Identification of the cell body, contour, primary dendrites, and connection with a semi-automatic algorithm. (C) Primary dendrite length measured with a customed software for dendrite tracking. Linear regression model in dashed lines (n≈50 cells per timepoint). Data are mean ± 95% c.i.

4.4.2 Cell proliferation

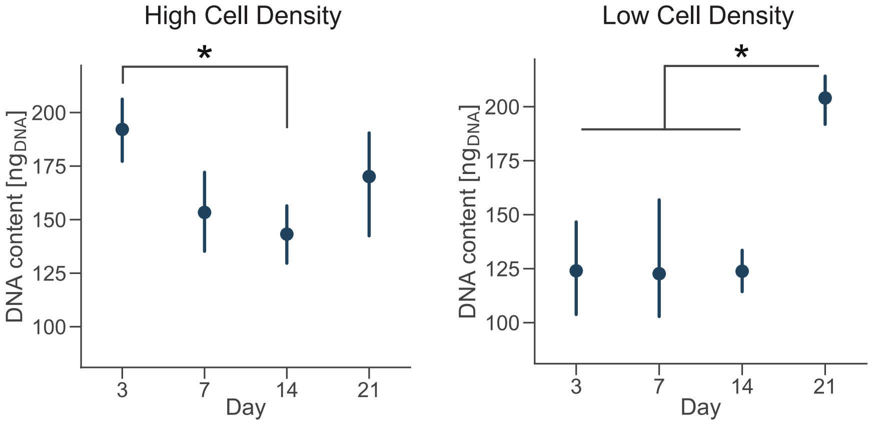

Figure 4.6: **Cells cultured at low density proliferate over time.** DNA content of each group at day 3, 7, 14 and 21. Point plots denote the mean of n=6 samples with error bars representing 95% of confidence interval. * represents statistical significance ($p<0.05$) between indicated groups using one-way ANOVA with Tukey's post-hoc test.

Cell proliferation in the bone-on-a-chip was associated to measured DNA content over the period of culture. DNA showed a negative trend over time for the high cell density group, as suggested by the lower DNA content at day 14 compared to day 3 (Figure 4.6). In the low cell density group, by day 21 the DNA content was significantly higher than early timepoints (Figure 4.6).

4.4.3 Osteogenic activity and mineralization

Extracellular ALP activity was normalized by the DNA content and showed an upregulation for the high density group compared to the low density in both donors (Figure 4.7). The ALP activity had increasing trend for cells cultured at high density, even though the magnitudes of the ALP measurements were higher for donor 2 compared to the donor 1. Moreover, cells from the donor 1 showed a significantly higher ALP activity by day 7 followed by a decreasing trend (Figure 4.7-a).

Calcium staining with calcein at days 7, 14 and 21 showed that primary human osteoblasts mineralized the extracellular matrix over the whole period of culture. Images qualitatively showed a higher presence of calcium ions for the cells cultured at high density (Figure 4.8).

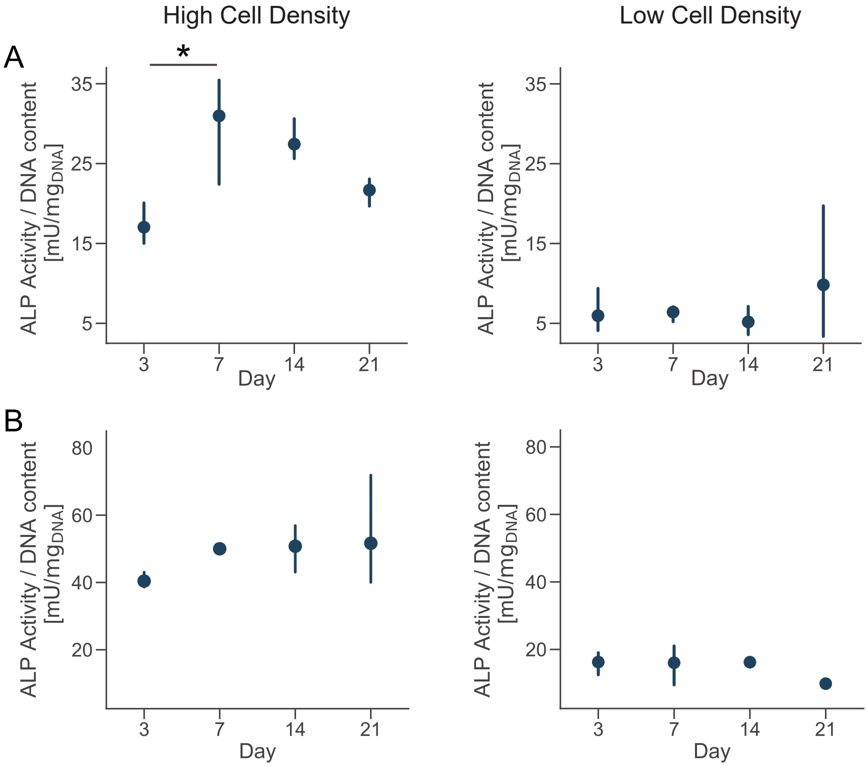

Figure 4.7: **Cells cultured at high density upregulate alkaline phosphatase (ALP) activity.** Extracellular ALP activity of each group at day 3, 7, 14 and 21. Point plots denote the mean of n=3 samples (row A - donor 1, row B - donor 2) with error bars representing 95% of confidence interval. * represents statistical significance ($p<0.05$) between indicated groups using one-way ANOVA with Tukey's post-hoc test.

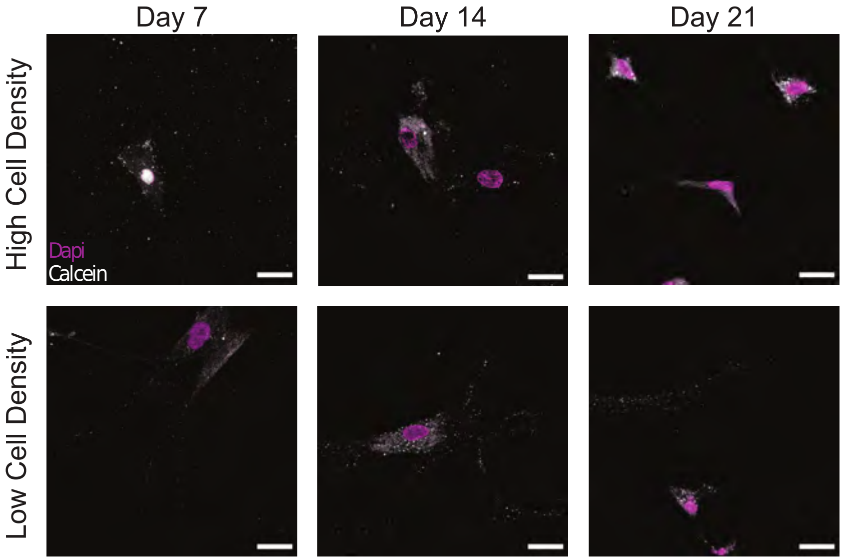

Figure 4.8: **Primary human osteoblasts cultured in the bone-on-a-chip device mineralize the 3D collagen matrix.** Cell nuclei (DAPI) and calcium ions (calcein). Scale bar, 30 µm.

4.4.4 Synthesis of osteogenic markers

Immunofluorescent staining for BSP2 demonstrated positive synthesis within the proximity of cells in the earliest days of culture for both cell density groups. Osteoblasts cultured at low density produced BSP2 at all timepoints (Figure 4.9). Conversly, the high density group reduced BSP2 expression at the end of the culture (21 days, Figure 4.9).

Low presence of DMP1 staining were observed for cells cultured at low density, while DMP1 was more expressed by the human osteoblasts cultured at high density at all timepoints (Figure 4.10).

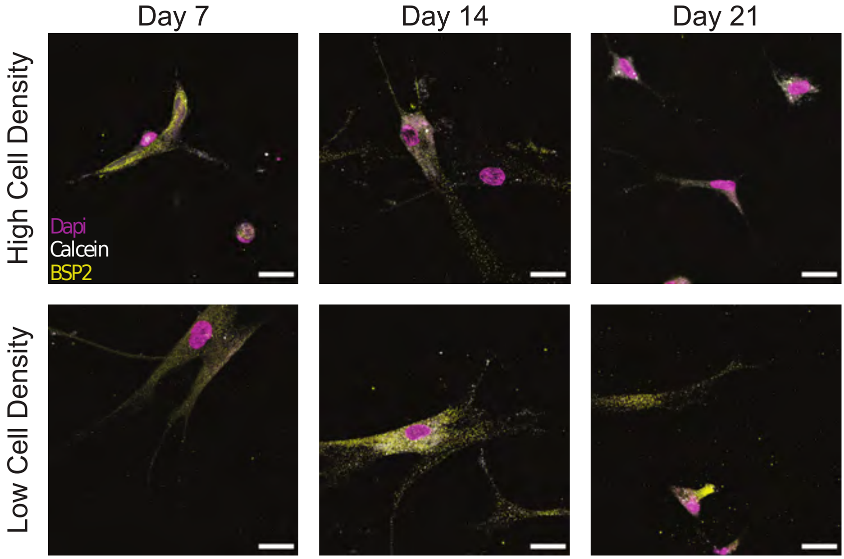

Figure 4.9: **Cells at low density synthesize bone sialoprotein 2 (BSP2) at all timepoints.** Cell nuclei (DAPI), calcium (calcein) and BSP2. Scale bar, 30 µm.

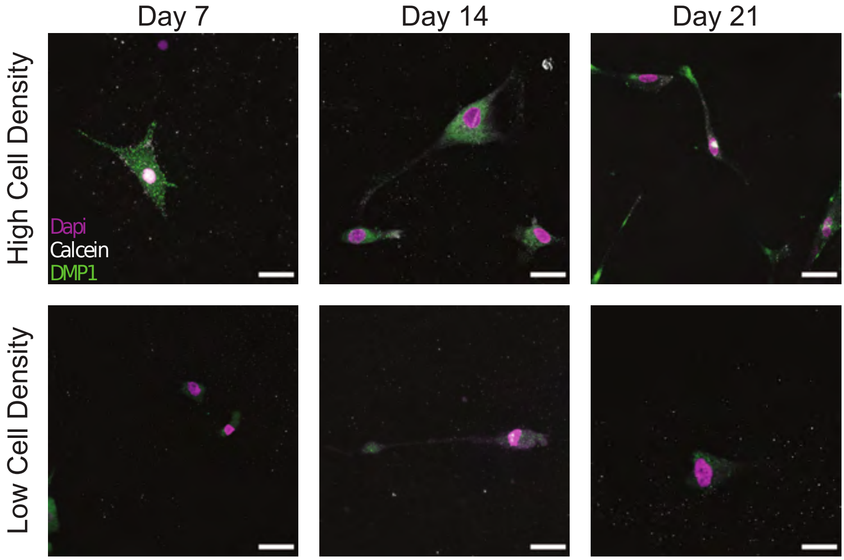

Figure 4.10: **Cells cultured at high density synthesize dental matrix protein 1 (DMP1).** Cell nuclei (DAPI), calcium (calcein) and DMP1. Scale bar, 30 µm.

4.5 Discussion

Recent advances in mimicking bone with microengineered platforms are reducing the gap between the tissue and other more developed organ-on-chip models but they did not reach to show the development of a device with differentiated osteocytes and a 3D mineralized matrix.

Given that primary human osteoblasts embedded in a 3D fibrous collagen matrix is an optimal environment to encourage osteocyte differentiation [214, 228, 225], it is hypothesized that the same environment translated to organ-on-a-chip scale recapitulates two key *in vivo* bone properties: osteoblast maturation and matrix mineralization. To determine the development of mature bone formation, the major aspects underlying osteoblast-osteocyte differentiation were investigated: cell morphology variation, mineralization and protein synthesis.

4.5.1 Cells show dendritic morphology while increasing primary dendrite length over time

The osteoblast-osteocyte differentiation is a complex mechanism, still under investigation, with relevant changes in cell morphology, polarization, cytoplasmic volume, number of cell organelles, proliferation, gene expression, type of collagen deposited and bone deposition rate. During these transitional stages, the extension of cellular dendrites or pseudopodia is the one of most recognizable variations [45].

Osteoblasts were already classified with a spread, aligned, transitional or dendritic morphology during their differentiation into osteocytes *in vitro* [237], and mineralizing conditions enhanced the development of a stellate morphology [225]. Microfluidics showed that pre-osteoblastic mouse cells adhere and spread differently along a stiffness gradient, but it did not highlight any morphological variation [244]. Here, the difference in cell shape suggests that human osteoblasts cultured at $1{\cdot}10^6$ cells/ml (high density) are more differentiated into osteocytes than cells cultured at $2.5{\cdot}10^5$ cells/ml (low density) (Figure 4.2). The dendritic morphology for the high density group reported here is consistent with the results in a traditional 3D *in vitro* systems, where mouse bone cells cultured at a low cell density ($2.5{\cdot}10^5$ cells/ml) had a lower percentage of dendritic cells with respect to cells cultured at high density ($2{\cdot}10^6$ cells/ml) [214]. Dendritic protrusions of primary human osteoblasts in collagen hydrogels is documented in the literature for initial cell seeding densities lower than $2.5{\cdot}10^5$ cells/ml [225, 226, 227]. In these cases, the maximum collagen concentration in the hydrogel was 3 mg/ml, which is half of the 6 mg/ml used in this study. Hydrogels with lower collagen concentration have lower mechanical properties [233], which favor a dendritic cell morphology even at lower cell seeding densities [214]. Osteoblast differentiation was reduced in hydrogels with low collagen concentration when they were modified with biomimetically or strontium-doped mineralized collagen, confirming that the higher stiffness of the matrix delays the differentiation for low cell seeding densities [227]. On the other hand, hydrogel contraction limits the use of high cell seeding densities. The present bone-on-a-chip system, where trapezoidal columns within the culture chamber reduces the hydrogel contraction, facilitated the use of hydrogels with higher collagen concentration, thus favoring the culture of cells at higher seeding densities and the exhibition of a dendritic morphology at higher collagen concentrations.

Experimental biology requires novel automatic tools for image analysis to support the conversion of microscopy images into quantitative data [245]. The customed image analysis software developed to track cell protrusions provided a semi-automatic quantification of cell morphology, less prone to user error. The software confirmed osteoblast change to a dendritic morphology when cultured at high density, given their significant dendrite growth over the period of culture (Figure 4.5-c). The same analysis did not show a quantitative change in cell morphology over time for the low density group (Figure 4.5-c), as suggested by the aligned shape observed in confocal imaging (Figure 4.2).

Compared to traditional *in vitro* culture, the ratio between the volumes of culture and the fewer number of cells used in microengineered devices make quantitative image analyses more representative of the whole cell population present in each sample. The number of cells tracked in this study (n$\approx$50 cells per timepoint) is 100 times lower than the total amount of cells in each sample ($\approx$5000 cells), while in traditional systems it is usually 1,000,000 times lower. Moreover, the high control of the geometries of the organ-on-a-chip culture chamber allows the identification of the same image location at each timepoint. The combination of the organ-on-chip technology with a semi-automatic software that decreases operator-dependent errors produce a more accurate and reliable platform for quantitative image analysis.

The evaluation of cell-cell connections showed a limited variation over time, due to the requirement for cell boundaries to be on the same image of the z-stack (Figure 4.3). However, it was observed a slight increase in cell connections for cells cultured at high density over time (Figure 4.5-a). Osteoblasts did not form an interconnected network, they rather showed exploratory dendrites to create transient connections and position themselves in the extracellular matrix [214, 246]. The dendritic morphology at the end of the culture and the increase in exploratory dendrite length indicated that osteoblasts cultured at high density underwent differentiation into an early osteocytic phenotype.

4.5.2 Alkaline phosphatase upregulation is associated with the interruption of cell proliferation

The cessation of cell proliferation and collagen matrix production follows the secretion of soft osteoid that surrounds osteoblasts initiating differentiation [210]. To determine whether the culture microenvironment regulated cell proliferation in the bone-on-a-chip, the 3D collagen matrix was degraded, cells were extracted and the evolution of the DNA content was quantified.

The amount of DNA measured from a unique cell type is proportional to the total number of cells. Thus, the negative trend in DNA content for osteoblasts cultured at high density indicated that those cells were not proliferating in the bone-on-a-chip system, plausibly because they were undergoing a differentiation process (Figure 4.6). Only a limited proportion of osteoblasts differentiates into osteocyte *in vivo* while the rest of the population follows other fates, including apoptosis [45]. If cells seeded at high density were differentiating into osteocytes, the decreasing trend in the DNA amount confirmed that the microenvironment also induced the apoptosis of a subpart of the osteoblast population.

A 3D culture environment made of a microbeads assembly already showed that osteoblastic cells cultured in a microfluidic system stop proliferating, compared to a control group cultured in a plate where cells were proliferating. The cell number quantification in the microbead assembly was estimated by the ratio of the number of cells and the number of microbeads imaged [111]. Here, it was developed a protocol to get a more direct measure of the amount of cells over time in the microengineered sample.

The higher DNA content in the low cell density group by day 21 suggested that cells started proliferating under these culture conditions (Figure 4.6). Results show that after an initial period of quiescence, osteoblasts seeded at low density maintained their proliferative capacity in the bone-on-a-chip, supporting the hypothesis that they were not differentiating into osteocytes. The use of primary human cells was crucial to capture the difference between proliferative and non-proliferative conditions in the bone-on-a-chip model. Cell-lines have high proliferation rates which make them not very suitable to study this precise aspect of bone cells function [247]. For example, a mouse osteoblast cell-line (MC3T3-E1) showed to proliferate even if cells were differentiating into osteocytes and creating an interconnected network between dendritic cells [214]. The combination of primary human cells and microengineered technology give a valid solution to culture cells representative of the *in vivo* phenotype maximizing the number of samples. Such system is a unique representative model of osteoblast proliferation in a physiologic 3D environment.

The transition from a proliferative to a quiescent phase during osteoblast differentiation is concomitant to the upregulation of ALP and its later reduction

[209]. To assess osteoblast secretion of ALP during culture, the evolution of enzyme activity in the culture media and the effect of cell density was quantified.

The upregulation of ALP activity for cells cultured at higher density confirmed the higher potential for matrix mineralization and osteogenic differentiation for both donors (Figure 4.7). Differences in trends of the ALP measurements might be related to inter-donor variability, and more specifically to the differences in age and sex between donors. Cells from the younger male donor (donor 2) had higher absolute ALP activity and didn't show the trend observed in donor 1, but ALP was consistently higher for cells cultured at higher density (Figure 4.7). In tissue engineering, the upregulation of ALP expression relates to osteogenesis and is a precursor to mineralization of the tissue [241]. Previous studies in microfluidic devices only showed the upregulation of ALP activity at the end of the culture, proving that those platforms promoted osteogenesis [113, 248, 112]. Here, it was measured the temporal evolution of ALP activity during the whole culture and it suggested that osteoblasts cultured at high density had a phase of increase of mineralization in the first week of culture and later continued the differentiation process.

Calcein is a fluorochrome binding calcium at bone mineralization front [249], thus identifying newly mineralized matrix. Calcium staining with calcein confirmed the results of ALP activity: the lower presence of calcium ions for the cells cultured at low density indicates that this cell seeding density ($2.5{\cdot}10^5$ cells/ml) was probably insufficient to initiate osteoblasts differentiation in this hydrogel, while cells needed to proliferate more before undertaking this pathway.

4.5.3 Cell density regulates osteogenic marker synthesis

Osteoblasts transitional stages during bone formation involve changes in cell morphology and protein synthesis. Given the differences observed in cell morphology, protrusion length dynamics, proliferation and osteogenesis, further investigation required the qualitative assessment of bone matrix proteins. Two specific proteins BSP2 and DMP1, representative of osteoblast and osteocyte phenotype respectively, were selected to determine the effect of cell density on their production.

The lower presence of BSP2 at the end of the culture denoted that cells cultured at high density group changed differentiation stage in the bone-on-a-chip devices, while BSP2 production at all timepoints suggested that no transition to osteocyte occurred for this group (Figure 4.9). BSP2 expression is characteristic of osteoblast phenotype, even if it was observed in lower amounts in osteocytes [45]. Another osteocytic marker needs to determine whether cells of the high density group underwent this specific fate.

The limited transition into the osteocyte stage during the whole culture period for cells cultured at low density was confirmed by the absence of DMP1 staining (Figure 4.10). On the contrary the higher presence of the osteocytic marker for cells cultured at high density, together with the decreased presence of the osteoblast marker BSP2 (Figure 4.9), indicated their faster osteoblasts transition to osteocytes. The positive DMP1 staining for cells cultured at high density reported here is consistent with the results in a traditional 3D *in vitro* systems, where cells cultured at higher density ($2 \cdot 10^6$ cells/ml) produced more DMP1 as dispersed nodules within the surrounding matrix [214].

4.5.4 Cells cultured at higher density differentiated faster into osteocytes

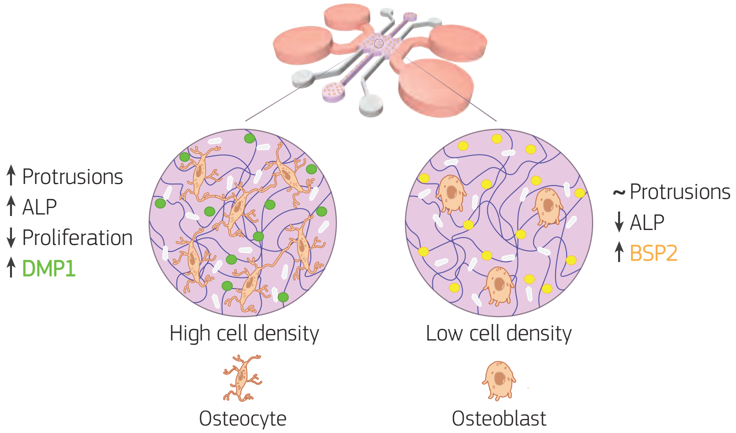

Figure 4.11: **Bone-on-a-chip development with two cell seeding densities.** Primary human osteoblasts were encapsulated in type I collagen hydrogel (purple in the figure) at $2.5 \cdot 10^5$ (low cell density) and $1 \cdot 10^6$ (high cell density) cells/ml, then loaded in the bone-on-a-chip devices and cultured up to 21 days to study matrix mineralization and cell differentiation into osteocytes. Cell morphology, dendrite tracking, DNA content, alkaline phosphatase (ALP) production, calcium deposition (white in the figure), and immunofluorescent staining of bone sialoprotein 2 (BSP2, yellow in the figure) and dentin matrix protein 1 (DMP1, green in the figure) were performed to assess the osteogenic phenotype of the cells. At low cell density, the biochemical 3D microenvironment induced only the expression of osteoblast markers (ALP, BSP2). While the change in cell morphology, the upregulation of ALP and the expression of DMP1 suggested that osteoblast transition to osteocytes occurred faster for cells cultured at high density.

Overall, the data presented in this chapter showed how the 3D microenvironment in the bone-on-a-chip regulated osteoblast-osteocyte differentiation (Figure 4.11). The microengineered technology created a highly controllable environment to study the maturation of primary human bone cells in a 3D extracellular matrix made of the most abundant organic component in bone tissue. A custom semi-automatic image analysis software led to the extraction of quantitative data on the cellular morphology from microscopy images. In addition, the use of primary human cells at high cell density was crucial to mimic the physiological shift from proliferative to non-proliferative conditions during the differentiation process. The expression of characteristics osteoblast and osteocyte markers confirmed differentation with changes in synthesis of extracellular matrix proteins. Furthermore, by 21 days of *in vitro* culture, osteoblasts cultured at high density increased the protrusion length over time, exhibited dendritic morphology, did not increase cell number, upregulated ALP activity, downregulated BSP2 synthesis and produced more DMP1. Thus they underwent changes in cell morphology, proliferation, mineral deposition and protein production that are specific of the differentiation into osteocytes. Conversely, osteoblasts cultured at low density had constant protrusion length up to 21 days, proliferated, had constant ALP activity and produced only BSP2. They consistently exhibited no transition towards the osteocytic phenotype.

One limitation of this study is the presence of a 3D hydrogel embedding cells in a narrow space that made RNA purification not possible after extraction for gene expression analysis. Moreover, the cell extraction protocol took one night for the complete digestion of the collagen matrix, which would inexorably affect results from PCR. Previous works on cell differentiation in microfluidic systems focused on the protein expression rather than gene profiles [250, 251, 252, 253, 254], considering the technical challenges and that protein biosynthesis depends on transcript levels as well as other factors such as the local availability of resources [255]. Results on dendritic morphology, cell proliferation, alkaline phsphatase activity and protein synthesis firmly indicate osteoblasts differentiation and the effectiveness of the microengineered technology used.

4.6 Conclusions

Traditional *in vitro* systems already showed that primary human osteoblasts embedded in a 3D fibrous collagen matrix differentiates into osteocytes under specific conditions. Here, the findings of traditional macro-models on osteoblast differentiation were translated to the organ-on-a-chip scale. A minimal microengineered functional unit captured the major aspects underlying the differentiation of primary human osteoblasts into osteocytes, which depends on the cell seeding density. A custom image analysis software was developed to support the semi-automatic analysis of cell dendrite elongation. Only the human osteoblasts seeded at higher density underwent the change in cell morphology, proliferation, mineral deposition and protein synthesis that are specific of the differentiation into osteocytes. The use of the microengineered technology to study the maturation of primary human osteoblasts in a 3D fibrous extracellular matrix takes advantage of the limited number of cells required by these systems, creating a unique platform to represent the phenotype variability as well as to elucidate the role of single or simultaneous stimulation in osteoblast maturation. From a clinical perspective, the bone-on-a-chip presented in this work provides the minimal functional microenvironment to build patient-specific bone models to study the individual osteogenic potential and the effect of alternative therapies.

Code availability

The image analysis software used for cell protrusion tracking in this study was developed in Python 3, and is available under the following link:
github.com/gabnasello/cellprotrusiontracker-frontiers2020

Chapter 5

Towards patient-specific bone scaffolds

5.1 Introduction

This chapter draws together the main findings of each *in silico* and the *in vitro* study carried out in the thesis. The results of the individual research chapters are summarized in section 5.2, with a focus on the evaluation of 3D printed scaffold performances and their regenerative potential for patient-specific bone applications. Section 5.3 outlines the implications for the field of bone tissue engineering as well as for personalized treatments. Finally, section 5.4 provides recommendations for further work and future perspectives in the field combining personalized and regenerative medicine.

5.2 Main achievements of the thesis

The research presented in this doctoral thesis explored different factors that regulate the regenerative potential of 3D printed bone scaffolds, ranging from the scaffold mechanical interaction to the osteogenic response of patient-specific bone cells (Figure 5.1). Different modeling systems were developed to reveal specific information of the main actors in the bone regeneration process for patient-specific scaffolds. On the scaffold side, an *in silico* model predicted differences in the *in vivo* regenerative outcome of 3D printed bone scaffolds based on the patient-specific mechanical parameters. On the patient side, a micro-engineered system provided an *in vitro* strategy to culture bone cells from individual patients and evaluate their osteogenic differentiation. The key contributions of the research performed to each hypothesis listed in section 1.3 are summarized below.

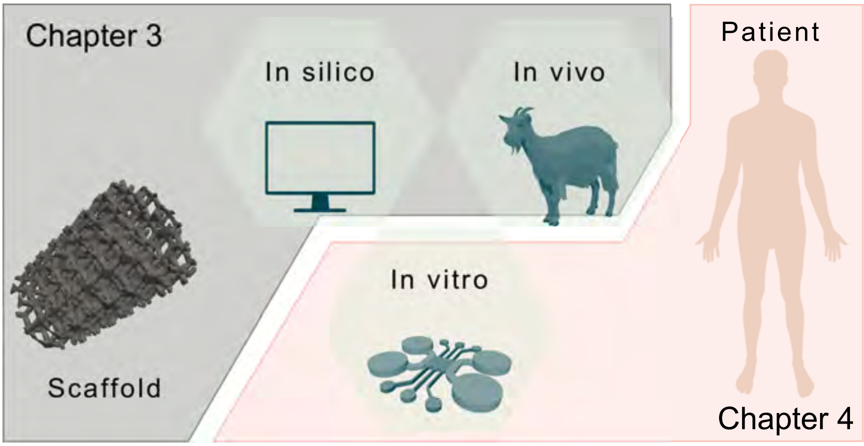

Figure 5.1: **Graphical representation of the chapters of this thesis**. Use of multiple modeling systems to evaluate the bone regeneration process guided by patient-specific 3D printed scaffolds.

Research achievement 1

A mechano-driven regeneration algorithm predicts differences in bone ingrowth distribution depending on the scaffold implantation site and individual mechano-sensitivity.

The *in silico* model presented in this thesis (chapter 3) determined the *in vivo* regenerative outcome of porous titanium scaffolds in a patient-specific context. It was demonstrated that a mechano-driven regeneration algorithm predicts differences in bone ingrowth distribution depending on the scaffold implantation site. On the one hand, homogeneous *in vivo* bone ingrowth corresponded to uniform mechanical stimulus for scaffolds inserted into the femoral and tibial epiphysis. On the other hand, localized *in vivo* bone ingrowth in the periosteal subregion corresponded to higher mechanical stimulation for scaffolds inserted closer to the tibial diaphysis.

Detailed patient-specific and location-specific predictions of bone regeneration required only two fitted parameters, suggesting that a mechanistic description of the bone regeneration process may not be needed to predict the scaffold regenerative performance. By fitting *in vivo* bone ingrowth data, the computational model identified differences in mechano-sensitivity between recipients. Therefore, evaluating the regenerative outcome of patient-specific bone scaffolds requires both bone cells mechano-sensitivity evaluation and location-specific information to be implemented in the computational model of a mechano-driven bone regeneration.

Research achievement 2

Human osteoblasts cultured in a bone-on-chip differentiate into osteocytes and their differentiation depends on the initial cell seeding density.

The research study presented in chapter 4 demonstrated that human osteoblasts cultured in a bone-on-chip microenvironment exhibit characteristic features of their differentiation into osteocytes. Similarly to a previous macro-scale model of osteoblast differentiation in 3D hydrogel [214], the results from this chapter showed that osteoblasts seeded at higher density in the 3D microenvironment increased the cell primary dendrite length over time, upregulated alkaline phosphatase, interrupted cell proliferation and synthesized an osteocyte marker (DMP1).

Moreover, the limited volumes of the culture facilitated the use of primary human osteoblasts isolated from single individuals for each sample. The use of patient-specific bone-on-chip revealed different magnitudes in the alkaline phosphatase activity for osteoblasts isolated from two different donors, indicating differences in their osteogenic activity. Overall, results from this study demonstrated for the first time that a 3D microengineered environment can investigate the osteogenic activity of bone cells isolated from individual subjects.

Global achievement of the thesis

Patient-specific orthopedic applications require the synergy of advanced modeling techniques to assess scaffold-guided bone regeneration based on the patient-specific regenerative capacity and location-specific requirements.

Taken together, the results of this thesis emphasize the importance of using multiple modeling systems when investigating the *in vivo* regeneration process guided by patient-specific bone scaffolds. Both actors of a cell-free *in situ* regenerative strategy, namely the scaffold and the patient, have a significant effect on the final regenerative outcome and needs to be modeled. An *in silico* model was developed to predict bone formation based on the scaffold design and the host mechanical environment, while the microengineering *in vitro* technology was used to evaluate the osteogenic potential of human osteoblasts isolated from single donors. The BOC can inform on the regenerative capacity and mechano-sensitivity of the patient-specific osteoblasts, providing a key element of scaffold design coupled in the *in silico* model to the anatomical requirements. Through the multiple models and the results presented in this thesis, it is possible to represent the variability of the regenerative response and evaluate the potential scaffold performance for each unique case.

5.3 Implications for the field of tissue engineering

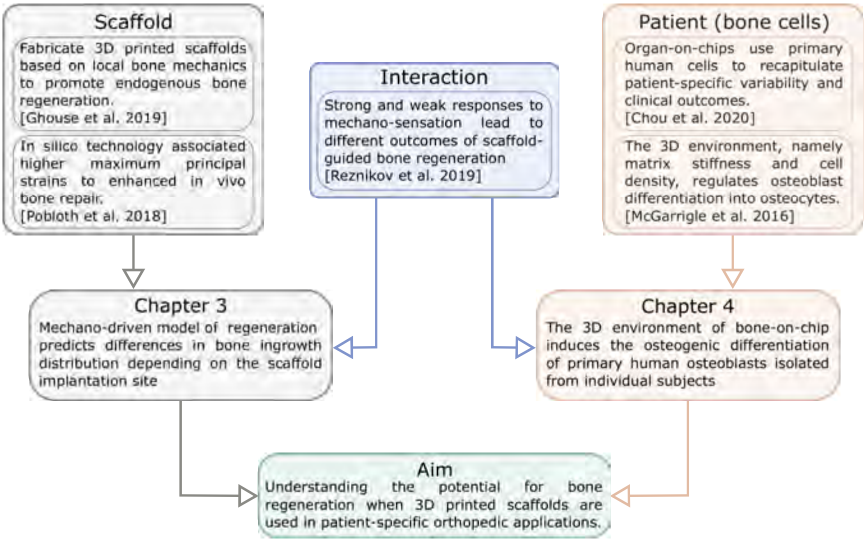

Fabricate 3D printed scaffolds based on local bone mechanics to promote endogenous bone regeneration. [Ghouse et al. 2019]

In silico technology associated higher maximum principal strains to enhanced in vivo bone repair. [Pobloth et al. 2018]

Strong and weak responses to mechano-sensation lead to different outcomes of scaffold-guided bone regeneration [Reznikov et al. 2019]

Organ-on-chips use primary human cells to recapitulate patient-specific variability and clinical outcomes. [Chou et al. 2020]

The 3D environment, namely matrix stiffness and cell density, regulates osteoblast differentiation into osteocytes. [McGarrigle et al. 2016]

Mechano-driven model of regeneration predicts differences in bone ingrowth distribution depending on the scaffold implantation site

The 3D environment of bone-on-chip induces the osteogenic differentiation of primary human osteoblasts isolated from individual subjects

Understanding the potential for bone regeneration when 3D printed scaffolds are used in patient-specific orthopedic applications.

Figure 5.2: **Implications for the tissue engineering field**. Graphical representation of the work presented in the research chapters of the thesis. Results and global aim of the thesis are in context with the state-of-art of the tissue engineering field.

Matching the mechanical properties of natural bone tissue has been a widely investigated strategy to design novel scaffolds [83, 99, 256, 257, 258, 259]. However, a single TE approach is unlikely to meet all regenerative requirements from different patients, leading to unsatisfactory outcomes when tested in a clinically relevant scenario [260]. There are growing concerns on the detrimental impact of patient-related factors to the variability outcome of TE products [86, 260, 261]. In view of defining a cell-free TE strategy for patient-specific orthopedic applications, each research study conducted as part of this thesis has advanced the current understanding of both the scaffold and the patient role in the bone regeneration process (Figure 5.2).

When optimized from a mechanobiological perspective, bone scaffolds promote endogenous bone regeneration. Ghouse et al. [99] designed bone scaffolds with inner stiffness gradients matching the local mechanical variations of the bone being replaced. Although the aim of the study was not to maximize bone ingrowth into a porous scaffold, the authors proposed a clinical applicable approach to fabricate porous scaffolds based on the local bone mechanical properties [99]. In order to maximize the rate and quantity of bone repair, Pobloth et al. [144] used the computational technology to evaluate the mechanobiological environment of 3D printed titanium scaffolds with different mechanical properties. The *in vivo* results of endogenous bone defect regeneration in large animal models verified that lower scaffold stiffness induced higher maximum principal strains and enhanced bone repair [144]. Similarly, Reznikov et al. reported higher bone ingrowth for scaffolds with a lower apparent modulus, although the authors identified two different groups within animals tested. One group, made of 7 animals out of 12, showed mechano-sensation capacity and higher regenerative potential, while animals of the other group did not have any mechano-sensation capacity and showed lower regenerative outcomes [89]. The results of chapter 3 demonstrated the importance of modeling both the mechano-sensation capacity and the local bone mechanical environment for patient-specific and location-specific predictions of bone ingrowth (Figure 5.2). Although mechanics cannot be the only regulator of the bone regeneration process, the mechano-driven model presented can evaluate the regenerative potential of porous bone scaffolds based on two individual parameters. Therefore, such model can guide the design of a bone scaffold that meets the mechanical and biological requirements of the specific patient.

The heterogeneous response reported by Reznikov et al. [89] showed the central role of host variability in the scaffold-guided bone regeneration, corroborating the clinical observation that patient variability might have a greater impact on the regenerative outcome than the scaffold itself [260]. Although there is a clear need to model patient regenerative variability, *in vitro* bone models have traditionally preferred osteoblastic cell lines to primary human osteoblasts because of their almost unlimited availability, their ease of maintenance and their phenotype stability [262]. McGarrigle et al. used a pre-osteoblastic mouse cell line (MC3T3-E1) to prove the regulation of the 3D environment, namely ECM stiffness and cell density, on osteoblast differentiation into osteocytes [214]. However, bone tissue models made by cell lines do not represent the biological variability associated to donor-related factors, which is essential in the context of personalized medicine. Although different organ-on-chips used primary human cells to recapitulate patient-specific clinical outcomes [105, 108, 263], no approach combined primary human bone cells from single donors and organ-on-chip technology. The experimental study from chapter 4 revealed that a bone-on-chip system made of primary human osteoblasts embedded in a 3D fibrous collagen matrix recapitulate osteoblast maturation towards osteocytes (Figure 5.2). While osteogenic differentiation were observed for both batches of osteoblasts tested, the magnitudes of the ALP measurements differed for the two donors used. Although a 3D microengineered system of osteoblasts embedded in a collagen gel is an extreme simplification of the structural and cellular complexity of the bone tissue, this study demonstrated for the first time that the bone-on-chip technology models the variability of the osteoblast phenotype and can investigate the osteogenic activity of patient-specific bone cells.

5.4 Recommendations for future work

The research carried out in this thesis provided a novel experimental approach to investigate the bone regeneration process guided by patient-specific scaffolds, made up of both *in silico* and *in vitro* modeling systems. The development of each system presented as well as their final integration can get closer to a personalized evaluation of the regenerative performance associated to 3D printed bone scaffolds, as discussed in the present section.

5.4.1 Scaffold mechanobiological optimization for case-specific applications

Scaffold design evaluation for optimal primary and secondary stability

The mechano-driven model of bone regeneration described in chapter 3 could brings a new tool to optimize the design of orthopedic implants for a better osteointegration in patient-specific applications. As the 3D printed porous surface of regenerative implants enhances the biological engraft, future studies should evaluate the regenerative performance of complex 3D printed implants design for clinically relevant cases. However, it is important to mention that the transition from granulation or woven tissue to bone formation might not happen if fibrotic scar-like tissue is formed. In fact, the computational analysis of chapter 3 assumed that micromotion at the bone-scaffold interface was negligible due to the press-fit insertion of the scaffold into the bone. The absence of micromotions is an ideal condition for the scaffold osteointegration and primary stability, while the presence of micromotions favors interfacial fibrous tissue formation [203, 264]. In a clinical scenario, orthopedic implants require immediate (i.e. primary) stability using screws, followed by a long-term (i.e. secondary) stability given by the bone growth into the porous surface [265]. Future studies should combine the bone regeneration model with a state-of-art screw fixation model [266] to evaluate both the parimary and secondary stability of orthopedic implants. Different screw configurations drastically alter the initial implant stability affecting bone ingrowth [267, 268]. Therefore, a combined model of bone regeneration and screw fixation would reduce micromotion in the short-term while maximizing bone ingrowth in the long-term.

Identify patients where scaffold degradation or stiffness gradients are beneficial

In search of maximizing bone regeneration, both the mechanical [99, 259, 269] and the degradation [270, 271, 272] behavior of 3D printed scaffolds have been widely investigated. From a mechanical perspective, it is clear that softer scaffolds enhance bone regeneration until they withstand both mechanical and fixation failures [144]. For this reason, novel meta-biomaterials were recently proposed to minimize the risk of mechanical and interface failure of bone scaffolds, since they present structural properties that are not found in naturally occurring biomaterials [273, 274]. From a degradation perspective, additively manufactured biodegradable metals, such as magnesium alloys [275], and calcium phosphates [276], as well as their combination [277], have been developed as suitable bone substitutes for load bearing applications. The degradation dynamics depend on the scaffold topology [278], thus the design of degradable scaffolds would benefit from computational predictive tools of their degradative state in physiological environments [146].

Incorporating material degradation in the bone regeneration model described in chapter 3, together with simulating unprecedented scaffold micro-architectures, would guide the design of degradable scaffolds and meta-biomaterials. However, degradable and mechanobiologically-optimized scaffolds are not expected to improve bone regeneration in all patients [89]. Therefore, future studies should use the patient-specific computational model presented in chapter 3 to identify which patients would benefit from degradable scaffolds or complex microscale structures while the primary stability of the bone substitute is preserved.

FUTURE RESEARCH DIRECTION - Scaffold mechanobiological optimization for case-specific applications

Bone regeneration predictions for 3D printed orthopedic scaffolds requires the combination of bone regeneration with screw fixation models to guarantee the initial stability of the implant while maximizing its osteointegration in the long term. Given that dramatic influence of individual characteristics on the scaffold regenerative response, patient-specific computational models of bone regeneration should identify which patients benefit from degradable or mechanobiologically-optimized scaffolds.

5.4.2 Individual mechano-sensitivity in bone-on-chips

Interindividual variability is a critical challenge for TE therapies, and organ-on-chips offer innovative systems to predict variability in patient-specific response to a designed microenvironment [91, 105]. The bone-on-chip system described in chapter 4 can compare the osteogenic activity of bone cells from different patients that are laden in a collagen hydrogel. Thus, future studies might determine how bone-related disorders alter the osteogenic activity, or the regenerative capacity, of primary human bone cells with controlled experimentation in patient-specific bone-on-chips.

Hydrogels play an important role in engineering BOCs to mimic the specific characteristics of the microenvironment under investigation. Collagen-based hydrogels are the most common choice in BOCs as this protein is the principal components of the mineralized bone matrix and the marrow matrix. Bone marrow niches are commonoly assocaited to lower collagen concentrations, thus lower hydrogel mehcanical properties [108, 122, 120], while an osteogenic microenvironment corresponded to higher collagen concentrations or incorporating hydroxyapatite [118, 129]. Besides collagen, fibrin hydrogels can model the early stage extracellular environment of bone diseases such as fracture healing [279] or cancer tumor-fibrin matrix [280]. Conversely, synthetic hydrogels offer wider control over the structural, chemical and mechanical properties. For example, thermo-responsive hydrogels could exponentially increase their stiffness after gelation, being an ideal model to investigate the cortical matrix or the pathological environment related to osteopetrosis.

Tuning, as well as monitoring, hydrogel structural properties over time can be used to model both physiological and pathological processes of the bone tissue. For example, the bone remodelling process has direct effects on matrix architecture and BOCs provide an unprecedented system where osteoblasts, osteoclasts and osteocytes can be simultaneously culture in a 3D environment while monitoring the bone formation/resorption balance. As for pathological mechanisms, a precise control of the hydrogel architecture could replicate trabecula thickness of single individuals, which is considered a risk factor for postmenopausal bone loss [281]. Thus, BOCs could define patient-specific matrices and predict the outcome of osteoporosis based on the initial trabecula thickness. It is then clear that BOCs can help predicting the outcome of treatments by designing different bone characteristics with specific hydrogel composition.

In addition, the organ-on-chip technology relies on the use of microfluidic systems to apply various mechanical stimuli on cells. Human tissues are characterized by different mechanotransduction signals, thus organ-on-chips offer alternative solutions to apply multiple stimuli, such as shear and interstitial flow, cyclic stretching, stiffness gradient or geometric confinement [282]. As for the bone tissue, osteocyte regulatory role of both bone formation and resorption processes is directly related to fluid shear stress in the lacunocanalicular network. It is know that extracellular proteins, such as glycocalyx, bind cell receptors, such as integrins, and activate mechanotransduction pathways by stretching the cell membrane [51]. Therefore, BOC platforms could investigate the osteocyte mechanotransduction with a direct control on the 3D matrix where cells are embedded and the interstitial fluid flow that replicates the *in vivo* mechanical signal.

Not only does a bone-on-chip personalize device for precision medicine, but it also provides mechanotransduction signals. Therefore, bone-on-chips are the ideal candidates to predict the individual mechano-sensitivity introduced in the patient-specific model of bone regeneration in chapter 3. By associating the bone cell mechano-sensation in microfluidic devices to circulating levels of specific markers, such as estrogen [199] or genetic differences between individual humans [198], future studies might predict the individual mechano-sensitivity for bone regeneration in *in vitro* microenvironments reproducing pathological conditions. However, the bone regeneration potential cannot be just reduced to variations in the osteogenic activity of osteoblast/osteocytes embedded in a 3D matrix. In order to build relevant models of bone regeneration, further research is needed to recapitulate the structural complexity of the bone tissue, as well as its interaction with any other tissue affecting the regeneration process [104].

FUTURE RESEARCH DIRECTION - Individual mechano-sensitivity in bone-on-chips

The organ-on-chip technology predicts the variability between individuals associated to specific biological processes. From a mechanobiological perspective, bone-on-chips can evaluate the mechano-sensitivity of patient-specific bone cells by applying interstitial fluid flow. In order to build relevant models of bone regeneration, hydrogel-based bone-on-chips need to recapitulate the structural complexity of the bone tissue.

5.5 Conclusion

The convergence of personalized and regenerative medicine helps the translation of tissue engineering products to the clinics by reducing the variability of the final clinical outcome. Although it is a fascinating strategy, a patient-specific approach requires a thorough understanding of all sources of variability, from product manufacturing to patient response, before learning how to mitigate those effects. This thesis has presented the experimental research performed throughout the course of the author's PhD studies to investigate the bone regeneration process associated to patient-specific 3D printed scaffolds. The experimental research relied on the use of multiple modeling systems to understand the effects of both the scaffold and the patient on bone regeneration.

A computational method of mechano-driven bone regeneration was applied to simulate the mineralization process within the pores of 3D printed bone scaffolds based on the mechanical interaction between the scaffold and the host environment, described by subject and location-specific parameters. Besides predicting variations in the bone ingrowth distribution when a cell-free titanium scaffold is inserted closer to the tibial diaphysis, the model proposed that the limited bone ingrowth in the scaffold core, observed both *in vivo* and *in silico*, was associated to low mechanical stimulation. By modeling the mechano-sensation capacity of both the individual and the local bone tissue, such computational model can guide the design of bone scaffolds that meet patient-specific requirements.

To understand the intrinsic variability of the patient response, a bone-on-chip system was developed to culture primary human osteoblasts and assess their osteogenic activity. The differentiation process towards osteocytes was recreated in a 3D collagen hydrogel where cells, during 21 days, underwent the characteristic changes protrusion length, cellular morphology, proliferation, alkaline phosphatase and protein secretion. As already observed in traditional culture systems, increasing the cell seeding density favored osteoblast differentiation into osteocytes but osteoblasts isolated form different donors showed differences in the alkaline phosphatase activity. The limited volumes of culture of such micro-engineered device facilitates modeling patient-specific variations in the osteoblast phenotype.

The results from this thesis provide a novel perspective to evaluate the performance of a tissue engineering product, where advanced *in vitro* and *in silico* techniques, combined with *in vivo* data, evaluate distinctive aspects of the bone regeneration process for patient-specific applications. A computational approach predicted, for the first time, differences in bone regeneration for different scaffold implantation sites and individual mechano-sensitivity. The bone-on-chip technology was used to evaluate the osteogenic activity of human osteoblasts from single donors, showing that their differentiation into osteocytes depends on the initial seeding density. The synergy of the modeling techniques developed in this thesis define an innovative approach to maximize the scaffold osteointegration based on the mechanosensation of patient-specific bone cells and the local mechanical environment. Future personalized tissue engineering strategies could rely on the integration of those models to ultimately mitigate variability in the bone regeneration process guided by a patient-specific scaffold.

5.6 Conclusiones

La convergencia de la medicina personalizada y la regenerativa aporta terapias específicas para el paciente que pueden ayudar a trasladar los productos de ingeniería de tejidos a las clínicas al reducir la variabilidad del resultado clínico final. Aunque es una estrategia fascinante, un enfoque específico para el paciente requiere una comprensión profunda de todas las fuentes de variabilidad, desde la fabricación del producto hasta la respuesta del paciente, antes de aprender a mitigar esos efectos. Esta tesis ha presentado la investigación experimental realizada a lo largo de los estudios de doctorado del autor para investigar el proceso de regeneración ósea asociado a los andamios impresos en 3D específicos del paciente. La investigación experimental se basó en el uso de múltiples sistemas de modelado para comprender los efectos tanto del andamio como del paciente sobre la regeneración ósea.

Se aplicó un método computacional de regeneración ósea impulsada por un mecanismo para simular el proceso de mineralización dentro de los poros de los andamios óseos impresos en 3D en función de la interacción mecánica entre el andamio y el entorno del anfitrión, descrito por parámetros específicos del sujeto y la ubicación. Además de predecir variaciones en la distribución del crecimiento óseo cuando se inserta un andamio de titanio libre de células más cerca de la diáfisis tibial, el modelo propuso que el crecimiento óseo limitado en el núcleo del andamio se observó tanto en *in vivo* como en *in silico*, se asoció a una baja estimulación mecánica. Al modelar la capacidad de sensación mecánica tanto del individuo como del tejido óseo local, dicho modelo computacional puede guiar el diseño de andamios óseos que cumplan con los requisitos específicos del paciente.

Para comprender la variabilidad intrínseca de la respuesta del paciente, se desarrolló un sistema de hueso en chip para cultivar osteoblastos humanos primarios y evaluar su actividad osteogénica. El proceso de diferenciación hacia los osteocitos se recreó en un hidrogel de colágeno 3D donde las células, durante 21 días, experimentaron los cambios característicos de longitud de protrusión, morfología celular, proliferación, fosfatasa alcalina y secreción de proteínas. Como ya se ha observado en los sistemas de cultivo tradicionales, el aumento de la densidad de siembra celular favoreció la diferenciación de osteoblastos en osteocitos, pero los osteoblastos aislados de diferentes donantes mostraron diferencias en la actividad de la fosfatasa alcalina. Los volúmenes limitados de cultivo de tal dispositivo de microingeniería facilitan el modelado de variaciones específicas del paciente en el fenotipo de osteoblastos.

Los resultados de esta tesis proporcionan una perspectiva novedosa para evaluar el rendimiento de un producto de ingeniería de tejidos, donde las técnicas avanzadas de *in vitro* y *in silico*, combinadas con datos de *in vivo*, evalúan aspectos distintivos de el proceso de regeneración ósea para aplicaciones específicas de pacientes. Un enfoque computacional predijo, por primera vez, diferencias en la regeneración ósea para diferentes sitios de implantación de andamios y mecano-sensibilidad individual. La tecnología de hueso en chip se utilizó para evaluar la actividad osteogénica de los osteoblastos humanos de donantes únicos, lo que demuestra que su diferenciación en osteocitos depende de la densidad de siembra inicial. La sinergia de las técnicas de modelado desarrolladas en esta tesis define un enfoque innovador para maximizar la osteointegración del andamio basado en la mecanosensación de las células óseas específicas del paciente y el entorno mecánico local. Las futuras estrategias personalizadas de ingeniería de tejidos podrían depender de la integración de esos modelos para mitigar en última instancia la variabilidad en el proceso de regeneración ósea guiado por un andamio específico del paciente.

Appendix A

Mathematical formulation of mechano-driven bone regeneration

In this model, it is simulated a simultaneous process of cell invasion and bone formation regulated by the mechanical stimulus [134]. Cell invasion is treated as a diffusion process, according to Fick's law

$$\frac{\partial c}{\partial t} = D \cdot \frac{\partial^2 c}{\partial \underline{x}^2} \tag{A.1}$$

where t and $\underline{x}$ represent time and space, respectively. Cell concentration in the scaffold pores c is normalized to the maximum cell concentration, which is assumed to be in the surrounding bone tissue [141]. D is the diffusion constant, with no distinction between the single contributions of migrating cells and other cell types.

The role of mechanics on bone regulation is based on the effective tissue microstrain $\bar{\epsilon}$, calculated from the strain energy density W and the Young's modulus E [163]

$$\bar{\epsilon} = \sqrt{2 \cdot \frac{W}{E}} \cdot 10^6 \tag{A.2}$$

The daily strain history depends on the strain levels and the load cases, which defines the daily strain stimulus for bone formation Ψ

$$\Psi = \sum_{i=1}^{N} (n_i \cdot \bar{\varepsilon}^m)^{1/m} \tag{A.3}$$

where N is the number of different daily load cases, n_i is the average number of daily cycles and m is a model parameter [164].

Mechanical stimulus regulates bone deposition by the remodeling error, which is the difference between the mechanical stimulus and a reference value [63]. In this model, the local daily strain stimulus Ψ^*_{local} in the peri-implant region is the reference value above which bone formation occurs [165]. The mathematical formulation of the bone volume deposition rate inside the pores of a bone scaffold

$$\dot{V} = \begin{cases} 0, & \text{if } \Psi \leq \alpha \cdot \Psi^*_{local} \\ k \cdot (\Psi - \alpha \cdot \Psi^*_{local}), & \text{if } \Psi > \alpha \cdot \Psi^*_{local} \\ \dot{V}_{max}, & \text{if } k \cdot (\Psi - \alpha \cdot \Psi^*_{local}) \geq \dot{V}_{max} \end{cases} \tag{A.4}$$

assumes that:

- no bone resorption takes place for low mechanical stimuli [134]
- the daily strain stimulus initiating bone formation is reduced by a factor α (experimentally observed in the peri-implant region [64])
- bone formation is proportional to mechanical stimulus up to a maximum bone deposition rate $\dot{V}_{max}$ [166].

Bone formation is intrinsically related to the increase of apparent mineral density and matrix mechanical properties. The apparent density rate $\dot{\rho}$ is the product of the cell concentration, the bone volume deposition rate and the maximum bone mineral density ρ_{max} [134]

$$\dot{\rho} = \bar{c} \cdot \dot{V} \cdot \rho_{max} \tag{A.5}$$

Table A.1 lists all symbols used in this mathematical formulation as well as their physical meaning and their units.

Symbol	Meaning	Unit
c	Normalized cell concentration	$adimensional$
D	Diffusion constant	$\frac{cm^2}{s}$
W	Strain energy density	Pa
E	Young's modulus	Pa
$\bar{\epsilon}$	Effective tissue microstrain	$\mu strains$
Ψ	Daily strain stimulus for bone formation	$\mu strains$
N	Number of different daily load cases	$adimensional$
n_i	Average daily cycles	$adimensional$
m	Daily strain history parameter	$adimensional$
Ψ^*_{local}	Local daily strain stimulus in the peri-implant region	$\mu strains$
$\dot{V}$	Bone volume deposition rate inside the pores of a bone scaffold	$\frac{\% \left[\frac{mm^3_{bone}}{mm^3_{tissue}}\right]}{day}$
k	Constant of bone volume deposition rate	$\frac{\% \left[\frac{mm^3_{bone}}{mm^3_{tissue}}\right]}{\mu strains \cdot day}$
α	Fraction of reference daily stimulus	$\%$
$\dot{V}_{max}$	Maximum bone deposition rate	$\frac{\% \left[\frac{mm^3_{bone}}{mm^3_{tissue}}\right]}{day}$
$\dot{\rho}$	Bone mineral density rate	$\frac{g}{cm^3 \cdot day}$
ρ_{max}	Maximum bone mineral density	$\frac{g}{cm^3}$

Table A.1: **List of symbols used in the mechano-driven model of bone regeneration.** Symbols are listed in their order of usage in the text.

References

[1] United States Bone and Joint Initiative, *The Burden of Musculoskeletal Diseases in the United States (BMUS).* third edit ed., 2014.

[2] J. Plannel and M. Navarro, "Challenges of bone repair," in *Bone Repair Biomaterials*, pp. 3–24, Elsevier, 2009.

[3] L. J. Donaldson, I. P. Reckless, S. Scholes, J. S. Mindell, and N. J. Shelton, "The epidemiology of fractures in England," *Journal of Epidemiology & Community Health*, vol. 62, no. 2, pp. 174–180, 2008.

[4] J. Buza, "Bone healing in 2016," *Clinical Cases in Mineral and Bone Metabolism*, 2016.

[5] T. A. Einhorn, "Enhancement of fracture-healing.," *The Journal of Bone & Joint Surgery*, vol. 77, no. 6, pp. 940–956, 1995.

[6] F. Borgström, L. Karlsson, G. Ortsäter, N. Norton, P. Halbout, C. Cooper, M. Lorentzon, E. V. McCloskey, N. C. Harvey, M. K. Javaid, and J. A. Kanis, "Fragility fractures in Europe: burden, management and opportunities," *Archives of Osteoporosis*, vol. 15, no. 1, p. 59, 2020.

[7] A. S. Brydone, D. Meek, and S. Maclaine, "Bone grafting, orthopaedic biomaterials, and the clinical need for bone engineering," *Proceedings of the Institution of Mechanical Engineers, Part H: Journal of Engineering in Medicine*, vol. 224, no. 12, pp. 1329–1343, 2010.

[8] R. Iorio, B. Schwartz, W. Macaulay, S. M. Teeney, W. L. Healy, and S. York, "Surgical Treatment of Displaced Femoral Neck Fractures in the Elderly," *The Journal of Arthroplasty*, vol. 21, no. 8, pp. 1124–1133, 2006.

[9] S. Glyn-Jones, A. J. R. Palmer, R. Agricola, A. J. Price, T. L. Vincent, H. Weinans, and A. J. Carr, "Osteoarthritis," *The Lancet*, vol. 386, no. 9991, pp. 376–387, 2015.

[10] Y. Zhang and J. M. Jordan, "Epidemiology of Osteoarthritis," *Clinics in Geriatric Medicine*, vol. 26, no. 3, pp. 355–369, 2010.

[11] M. Hiligsmann, C. Cooper, N. Arden, M. Boers, J. C. Branco, M. Luisa Brandi, O. Bruyère, F. Guillemin, M. C. Hochberg, D. J. Hunter, J. A. Kanis,

T. K. Kvien, A. Laslop, J.-P. Pelletier, D. Pinto, S. Reiter-Niesert, R. Rizzoli, L. C. Rovati, J. L. H. Severens, S. Silverman, Y. Tsouderos, P. Tugwell, and J.-Y. Reginster, "Health economics in the field of osteoarthritis: An Expert's consensus paper from the European Society for Clinical and Economic Aspects of Osteoporosis and Osteoarthritis (ESCEO)," *Seminars in Arthritis and Rheumatism*, vol. 43, no. 3, pp. 303–313, 2013.

[12] L. Mirabello, R. J. Troisi, and S. A. Savage, "Osteosarcoma incidence and survival rates from 1973 to 2004," *Cancer*, vol. 115, no. 7, pp. 1531–1543, 2009.

[13] D. Biau, F. Faure, S. Katsahian, C. Jeanrot, B. Tomeno, and P. Anract, "Survival of Total Knee Replacement with a Megaprosthesis After Bone Tumor Resection," *The Journal of Bone & Joint Surgery*, vol. 88, no. 6, pp. 1285–1293, 2006.

[14] X. Li, Y. Zhang, S. Wan, H. Li, D. Li, J. Xia, Z. Yuan, M. Ren, S. Yu, S. Li, Y. Yang, L. Han, and Z. Yang, "A comparative study between limb-salvage and amputation for treating osteosarcoma," *Journal of Bone Oncology*, vol. 5, no. 1, pp. 15–21, 2016.

[15] B. Vamsi Krishna, W. Xue, S. Bose, and A. Bandyopadhyay, "Engineered porous metals for implants," *JOM*, vol. 60, no. 5, pp. 45–48, 2008.

[16] K. J. Bozic, A. F. Kamath, K. Ong, E. Lau, S. Kurtz, V. Chan, T. P. Vail, H. Rubash, and D. J. Berry, "Comparative Epidemiology of Revision Arthroplasty: Failed THA Poses Greater Clinical and Economic Burdens Than Failed TKA," *Clinical Orthopaedics and Related Research®*, vol. 473, no. 6, pp. 2131–2138, 2015.

[17] S. Kurtz, K. Ong, E. Lau, F. Mowat, and M. Halpern, "Projections of Primary and Revision Hip and Knee Arthroplasty in the United States from 2005 to 2030," *The Journal of Bone & Joint Surgery*, vol. 89, no. 4, pp. 780–785, 2007.

[18] S. Kim, "Changes in surgical loads and economic burden of hip and knee replacements in the US: 1997–2004," *Arthritis & Rheumatism*, vol. 59, no. 4, pp. 481–488, 2008.

[19] J. Muth, M. Poggie, G. Kulesha, and R. Michael Meneghini, "Novel Highly Porous Metal Technology in Artificial Hip and Knee Replacement: Processing Methodologies and Clinical Applications," *JOM*, vol. 65, no. 2, pp. 318–325, 2013.

[20] K. Willemsen, R. Nizak, H. J. Noordmans, R. M. Castelein, H. Weinans, and M. C. Kruyt, "Challenges in the design and regulatory approval of 3D-printed surgical implants: a two-case series," *The Lancet Digital Health*, vol. 1, no. 4, pp. e163–e171, 2019.

[21] C. Loebel and J. A. Burdick, "Engineering Stem and Stromal Cell Therapies for Musculoskeletal Tissue Repair," *Cell Stem Cell*, vol. 22, no. 3, pp. 325–339,

2018.

[22] A. R. Amini, C. T. Laurencin, and S. P. Nukavarapu, "Bone Tissue Engineering: Recent Advances and Challenges," *Critical Reviews in Biomedical Engineering*, vol. 40, no. 5, pp. 363–408, 2012.

[23] S. Bose, S. Vahabzadeh, and A. Bandyopadhyay, "Bone tissue engineering using 3D printing," *Materials Today*, vol. 16, no. 12, pp. 496–504, 2013.

[24] W. Reichert, B. D. Ratner, J. Anderson, A. Coury, A. S. Hoffman, C. T. Laurencin, and D. Tirrell, "2010 Panel on the Biomaterials Grand Challenges," *Journal of Biomedical Materials Research Part A*, vol. 96A, no. 2, pp. 275–287, 2011.

[25] L. S. Neves, M. T. Rodrigues, R. L. Reis, and M. E. Gomes, "Current approaches and future perspectives on strategies for the development of personalized tissue engineering therapies," *Expert Review of Precision Medicine and Drug Development*, vol. 1, no. 1, pp. 93–108, 2016.

[26] T. Aghaloo, J. Pi-Anfruns, A. Moshaverinia, D. Sim, T. Grogan, and D. Hadaya, "The Effects of Systemic Diseases and Medications on Implant Osseointegration: A Systematic Review," *The International Journal of Oral & Maxillofacial Implants*, vol. 34, pp. s35–s49, 2019.

[27] G. F. Muschler, V. P. Raut, T. E. Patterson, J. C. Wenke, and J. O. Hollinger, "The Design and Use of Animal Models for Translational Research in Bone Tissue Engineering and Regenerative Medicine," *Tissue Engineering Part B: Reviews*, vol. 16, no. 1, pp. 123–145, 2010.

[28] S. Caddeo, M. Boffito, and S. Sartori, "Tissue Engineering Approaches in the Design of Healthy and Pathological In Vitro Tissue Models," *Frontiers in Bioengineering and Biotechnology*, vol. 5, 2017.

[29] A. Boussommier-Calleja, R. Li, M. B. Chen, S. C. Wong, and R. D. Kamm, "Microfluidics: A New Tool for Modeling Cancer–Immune Interactions," *Trends in Cancer*, vol. 2, no. 1, pp. 6–19, 2016.

[30] L. Geris, "Regenerative orthopaedics: in vitro, in vivo ... in silico," *International Orthopaedics*, vol. 38, no. 9, pp. 1771–1778, 2014.

[31] L. Geris, T. Lambrechts, A. Carlier, and I. Papantoniou, "The future is digital: In silico tissue engineering," *Current Opinion in Biomedical Engineering*, vol. 6, pp. 92–98, 2018.

[32] D. B. Burr and O. Akkus, "Bone Morphology and Organization," in *Basic and Applied Bone Biology*, pp. 3–25, Elsevier, 2014.

[33] N. Reznikov, R. Shahar, and S. Weiner, "Bone hierarchical structure in three dimensions," *Acta Biomaterialia*, vol. 10, no. 9, pp. 3815–3826, 2014.

[34] R. Bartl and C. Bartl, "Structure and Architecture of Bone," in *Bone Disorders*, pp. 11–20, Cham: Springer International Publishing, 2017.

[35] X. Wang, S. Xu, S. Zhou, W. Xu, M. Leary, P. Choong, M. Qian, M. Brandt, and Y. M. Xie, "Topological design and additive manufacturing of porous metals for bone scaffolds and orthopaedic implants: A review," *Biomaterials*, vol. 83, pp. 127–141, 2016.

[36] A. Salhotra, H. N. Shah, B. Levi, and M. T. Longaker, "Mechanisms of bone development and repair," *Nature Reviews Molecular Cell Biology*, vol. 21, no. 11, pp. 696–711, 2020.

[37] F. Long, "Building strong bones: molecular regulation of the osteoblast lineage," *Nature Reviews Molecular Cell Biology*, vol. 13, no. 1, pp. 27–38, 2012.

[38] M. F. Pittenger, D. E. Discher, B. M. Péault, D. G. Phinney, J. M. Hare, and A. I. Caplan, "Mesenchymal stem cell perspective: cell biology to clinical progress," *npj Regenerative Medicine*, vol. 4, no. 1, p. 22, 2019.

[39] M. Dominici, K. Le Blanc, I. Mueller, I. Slaper-Cortenbach, F. Marini, D. Krause, R. Deans, A. Keating, D. Prockop, and E. Horwitz, "Minimal criteria for defining multipotent mesenchymal stromal cells. The International Society for Cellular Therapy position statement," *Cytotherapy*, vol. 8, no. 4, pp. 315–317, 2006.

[40] R. A. Somoza, D. Correa, and A. I. Caplan, "Roles for mesenchymal stem cells as medicinal signaling cells," *Nat Protoc*, vol. 11, no. 1, 2016.

[41] M. Crisan, S. Yap, L. Casteilla, C.-W. Chen, M. Corselli, T. S. Park, G. Andriolo, B. Sun, B. Zheng, L. Zhang, C. Norotte, P.-N. Teng, J. Traas, R. Schugar, B. M. Deasy, S. Badylak, H.-J. Bűhring, J.-P. Giacobino, L. Lazzari, J. Huard, and B. Péault, "A Perivascular Origin for Mesenchymal Stem Cells in Multiple Human Organs," *Cell Stem Cell*, vol. 3, no. 3, pp. 301–313, 2008.

[42] W. L. Grayson, B. A. Bunnell, E. Martin, T. Frazier, B. P. Hung, and J. M. Gimble, "Stromal cells and stem cells in clinical bone regeneration," *Nature Reviews Endocrinology*, vol. 11, no. 3, pp. 140–150, 2015.

[43] A. I. Caplan, "Mesenchymal Stem Cells: Time to Change the Name!," *STEM CELLS Translational Medicine*, vol. 6, no. 6, pp. 1445–1451, 2017.

[44] S. J. Roberts, N. van Gastel, G. Carmeliet, and F. P. Luyten, "Uncovering the periosteum for skeletal regeneration: The stem cell that lies beneath," *Bone*, vol. 70, pp. 10–18, 2015.

[45] T. A. Franz-Odendaal, B. K. Hall, and P. E. Witten, "Buried alive: How osteoblasts become osteocytes," *Developmental Dynamics*, vol. 235, no. 1, pp. 176–190, 2006.

[46] T. Bellido, L. I. Plotkin, and A. Bruzzaniti, "Bone Cells," in *Basic and Applied Bone Biology*, pp. 27–45, Elsevier, 2014.

[47] A. L. Mescher, *Junqueira's Basic Histology Text and Atlas*. McGraw-Hill Education, 2018.

[48] L. F. Bonewald, "The amazing osteocyte," *Journal of Bone and Mineral Research*, vol. 26, no. 2, pp. 229–238, 2011.

[49] J. C. Reichert, A. Cipitria, D. R. Epari, S. Saifzadeh, P. Krishnakanth, A. Berner, M. A. Woodruff, H. Schell, M. Mehta, M. A. Schuetz, G. N. Duda, and D. W. Hutmacher, "A Tissue Engineering Solution for Segmental Defect Regeneration in Load-Bearing Long Bones," *Science Translational Medicine*, vol. 4, no. 141, pp. 141ra93–141ra93, 2012.

[50] W. Ji, G. Kerckhofs, C. Geeroms, M. Marechal, L. Geris, and F. P. Luyten, "Deciphering the combined effect of bone morphogenetic protein 6 and calcium phosphate on bone formation capacity of periosteum derived cell-based tissue engineering constructs," *Acta Biomaterialia*, vol. 80, pp. 97–107, 2018.

[51] S. Burra, D. P. Nicolella, and J. X. Jiang, "Dark horse in osteocyte biology: Glycocalyx around the dendrites is critical for osteocyte mechanosensing," *Communicative & integrative biology*, vol. 4, no. 1, pp. 48–50, 2011.

[52] S. W. Verbruggen, T. J. Vaughan, and L. M. McNamara, "Strain amplification in bone mechanobiology: a computational investigation of the in vivo mechanics of osteocytes," *Journal of The Royal Society Interface*, vol. 9, no. 75, pp. 2735–2744, 2012.

[53] H. K. Väänänen and T. Laitala-Leinonen, "Osteoclast lineage and function," *Archives of Biochemistry and Biophysics*, vol. 473, no. 2, pp. 132–138, 2008.

[54] F. Xu and S. L. Teitelbaum, "Osteoclasts: New Insights," *Bone Research*, vol. 1, no. 1, pp. 11–26, 2013.

[55] T. Nakashima, M. Hayashi, T. Fukunaga, K. Kurata, M. Oh-hora, J. Q. Feng, L. F. Bonewald, T. Kodama, A. Wutz, E. F. Wagner, J. M. Penninger, and H. Takayanagi, "Evidence for osteocyte regulation of bone homeostasis through RANKL expression," *Nature Medicine*, vol. 17, no. 10, pp. 1231–1234, 2011.

[56] M. R. Allen and D. B. Burr, "Bone Growth, Modeling, and Remodeling," in *Basic and Applied Bone Biology*, pp. 85–100, Elsevier, 2019.

[57] R. Bartl and C. Bartl, "Modelling and Remodelling of Bone," in *Bone Disorders*, pp. 21–30, Cham: Springer International Publishing, 2017.

[58] R. Bartl and C. Bartl, "Control and Regulation of Bone Remodelling," in *Bone Disorders*, pp. 31–38, Cham: Springer International Publishing, 2017.

[59] R. B. Martin, D. B. Burr, N. A. Sharkey, and D. P. Fyhrie, "Growth, Modeling and Remodeling of Bone," in *Skeletal Tissue Mechanics*, pp. 95–173, New York, NY: Springer New York, 2015.

[60] A. G. Robling, R. Daly, R. K. Fuchs, and D. B. Burr, "Mechanical Adaptation," in *Basic and Applied Bone Biology*, pp. 203–233, Elsevier, 2019.

[61] A. G. Robling and C. H. Turner, "Mechanical Signaling for Bone Modeling and Remodeling," *Critical Reviews^{TM} in Eukaryotic Gene Expression*, vol. 19,

no. 4, pp. 319–338, 2009.

[62] H. M. Frost, “Bone "mass" and the "mechanostat": A proposal,” *The Anatomical Record*, vol. 219, no. 1, pp. 1–9, 1987.

[63] D. R. Carter and G. S. Beaupré, “Cancellous Bone,” in *Skeletal Function and Form*, vol. 13, pp. 138–160, Cambridge University Press, 2000.

[64] Z. Li, D. Betts, G. Kuhn, M. Schirmer, R. Müller, and D. Ruffoni, “Mechanical regulation of bone formation and resorption around implants in a mouse model of osteopenic bone,” *Journal of The Royal Society Interface*, vol. 16, no. 152, p. 20180667, 2019.

[65] R. Bartl and C. Bartl, “Fracture Healing,” in *Bone Disorders*, pp. 239–242, Cham: Springer International Publishing, 2017.

[66] J. Li, M. A. Kacena, and D. L. Stocum, “Fracture Healing,” in *Basic and Applied Bone Biology*, pp. 235–253, Elsevier, 2019.

[67] D. S. Sparks, S. Saifzadeh, F. M. Savi, C. E. Dlaska, A. Berner, J. Henkel, J. C. Reichert, M. Wullschleger, J. Ren, A. Cipitria, J. A. McGovern, R. Steck, M. Wagels, M. A. Woodruff, M. A. Schuetz, and D. W. Hutmacher, “A preclinical large-animal model for the assessment of critical-size load-bearing bone defect reconstruction,” *Nature Protocols*, vol. 15, no. 3, pp. 877–924, 2020.

[68] R. Mora, L. Pedrotti, and G. B. Galli, “Failure of Union,” in *Nonunion of the Long Bones*, pp. 27–37, Milan: Springer-Verlag, 2006.

[69] D. Holmes, “Closing the gap,” *Nature*, vol. 550, no. 7677, pp. S194–S195, 2017.

[70] R. Langer and J. Vacanti, “Tissue engineering,” *Science*, vol. 260, no. 5110, pp. 920–926, 1993.

[71] M. A. Woodruff, C. Lange, J. Reichert, A. Berner, F. Chen, P. Fratzl, J.-T. Schantz, and D. W. Hutmacher, “Bone tissue engineering: from bench to bedside,” *Materials Today*, vol. 15, no. 10, pp. 430–435, 2012.

[72] F. J. O’Brien, “Biomaterials & scaffolds for tissue engineering,” *Materials Today*, vol. 14, no. 3, pp. 88–95, 2011.

[73] T.-M. De Witte, L. E. Fratila-Apachitei, A. A. Zadpoor, and N. A. Peppas, “Bone tissue engineering via growth factor delivery: from scaffolds to complex matrices,” *Regenerative Biomaterials*, vol. 5, no. 4, pp. 197–211, 2018.

[74] T. Dvir, B. P. Timko, D. S. Kohane, and R. Langer, “Nanotechnological strategies for engineering complex tissues,” *Nature Nanotechnology*, vol. 6, no. 1, pp. 13–22, 2011.

[75] C. T. Laurencin and Y. Khan, “Regenerative Engineering,” *Science Translational Medicine*, vol. 4, no. 160, pp. 160ed9–160ed9, 2012.

[76] J. A. Burdick, R. L. Mauck, J. H. Gorman, and R. C. Gorman, "Acellular Biomaterials: An Evolving Alternative to Cell-Based Therapies," *Science Translational Medicine*, vol. 5, no. 176, pp. 176ps4–176ps4, 2013.

[77] Y. S. Kim, M. M. Smoak, A. J. Melchiorri, and A. G. Mikos, "An Overview of the Tissue Engineering Market in the United States from 2011 to 2018," *Tissue Engineering Part A*, vol. 25, no. 1-2, pp. 1–8, 2019.

[78] A. I. Smits and C. V. Bouten, "Tissue engineering meets immunoengineering: Prospective on personalized in situ tissue engineering strategies," *Current Opinion in Biomedical Engineering*, vol. 6, pp. 17–26, 2018.

[79] M. Bez, D. Sheyn, W. Tawackoli, P. Avalos, G. Shapiro, J. C. Giaconi, X. Da, S. B. David, J. Gavrity, H. A. Awad, H. W. Bae, E. J. Ley, T. J. Kremen, Z. Gazit, K. W. Ferrara, G. Pelled, and D. Gazit, "In situ bone tissue engineering via ultrasound-mediated gene delivery to endogenous progenitor cells in mini-pigs," *Science Translational Medicine*, vol. 9, no. 390, p. eaal3128, 2017.

[80] T. B. Wissing, V. Bonito, C. V. C. Bouten, and A. I. P. M. Smits, "Biomaterial-driven in situ cardiovascular tissue engineering—a multi-disciplinary perspective," *npj Regenerative Medicine*, vol. 2, no. 1, p. 18, 2017.

[81] H. Xia, X. Li, W. Gao, X. Fu, R. H. Fang, L. Zhang, and K. Zhang, "Tissue repair and regeneration with endogenous stem cells," *Nature Reviews Materials*, vol. 3, no. 7, pp. 174–193, 2018.

[82] G. L. Koons, M. Diba, and A. G. Mikos, "Materials design for bone-tissue engineering," *Nature Reviews Materials*, 2020.

[83] M. Zhang, R. Lin, X. Wang, J. Xue, C. Deng, C. Feng, H. Zhuang, J. Ma, C. Qin, L. Wan, J. Chang, and C. Wu, "3D printing of Haversian bone–mimicking scaffolds for multicellular delivery in bone regeneration," *Science Advances*, vol. 6, no. 12, p. eaaz6725, 2020.

[84] Z. M. Jessop, A. Al-Sabah, W. R. Francis, and I. S. Whitaker, "Transforming healthcare through regenerative medicine," *BMC Medicine*, vol. 14, no. 1, p. 115, 2016.

[85] F. Fernández-Avilés, R. Sanz-Ruiz, A. M. Climent, L. Badimon, R. Bolli, D. Charron, V. Fuster, S. Janssens, J. Kastrup, H.-S. Kim, T. F. Lüscher, J. F. Martin, P. Menasché, R. D. Simari, G. W. Stone, A. Terzic, J. T. Willerson, J. C. Wu, F. Fernández-Avilés, A. Terzic, L. Badimon, K. Broughton, D. L. DiFede, S. Dimmeler, R. Madonna, M. S. Penn, M. A. Sussman, J. P. Sluijter, K. C. Wollert, W. Balkan, R. Bolli, S. Chamuleau, D. Charron, M. E. Fernández-Santos, V. Fuster, G. Goliasch, M. Gyöngyösi, J. M. Hare, T. F. Lüscher, B. A. Tompkins, J. Winkler, A. Bayés-Genís, T. D. Henry, D. A. Taylor, A. M. Climent, A. Lerman, B. Pelacho, F. Prosper, R. Sanz-Ruiz, E. C. Perin, G. Pompilio, B. Gersh, J. Bartunek, E. Duckers, P. Ferdinandy,

S. Janssens, D. W. Losordo, P. L. Sánchez, W. Sherman, W. Wojakowski, A. Zeiher, J. Kastrup, J. Roncalli, A. Mathur, F. Crea, D. D´Amario, T. J. Povsic, J. Traverse, and S. Ylä-Herttuala, "Global position paper on cardiovascular regenerative medicine," *European Heart Journal*, vol. 38, no. 33, pp. 2532–2546, 2017.

[86] M. Hackmann, T. Wizemann, and S. H. Beachy, eds., *Exploring Sources of Variability Related to the Clinical Translation of Regenerative Engineering Products*. Washington, D.C.: National Academies Press, 2019.

[87] H. Razi, A. I. Birkhold, R. Weinkamer, G. N. Duda, B. M. Willie, and S. Checa, "Aging Leads to a Dysregulation in Mechanically Driven Bone Formation and Resorption," *Journal of Bone and Mineral Research*, vol. 30, no. 10, pp. 1864–1873, 2015.

[88] K. Newell, J. Chitty, and F. M. Henson, ""Patient reported outcomes" following experimental surgery-using telemetry to assess movement in experimental ovine models," *Journal of Orthopaedic Research®*, vol. 36, no. 5, pp. 1498–1507, 2018.

[89] N. Reznikov, O. R. Boughton, S. Ghouse, A. E. Weston, L. Collinson, G. W. Blunn, J. R. Jeffers, J. P. Cobb, and M. M. Stevens, "Individual response variations in scaffold-guided bone regeneration are determined by independent strain- and injury-induced mechanisms," *Biomaterials*, vol. 194, pp. 183–194, 2019.

[90] B. Zhang, A. Korolj, B. F. L. Lai, and M. Radisic, "Advances in organ-on-a-chip engineering," *Nature Reviews Materials*, vol. 3, no. 8, pp. 257–278, 2018.

[91] A. van den Berg, C. L. Mummery, R. Passier, and A. D. van der Meer, "Personalised organs-on-chips: functional testing for precision medicine," *Lab on a Chip*, vol. 19, no. 2, pp. 198–205, 2019.

[92] A. Williamson, S. Singh, U. Fernekorn, and A. Schober, "The future of the patient-specific Body-on-a-chip," *Lab on a Chip*, vol. 13, no. 18, p. 3471, 2013.

[93] A. A. Zadpoor, "Additively manufactured porous metallic biomaterials," *Journal of Materials Chemistry B*, vol. 7, no. 26, pp. 4088–4117, 2019.

[94] J. Henkel, M. A. Woodruff, D. R. Epari, R. Steck, V. Glatt, I. C. Dickinson, P. F. M. Choong, M. A. Schuetz, and D. W. Hutmacher, "Bone Regeneration Based on Tissue Engineering Conceptions — A 21st Century Perspective," *Bone Research*, vol. 1, no. 3, pp. 216–248, 2013.

[95] A. Zadpoor, "Design for Additive Bio-Manufacturing: From Patient-Specific Medical Devices to Rationally Designed Meta-Biomaterials," *International Journal of Molecular Sciences*, vol. 18, no. 8, p. 1607, 2017.

[96] S. Amin Yavari, J. van der Stok, Y. C. Chai, R. Wauthle, Z. Tahmasebi Birgani, P. Habibovic, M. Mulier, J. Schrooten, H. Weinans, and A. A. Zadpoor, "Bone

regeneration performance of surface-treated porous titanium," *Biomaterials*, vol. 35, no. 24, pp. 6172–6181, 2014.

[97] M. Croes, S. Bakhshandeh, I. van Hengel, K. Lietaert, K. van Kessel, B. Pouran, B. van der Wal, H. Vogely, W. Van Hecke, A. Fluit, C. Boel, J. Alblas, A. Zadpoor, H. Weinans, and S. Amin Yavari, "Antibacterial and immunogenic behavior of silver coatings on additively manufactured porous titanium," *Acta Biomaterialia*, vol. 81, pp. 315–327, 2018.

[98] A. A. Zadpoor, "Bone tissue regeneration: The role of scaffold geometry," *Biomaterials Science*, vol. 3, no. 2, pp. 231–245, 2015.

[99] S. Ghouse, N. Reznikov, O. R. Boughton, S. Babu, K. C. Ng, G. Blunn, J. P. Cobb, M. M. Stevens, and J. R. Jeffers, "The design and in vivo testing of a locally stiffness-matched porous scaffold," *Applied Materials Today*, vol. 15, pp. 377–388, 2019.

[100] J. M. G. Aznar, C. Valero, C. Borau, and N. Garijo, "Computational mechano-chemo-biology: a tool for the design of tissue scaffolds," *Biomanufacturing Reviews*, vol. 1, no. 1, p. 2, 2016.

[101] D. Huh, G. A. Hamilton, and D. E. Ingber, "From 3D cell culture to organs-on-chips," *Trends in Cell Biology*, vol. 21, no. 12, pp. 745–754, 2011.

[102] Y. Shin, S. Han, J. Jeon, K. Yamamoto, I. Zervantonakis, R. Sudo, R. Kamm, and S. Chung, "Microfluidic assay for simultaneous culture of multiple cell types on surfaces or within hydrogels," *Nature Protocols*, vol. 7, no. 7, pp. 1247–1259, 2012.

[103] E. W. Esch, A. Bahinski, and D. Huh, "Organs-on-chips at the frontiers of drug discovery," *Nature Reviews Drug Discovery*, vol. 14, no. 4, pp. 248–260, 2015.

[104] B. Harink, S. Le Gac, R. Truckenmüller, C. van Blitterswijk, and P. Habibovic, "Regeneration-on-a-chip? The perspectives on use of microfluidics in regenerative medicine," *Lab on a Chip*, vol. 13, no. 18, p. 3512, 2013.

[105] G. D. Vatine, R. Barrile, M. J. Workman, S. Sances, B. K. Barriga, M. Rahnama, S. Barthakur, M. Kasendra, C. Lucchesi, J. Kerns, N. Wen, W. R. Spivia, Z. Chen, J. Van Eyk, and C. N. Svendsen, "Human iPSC-Derived Blood-Brain Barrier Chips Enable Disease Modeling and Personalized Medicine Applications," *Cell Stem Cell*, vol. 24, no. 6, pp. 995–1005.e6, 2019.

[106] K. H. Benam, R. Villenave, C. Lucchesi, A. Varone, C. Hubeau, H.-H. Lee, S. E. Alves, M. Salmon, T. C. Ferrante, J. C. Weaver, A. Bahinski, G. A. Hamilton, and D. E. Ingber, "Small airway-on-a-chip enables analysis of human lung inflammation and drug responses in vitro," *Nature Methods*, vol. 13, no. 2, pp. 151–157, 2016.

[107] W. Zhang, W. Y. Lee, D. S. Siegel, P. Tolias, and J. Zilberberg, "Patient-Specific 3D Microfluidic Tissue Model for Multiple Myeloma," *Tissue Engineering Part C: Methods*, vol. 20, no. 8, pp. 663–670, 2014.

[108] "On-chip recapitulation of clinical bone marrow toxicities and patient-specific pathophysiology," *Nature Biomedical Engineering*, vol. 4, no. 4, pp. 394–406, 2020.

[109] A. Mansoorifar, R. Gordon, R. C. Bergan, and L. E. Bertassoni, "Bone-on-a-Chip: Microfluidic Technologies and Microphysiologic Models of Bone Tissue," *Advanced Functional Materials*, p. 2006796, 2020.

[110] L. You, S. Temiyasathit, P. Lee, C. H. Kim, P. Tummala, W. Yao, W. Kingery, A. M. Malone, R. Y. Kwon, and C. R. Jacobs, "Osteocytes as mechanosensors in the inhibition of bone resorption due to mechanical loading," *Bone*, vol. 42, no. 1, pp. 172–179, 2008.

[111] Q. Sun, S. Choudhary, C. Mannion, Y. Kissin, J. Zilberberg, and W. Lee, "Ex vivo construction of human primary 3D–networked osteocytes," *Bone*, vol. 105, pp. 245–252, 2017.

[112] E. Leclerc, B. David, L. Griscom, B. Lepioufle, T. Fujii, P. Layrolle, and C. Legallaisa, "Study of osteoblastic cells in a microfluidic environment," *Biomaterials*, vol. 27, no. 4, pp. 586–595, 2006.

[113] S. Hao, L. Ha, G. Cheng, Y. Wan, Y. Xia, D. M. Sosnoski, A. M. Mastro, and S. Y. Zheng, "A Spontaneous 3D Bone-On-a-Chip for Bone Metastasis Study of Breast Cancer Cells," *Small*, vol. 14, no. 12, pp. 1–10, 2018.

[114] J. S. Jeon, S. Bersini, M. Gilardi, G. Dubini, J. L. Charest, M. Moretti, and R. D. Kamm, "Human 3D vascularized organotypic microfluidic assays to study breast cancer cell extravasation," *Proceedings of the National Academy of Sciences*, vol. 112, no. 1, pp. 214–219, 2015.

[115] E. Sano, C. Mori, Y. Nashimoto, R. Yokokawa, H. Kotera, and Y.-s. Torisawa, "Engineering of vascularized 3D cell constructs to model cellular interactions through a vascular network," *Biomicrofluidics*, vol. 12, no. 4, p. 042204, 2018.

[116] X. Shi, J. Zhou, Y. Zhao, L. Li, and H. Wu, "Gradient-Regulated Hydrogel for Interface Tissue Engineering: Steering Simultaneous Osteo/Chondrogenesis of Stem Cells on a Chip," *Advanced Healthcare Materials*, vol. 2, no. 6, pp. 846–853, 2013.

[117] X. Mei, K. Middleton, D. Shim, Q. Wan, L. Xu, Y.-H. V. Ma, D. Devadas, N. Walji, L. Wang, E. W. K. Young, and L. You, "Microfluidic platform for studying osteocyte mechanoregulation of breast cancer bone metastasis," *Integrative Biology*, vol. 11, no. 4, pp. 119–129, 2019.

[118] S. Bersini, J. S. Jeon, G. Dubini, C. Arrigoni, S. Chung, J. L. Charest, M. Moretti, and R. D. Kamm, "A microfluidic 3D in vitro model for specificity of breast cancer metastasis to bone," *Biomaterials*, vol. 35, no. 8, pp. 2454–2461, 2014.

[119] Y. Zheng, Y. Sun, X. Yu, Y. Shao, P. Zhang, G. Dai, and J. Fu, "Angiogenesis in Liquid Tumors: An In Vitro Assay for Leukemic-Cell-Induced Bone Marrow

Angiogenesis," *Advanced Healthcare Materials*, vol. 5, no. 9, pp. 1014–1024, 2016.

[120] A. Bruce, R. Evans, R. Mezan, L. Shi, B. S. Moses, K. H. Martin, L. F. Gibson, and Y. Yang, "Three-Dimensional Microfluidic Tri-Culture Model of the Bone Marrow Microenvironment for Study of Acute Lymphoblastic Leukemia," *PLOS ONE*, vol. 10, no. 10, p. e0140506, 2015.

[121] J. Ahn, J. Lim, N. Jusoh, J. Lee, T.-E. Park, Y. Kim, J. Kim, and N. L. Jeon, "3D Microfluidic Bone Tumor Microenvironment Comprised of Hydroxyapatite/Fibrin Composite," *Frontiers in Bioengineering and Biotechnology*, vol. 7, 2019.

[122] Y.-s. Torisawa, C. S. Spina, T. Mammoto, A. Mammoto, J. C. Weaver, T. Tat, J. J. Collins, and D. E. Ingber, "Bone marrow–on–a–chip replicates hematopoietic niche physiology in vitro," *Nature Methods*, vol. 11, no. 6, pp. 663–669, 2014.

[123] C. Del Amo, V. Olivares, M. Cóndor, A. Blanco, J. Santolaria, J. Asín, C. Borau, and J. M. García-Aznar, "Matrix architecture plays a pivotal role in 3D osteoblast migration: The effect of interstitial fluid flow," *Journal of the Mechanical Behavior of Biomedical Materials*, vol. 83, pp. 52–62, 2018.

[124] N. Movilla, C. Borau, C. Valero, and J. García-Aznar, "Degradation of extracellular matrix regulates osteoblast migration: A microfluidic-based study," *Bone*, vol. 107, pp. 10–17, 2018.

[125] D. Yoon, H. Kim, E. Lee, M. H. Park, S. Chung, H. Jeon, C.-H. Ahn, and K. Lee, "Study on chemotaxis and chemokinesis of bone marrow-derived mesenchymal stem cells in hydrogel-based 3D microfluidic devices," *Biomaterials Research*, vol. 20, no. 1, p. 25, 2016.

[126] C. Moraes, G. Mehta, S. C. Lesher-Perez, and S. Takayama, "Organs-on-a-Chip: A Focus on Compartmentalized Microdevices," *Annals of Biomedical Engineering*, vol. 40, no. 6, pp. 1211–1227, 2012.

[127] R. R. Rao, A. W. Peterson, J. Ceccarelli, A. J. Putnam, and J. P. Stegemann, "Matrix composition regulates three-dimensional network formation by endothelial cells and mesenchymal stem cells in collagen/fibrin materials," *Angiogenesis*, vol. 15, no. 2, pp. 253–264, 2012.

[128] Z. Zhao, C. Vizetto-Duarte, Z. K. Moay, M. I. Setyawati, M. Rakshit, M. H. Kathawala, and K. W. Ng, "Composite Hydrogels in Three-Dimensional in vitro Models," *Frontiers in Bioengineering and Biotechnology*, vol. 8, 2020.

[129] N. Jusoh, S. Oh, S. Kim, J. Kim, and N. L. Jeon, "Microfluidic vascularized bone tissue model with hydroxyapatite-incorporated extracellular matrix," *Lab on a Chip*, vol. 15, no. 20, pp. 3984–3988, 2015.

[130] S. Giannitelli, D. Accoto, M. Trombetta, and A. Rainer, "Current trends in the design of scaffolds for computer-aided tissue engineering," *Acta Biomaterialia*, vol. 10, no. 2, pp. 580–594, 2014.

[131] A. Carlier, L. Geris, J. Lammens, and H. Van Oosterwyck, “Bringing computational models of bone regeneration to the clinic,” *Wiley Interdisciplinary Reviews: Systems Biology and Medicine*, vol. 7, no. 4, pp. 183–194, 2015.

[132] A. Carlier, Y. Chai, M. Moesen, T. Theys, J. Schrooten, H. Van Oosterwyck, and L. Geris, “Designing optimal calcium phosphate scaffold–cell combinations using an integrative model-based approach,” *Acta Biomaterialia*, vol. 7, no. 10, pp. 3573–3585, 2011.

[133] D. C. Betts and R. Müller, “Mechanical Regulation of Bone Regeneration: Theories, Models, and Experiments,” *Frontiers in Endocrinology*, vol. 5, 2014.

[134] J. A. Sanz-Herrera, J. M. García-Aznar, and M. Doblaré, “A mathematical model for bone tissue regeneration inside a specific type of scaffold,” *Biomechanics and Modeling in Mechanobiology*, vol. 7, no. 5, pp. 355–366, 2008.

[135] W. J. Hendrikson, A. J. Deegan, Y. Yang, C. A. van Blitterswijk, N. Verdonschot, L. Moroni, and J. Rouwkema, “Influence of Additive Manufactured Scaffold Architecture on the Distribution of Surface Strains and Fluid Flow Shear Stresses and Expected Osteochondral Cell Differentiation,” *Frontiers in Bioengineering and Biotechnology*, vol. 5, 2017.

[136] F. Zhao, M. J. Mc Garrigle, T. J. Vaughan, and L. M. McNamara, “In silico study of bone tissue regeneration in an idealised porous hydrogel scaffold using a mechano-regulation algorithm,” *Biomechanics and Modeling in Mechanobiology*, vol. 17, no. 1, pp. 5–18, 2018.

[137] F. Zhao, T. J. Vaughan, and L. M. Mcnamara, “Multiscale fluid–structure interaction modelling to determine the mechanical stimulation of bone cells in a tissue engineered scaffold,” *Biomechanics and Modeling in Mechanobiology*, vol. 14, no. 2, pp. 231–243, 2015.

[138] C. Perier-Metz, G. N. Duda, and S. Checa, “Mechano-Biological Computer Model of Scaffold-Supported Bone Regeneration: Effect of Bone Graft and Scaffold Structure on Large Bone Defect Tissue Patterning,” *Frontiers in Bioengineering and Biotechnology*, vol. 8, 2020.

[139] F. O. Ribeiro, M. J. Gómez-Benito, J. Folgado, P. R. Fernandes, and J. M. García-Aznar, “In silico Mechano-Chemical Model of Bone Healing for the Regeneration of Critical Defects: The Effect of BMP-2,” *PLOS ONE*, vol. 10, no. 6, p. e0127722, 2015.

[140] L. Wang, Q. Shi, Y. Cai, Q. Chen, X. Guo, and Z. Li, “Mechanical–chemical coupled modeling of bone regeneration within a biodegradable polymer scaffold loaded with VEGF,” *Biomechanics and Modeling in Mechanobiology*, vol. 19, no. 6, pp. 2285–2306, 2020.

[141] J. A. Sanz-Herrera, J. M. García-Aznar, and M. Doblaré, “On scaffold designing for bone regeneration: A computational multiscale approach,” *Acta*

Biomaterialia, vol. 5, no. 1, pp. 219–229, 2009.

[142] A. Boccaccio, A. E. Uva, M. Fiorentino, G. Mori, and G. Monno, "Geometry Design Optimization of Functionally Graded Scaffolds for Bone Tissue Engineering: A Mechanobiological Approach," *PLOS ONE*, vol. 11, no. 1, p. e0146935, 2016.

[143] M. Bashkuev, S. Checa, S. Postigo, G. Duda, and H. Schmidt, "Computational analyses of different intervertebral cages for lumbar spinal fusion," *Journal of Biomechanics*, vol. 48, no. 12, pp. 3274–3282, 2015.

[144] A.-M. Pobloth, S. Checa, H. Razi, A. Petersen, J. C. Weaver, K. Schmidt-Bleek, M. Windolf, A. Á. Tatai, C. P. Roth, K.-D. Schaser, G. N. Duda, and P. Schwabe, "Mechanobiologically optimized 3D titanium-mesh scaffolds enhance bone regeneration in critical segmental defects in sheep," *Science Translational Medicine*, vol. 10, no. 423, p. eaam8828, 2018.

[145] F. Zhao, T. J. Vaughan, and L. M. McNamara, "Quantification of fluid shear stress in bone tissue engineering scaffolds with spherical and cubical pore architectures," *Biomechanics and Modeling in Mechanobiology*, vol. 15, no. 3, pp. 561–577, 2016.

[146] A. P. Md Saad, R. A. Abdul Rahim, M. N. Harun, H. Basri, J. Abdullah, M. R. Abdul Kadir, and A. Syahrom, "The influence of flow rates on the dynamic degradation behaviour of porous magnesium under a simulated environment of human cancellous bone," *Materials & Design*, vol. 122, pp. 268–279, 2017.

[147] Q. Shi, H. Shui, Q. Chen, and Z.-Y. Li, "How does mechanical stimulus affect the coupling process of the scaffold degradation and bone formation: An in silico approach," *Computers in Biology and Medicine*, vol. 117, p. 103588, 2020.

[148] C. Metz, G. N. Duda, and S. Checa, "Towards multi-dynamic mechano-biological optimization of 3D-printed scaffolds to foster bone regeneration," *Acta Biomaterialia*, vol. 101, pp. 117–127, 2020.

[149] G. Nasello, A. Vautrin, J. Pitocchi, M. Wesseling, J. H. Kuiper, M. Á. Pérez, and J. M. García-Aznar, "Mechano-driven regeneration predicts response variations in large animal model based on scaffold implantation site and individual mechano-sensitivity," *Bone*, p. 115769, 2020.

[150] L. Zhang, G. Yang, B. N. Johnson, and X. Jia, "Three-dimensional (3D) printed scaffold and material selection for bone repair," *Acta Biomaterialia*, vol. 84, pp. 16–33, 2019.

[151] C. N. Kelly, J. Francovich, S. Julmi, D. Safranski, R. E. Guldberg, H. J. Maier, and K. Gall, "Fatigue behavior of As-built selective laser melted titanium scaffolds with sheet-based gyroid microarchitecture for bone tissue engineering," *Acta Biomaterialia*, vol. 94, pp. 610–626, 2019.

[152] C. Turner, "Three rules for bone adaptation to mechanical stimuli," *Bone*, vol. 23, no. 5, pp. 399–407, 1998.

[153] X.-Y. Zhang, X.-C. Yan, G. Fang, and M. Liu, "Biomechanical influence of structural variation strategies on functionally graded scaffolds constructed with triply periodic minimal surface," *Additive Manufacturing*, vol. 32, p. 101015, 2020.

[154] A. I. Birkhold, H. Razi, G. N. Duda, R. Weinkamer, S. Checa, and B. M. Willie, "The influence of age on adaptive bone formation and bone resorption," *Biomaterials*, vol. 35, no. 34, pp. 9290–9301, 2014.

[155] E. Seeman, "Bone quality: the material and structural basis of bone strength," *Journal of Bone and Mineral Metabolism*, vol. 26, no. 1, pp. 1–8, 2008.

[156] G. R. Cointry, L. Nocciolino, A. Ireland, N. M. Hall, A. Kriechbaumer, J. L. Ferretti, J. Rittweger, and R. F. Capozza, "Structural differences in cortical shell properties between upper and lower human fibula as described by pQCT serial scans. A biomechanical interpretation," *Bone*, vol. 90, pp. 185–194, 2016.

[157] J. L. Schriefer, S. J. Warden, L. K. Saxon, A. G. Robling, and C. H. Turner, "Cellular accommodation and the response of bone to mechanical loading," *Journal of Biomechanics*, vol. 38, no. 9, pp. 1838–1845, 2005.

[158] J. M. García-Aznar, M. J. Gómez-Benito, M. Á. Pérez, and M. Doblaré, "Mechanobiological Models for Bone Tissue. Applications to Implant Design," in *Biomechanics of Hard Tissues*, pp. 123–143, Weinheim, Germany: Wiley-VCH Verlag GmbH & Co. KGaA, 2010.

[159] L. Geris, J. Vander Sloten, and H. Van Oosterwyck, "Connecting biology and mechanics in fracture healing: an integrated mathematical modeling framework for the study of nonunions," *Biomechanics and Modeling in Mechanobiology*, vol. 9, no. 6, pp. 713–724, 2010.

[160] Y. Chen, S. Zhou, and Q. Li, "Microstructure design of biodegradable scaffold and its effect on tissue regeneration," *Biomaterials*, vol. 32, no. 22, pp. 5003–5014, 2011.

[161] S. Sturm, S. Zhou, Y.-W. Mai, and Q. Li, "On stiffness of scaffolds for bone tissue engineering—a numerical study," *Journal of Biomechanics*, vol. 43, no. 9, pp. 1738–1744, 2010.

[162] A. Carriero, A. Pereira, A. Wilson, S. Castagno, B. Javaheri, A. Pitsillides, M. Marenzana, and S. Shefelbine, "Spatial relationship between bone formation and mechanical stimulus within cortical bone: Combining 3D fluorochrome mapping and poroelastic finite element modelling," *Bone Reports*, vol. 8, pp. 72–80, 2018.

[163] W. Pistoia, B. van Rietbergen, E.-M. Lochmüller, C. Lill, F. Eckstein, and P. Rüegsegger, "Estimation of distal radius failure load with micro-finite element analysis models based on three-dimensional peripheral quantitative computed tomography images," *Bone*, vol. 30, no. 6, pp. 842–848, 2002.

[164] J. M. García-Aznar, T. Rueberg, and M. Doblare, "A bone remodelling model coupling microdamage growth and repair by 3D BMU-activity," *Biomechanics and Modeling in Mechanobiology*, vol. 4, no. 2-3, pp. 147–167, 2005.

[165] T. Adachi, Y. Osako, M. Tanaka, M. Hojo, and S. J. Hollister, "Framework for optimal design of porous scaffold microstructure by computational simulation of bone regeneration," *Biomaterials*, vol. 27, no. 21, pp. 3964–3972, 2006.

[166] T. Adachi, Y. Kameo, and M. Hojo, "Trabecular bone remodelling simulation considering osteocytic response to fluid-induced shear stress.," *Philosophical transactions. Series A, Mathematical, physical, and engineering sciences*, vol. 368, no. 1920, pp. 2669–82, 2010.

[167] "ABAQUS/Standard User's Manual, Version 6.14," 2010.

[168] M. Sonnaert, G. Kerckhofs, I. Papantoniou, S. Van Vlierberghe, V. Boterberg, P. Dubruel, F. P. Luyten, J. Schrooten, and L. Geris, "Multifactorial Optimization of Contrast-Enhanced Nanofocus Computed Tomography for Quantitative Analysis of Neo-Tissue Formation in Tissue Engineering Constructs," *PLOS ONE*, vol. 10, no. 6, p. e0130227, 2015.

[169] J. M. Anderson, A. Rodriguez, and D. T. Chang, "Foreign body reaction to biomaterials," *Seminars in Immunology*, vol. 20, no. 2, pp. 86–100, 2008.

[170] E. C. Pegg and H. S. Gill, "An open source software tool to assign the material properties of bone for ABAQUS finite element simulations," *Journal of Biomechanics*, vol. 49, no. 13, pp. 3116–3121, 2016.

[171] B. Helgason, F. Taddei, H. Pálsson, E. Schileo, L. Cristofolini, M. Viceconti, and S. Brynjólfsson, "A modified method for assigning material properties to FE models of bones," *Medical Engineering & Physics*, vol. 30, no. 4, pp. 444–453, 2008.

[172] E. F. Morgan, H. H. Bayraktar, and T. M. Keaveny, "Trabecular bone modulus–density relationships depend on anatomic site," *Journal of Biomechanics*, vol. 36, no. 7, pp. 897–904, 2003.

[173] E. Schileo, F. Taddei, A. Malandrino, L. Cristofolini, and M. Viceconti, "Subject-specific finite element models can accurately predict strain levels in long bones," *Journal of Biomechanics*, vol. 40, no. 13, pp. 2982–2989, 2007.

[174] E. Schileo, F. Taddei, L. Cristofolini, and M. Viceconti, "Subject-specific finite element models implementing a maximum principal strain criterion are able to estimate failure risk and fracture location on human femurs tested in vitro," *Journal of Biomechanics*, vol. 41, no. 2, pp. 356–367, 2008.

[175] E. Schileo, E. Dall'Ara, F. Taddei, A. Malandrino, T. Schotkamp, M. Baleani, and M. Viceconti, "An accurate estimation of bone density improves the accuracy of subject-specific finite element models," *Journal of Biomechanics*, vol. 41, no. 11, pp. 2483–2491, 2008.

[176] J. Victor, D. Van Doninck, L. Labey, B. Innocenti, P. Parizel, and J. Bellemans, "How precise can bony landmarks be determined on a CT scan of the knee?," *The Knee*, vol. 16, no. 5, pp. 358–365, 2009.

[177] J. Victor, D. Van Doninck, L. Labey, F. Van Glabbeek, P. Parizel, and J. Bellemans, "A common reference frame for describing rotation of the distal femur," *The Journal of Bone and Joint Surgery. British volume*, vol. 91-B, no. 5, pp. 683–690, 2009.

[178] E. S. Grood and W. J. Suntay, "A Joint Coordinate System for the Clinical Description of Three-Dimensional Motions: Application to the Knee," *Journal of Biomechanical Engineering*, vol. 105, no. 2, pp. 136–144, 1983.

[179] A. D. Speirs, M. O. Heller, G. N. Duda, and W. R. Taylor, "Physiologically based boundary conditions in finite element modelling," *Journal of Biomechanics*, vol. 40, no. 10, pp. 2318–2323, 2007.

[180] G. N. Duda, K. Eckert-Hübner, R. Sokiranski, A. Kreutner, R. Miller, and L. Claes, "Analysis of inter-fragmentary movement as a function of musculoskeletal loading conditions in sheep," *Journal of Biomechanics*, vol. 31, no. 3, pp. 201–210, 1997.

[181] Z. F. Lerner, B. C. Gadomski, A. K. Ipson, K. K. Haussler, C. M. Puttlitz, and R. C. Browning, "Modulating tibiofemoral contact force in the sheep hind limb via treadmill walking: Predictions from an opensim musculoskeletal model," *Journal of Orthopaedic Research*, vol. 33, no. 8, pp. 1128–1133, 2015.

[182] V. Vanheule, H. P. Delport, M. S. Andersen, L. Scheys, R. Wirix-Speetjens, I. Jonkers, J. Victor, and J. Vander Sloten, "Evaluation of predicted knee function for component malrotation in total knee arthroplasty," *Medical Engineering & Physics*, vol. 40, pp. 56–64, 2017.

[183] A. Vahdati, S. Walscharts, I. Jonkers, J. Garcia-Aznar, J. Vander Sloten, and G. van Lenthe, "Role of subject-specific musculoskeletal loading on the prediction of bone density distribution in the proximal femur," *Journal of the Mechanical Behavior of Biomedical Materials*, vol. 30, pp. 244–252, 2014.

[184] M. Berli, C. Borau, O. Decco, G. Adams, R. B. Cook, J. M. García Aznar, and P. Zioupos, "Localized tissue mineralization regulated by bone remodelling: A computational approach," *PLOS ONE*, vol. 12, no. 3, p. e0173228, 2017.

[185] L. Geris, A. Gerisch, J. V. Sloten, R. Weiner, and H. V. Oosterwyck, "Angiogenesis in bone fracture healing: A bioregulatory model," *Journal of Theoretical Biology*, vol. 251, no. 1, pp. 137–158, 2008.

[186] K. Mohaghegh, M. A. Pérez, and J. M. García-Aznar, "Accelerating numerical simulations of strain-adaptive bone remodeling predictions," *Computer Methods in Applied Mechanics and Engineering*, vol. 273, pp. 255–272, 2014.

[187] J. Z. Bakdash and L. R. Marusich, "Repeated Measures Correlation," *Frontiers in Psychology*, vol. 8, 2017.

[188] J. Currey, "The many adaptations of bone," *Journal of Biomechanics*, vol. 36, no. 10, pp. 1487–1495, 2003.

[189] R. B. Martin, D. B. Burr, N. A. Sharkey, and D. P. Fyhrie, *Skeletal Tissue Mechanics*. New York, NY: Springer New York, 2015.

[190] D. Chen, N. Bertollo, A. Lau, N. Taki, T. Nishino, H. Mishima, H. Kawamura, and W. R. Walsh, "Osseointegration of porous titanium implants with and without electrochemically deposited DCPD coating in an ovine model," *Journal of Orthopaedic Surgery and Research*, vol. 6, no. 1, p. 56, 2011.

[191] L. Bonewald, "Use it or lose it to age: A review of bone and muscle communication," *Bone*, vol. 120, pp. 212–218, 2019.

[192] M. Viceconti, S. Olsen, L.-P. Nolte, and K. Burton, "Extracting clinically relevant data from finite element simulations," *Clinical Biomechanics*, vol. 20, no. 5, pp. 451–454, 2005.

[193] D. S. Elliott, K. J. H. Newman, D. P. Forward, D. M. Hahn, B. Ollivere, K. Kojima, R. Handley, N. D. Rossiter, J. J. Wixted, R. M. Smith, and C. G. Moran, "A unified theory of bone healing and nonunion," *The Bone & Joint Journal*, vol. 98-B, no. 7, pp. 884–891, 2016.

[194] Y. Li, J. Zhou, P. Pavanram, M. Leeflang, L. Fockaert, B. Pouran, N. Tümer, K.-U. Schröder, J. Mol, H. Weinans, H. Jahr, and A. Zadpoor, "Additively manufactured biodegradable porous magnesium," *Acta Biomaterialia*, vol. 67, pp. 378–392, 2018.

[195] C. Han, Y. Li, Q. Wang, S. Wen, Q. Wei, C. Yan, L. Hao, J. Liu, and Y. Shi, "Continuous functionally graded porous titanium scaffolds manufactured by selective laser melting for bone implants," *Journal of the Mechanical Behavior of Biomedical Materials*, vol. 80, pp. 119–127, 2018.

[196] A. A. Zadpoor and H. Weinans, "Patient-specific bone modeling and analysis: The role of integration and automation in clinical adoption," *Journal of Biomechanics*, vol. 48, no. 5, pp. 750–760, 2015.

[197] A. Robling and C. Turner, "Mechanotransduction in bone: genetic effects on mechanosensitivity in mice," *Bone*, vol. 31, no. 5, pp. 562–569, 2002.

[198] I. J. Wallace, B. Demes, and S. Judex, "Ontogenetic and Genetic Influences on Bone's Responsiveness to Mechanical Signals," in *Building Bones: Bone Formation and Development in Anthropology* (C. J. Percival and J. T. Richtsmeier, eds.), pp. 233–253, Cambridge: Cambridge University Press, 2017.

[199] I. P. Geoghegan, D. A. Hoey, and L. M. McNamara, "Estrogen deficiency impairs integrin αvβ3-mediated mechanosensation by osteocytes and alters osteoclastogenic paracrine signalling," *Scientific Reports*, vol. 9, no. 1, p. 4654, 2019.

[200] I. Simfia, J. Schiavi, and L. M. McNamara, "ROCK-II inhibition suppresses impaired mechanobiological responses in early estrogen deficient osteoblasts," *Experimental Cell Research*, vol. 396, no. 1, p. 112264, 2020.

[201] A. Torcasio, X. Zhang, H. Van Oosterwyck, J. Duyck, and G. H. van Lenthe, "Use of micro-CT-based finite element analysis to accurately quantify peri-implant bone strains: a validation in rat tibiae," *Biomechanics and Modeling in Mechanobiology*, vol. 11, no. 5, pp. 743–750, 2012.

[202] J. Ganghoffer, R. Rahouadj, J. Boisse, and J. Schiavi, "A phase field approach for bone remodeling based on a second-gradient model," *Mechanics Research Communications*, vol. 96, pp. 37–44, 2019.

[203] R. M. Wazen, J. A. Currey, H. Guo, J. B. Brunski, J. A. Helms, and A. Nanci, "Micromotion-induced strain fields influence early stages of repair at bone–implant interfaces," *Acta Biomaterialia*, vol. 9, no. 5, pp. 6663–6674, 2013.

[204] P. Moreo, M. Pérez, J. García-Aznar, and M. Doblaré, "Modelling the mechanical behaviour of living bony interfaces," *Computer Methods in Applied Mechanics and Engineering*, vol. 196, no. 35-36, pp. 3300–3314, 2007.

[205] E. G. Meyer, C. T. Buckley, S. D. Thorpe, and D. J. Kelly, "Low oxygen tension is a more potent promoter of chondrogenic differentiation than dynamic compression," *Journal of Biomechanics*, vol. 43, no. 13, pp. 2516–2523, 2010.

[206] E. Borgiani, G. N. Duda, and S. Checa, "Multiscale Modeling of Bone Healing: Toward a Systems Biology Approach," *Frontiers in Physiology*, vol. 8, 2017.

[207] G. Nasello, P. Alamán-Díez, J. Schiavi, M. Á. Pérez, L. McNamara, and J. M. García-Aznar, "Primary human osteoblasts cultured in a 3d microenvironment create a unique representative model of their differentiation into osteocytes," *Frontiers in Bioengineering and Biotechnology*, vol. 8, p. 336, 2020.

[208] Y. C. Chai, A. Carlier, J. Bolander, S. J. Roberts, L. Geris, J. Schrooten, H. Van Oosterwyck, and F. P. Luyten, "Current views on calcium phosphate osteogenicity and the translation into effective bone regeneration strategies," *Acta Biomaterialia*, vol. 8, no. 11, pp. 3876–3887, 2012.

[209] F. Boukhechba, T. Balaguer, J. F. Michiels, K. Ackermann, D. Quincey, J. M. Bouler, W. Pyerin, G. F. Carle, and N. Rochet, "Human primary osteocyte differentiation in a 3D culture system," *Journal of Bone and Mineral Research*, vol. 24, no. 11, pp. 1927–1935, 2009.

[210] G. Atkins, D. Findlay, P. Anderson, and H. Morris, "Target genes: Bone proteins," in *Vitamin D*, vol. 25, pp. 411–424, Elsevier, third edition ed., 2011.

[211] M. Prideaux, D. M. Findlay, and G. J. Atkins, "Osteocytes: The master cells in bone remodelling," *Current Opinion in Pharmacology*, vol. 28, pp. 24–30, 2016.

[212] S. L. Dallas and L. F. Bonewald, “Dynamics of the transition from osteoblast to osteocyte,” *Annals of the New York Academy of Sciences*, vol. 1192, pp. 437–443, 2010.

[213] K. Uchihashi, S. Aoki, A. Matsunobu, and S. Toda, “Osteoblast migration into type I collagen gel and differentiation to osteocyte-like cells within a self-produced mineralized matrix: A novel system for analyzing differentiation from osteoblast to osteocyte,” *Bone*, vol. 52, no. 1, pp. 102–110, 2013.

[214] M. J. McGarrigle, C. A. Mullen, M. G. Haugh, M. C. Voisin, and L. M. McNamara, “Osteocyte differentiation and the formation of an interconnected cellular network in vitro,” *European Cells and Materials*, vol. 31, no. 353, pp. 323–340, 2016.

[215] Q. Sun, Y. Gu, W. Zhang, L. Dziopa, J. Zilberberg, and W. Lee, “Ex vivo 3D osteocyte network construction with primary murine bone cells,” *Bone Research*, vol. 3, no. 1, p. 15026, 2015.

[216] A. Pirosa, R. Gottardi, P. G. Alexander, and R. S. Tuan, “Engineering in-vitro stem cell-based vascularized bone models for drug screening and predictive toxicology,” *Stem Cell Research & Therapy*, vol. 9, no. 1, p. 112, 2018.

[217] B. W. de Wildt, S. Ansari, N. A. Sommerdijk, K. Ito, A. Akiva, and S. Hofmann, “From bone regeneration to three-dimensional in vitro models: tissue engineering of organized bone extracellular matrix,” *Current Opinion in Biomedical Engineering*, vol. 10, pp. 107–115, 2019.

[218] C. Wittkowske, G. C. Reilly, D. Lacroix, and C. M. Perrault, “In Vitro Bone Cell Models: Impact of Fluid Shear Stress on Bone Formation,” *Frontiers in Bioengineering and Biotechnology*, vol. 4, no. NOV, 2016.

[219] K. Ronaldson-Bouchard and G. Vunjak-Novakovic, “Organs-on-a-Chip: A Fast Track for Engineered Human Tissues in Drug Development,” *Cell Stem Cell*, vol. 22, no. 3, pp. 310–324, 2018.

[220] T. Osaki, V. Sivathanu, and R. D. Kamm, “Vascularized microfluidic organ-chips for drug screening, disease models and tissue engineering,” *Current Opinion in Biotechnology*, vol. 52, pp. 116–123, 2018.

[221] L. E. Bertassoni, M. Cecconi, V. Manoharan, M. Nikkhah, J. Hjortnaes, A. L. Cristino, G. Barabaschi, D. Demarchi, M. R. Dokmeci, Y. Yang, and A. Khademhosseini, “Hydrogel bioprinted microchannel networks for vascularization of tissue engineering constructs,” *Lab Chip*, vol. 14, no. 13, pp. 2202–2211, 2014.

[222] K. Middleton, S. Al-Dujaili, X. Mei, A. Günther, and L. You, “Microfluidic co-culture platform for investigating osteocyte-osteoclast signalling during fluid shear stress mechanostimulation,” *Journal of Biomechanics*, vol. 59, pp. 35–42, 2017.

[223] A. Marturano-Kruik, M. M. Nava, K. Yeager, A. Chramiec, L. Hao, S. Robinson, E. Guo, M. T. Raimondi, and G. Vunjak-Novakovic, “Human

bone perivascular niche-on-a-chip for studying metastatic colonization," *Proceedings of the National Academy of Sciences*, vol. 115, no. 6, pp. 1256–1261, 2018.

[224] K. E. Poole, R. L. Van Bezooijen, N. Loveridge, H. Hamersma, S. E. Papapoulos, C. W. Löwik, and J. Reeve, "Sclerostin is a delayed secreted product of osteocytes that inhibits bone formation," *FASEB Journal*, vol. 19, no. 13, pp. 1842–1844, 2005.

[225] G. J. Atkins, K. J. Welldon, A. R. Wijenayaka, L. F. Bonewald, and D. M. Findlay, "Vitamin K promotes mineralization, osteoblast-to-osteocyte transition, and an anticatabolic phenotype by gamma-carboxylation-dependent and -independent mechanisms," *American journal of physiology. Cell physiology*, vol. 297, no. 6, pp. C1358–C1367, 2009.

[226] Skottke, Gelinsky, and Bernhardt, "In Vitro Co-culture Model of Primary Human Osteoblasts and Osteocytes in Collagen Gels," *International Journal of Molecular Sciences*, vol. 20, no. 8, p. 1998, 2019.

[227] A. Bernhardt, E. Weiser, S. Wolf, C. Vater, and M. Gelinsky, "Primary Human Osteocyte Networks in Pure and Modified Collagen Gels," *Tissue Engineering Part A*, vol. 25, no. 19-20, pp. 1347–1355, 2019.

[228] S. M. Woo, J. Rosser, V. Dusevich, I. Kalajzic, and L. F. Bonewald, "Cell line IDG-SW3 replicates osteoblast-to-late-osteocyte differentiation in vitro and accelerates bone formation in vivo," *Journal of Bone and Mineral Research*, vol. 26, no. 11, pp. 2634–2646, 2011.

[229] J. R. Lorsch, F. S. Collins, and J. Lippincott-Schwartz, "Fixing problems with cell lines," *Science*, vol. 346, no. 6216, pp. 1452–1453, 2014.

[230] Y. Gu, W. Zhang, Q. Sun, Y. Hao, J. Zilberberg, and W. Y. Lee, "Microbead-guided reconstruction of the 3D osteocyte network during microfluidic perfusion culture," *Journal of Materials Chemistry B*, vol. 3, no. 17, pp. 3625–3633, 2015.

[231] F. Langenbach and J. Handschel, "Effects of dexamethasone, ascorbic acid and β-glycerophosphate on the osteogenic differentiation of stem cells in vitro," *Stem Cell Research & Therapy*, vol. 4, no. 5, p. 117, 2013.

[232] C. Del Amo, C. Borau, N. Movilla, J. Asín, and J. M. García-Aznar, "Quantifying 3D chemotaxis in microfluidic-based chips with step gradients of collagen hydrogel concentrations," *Integrative Biology*, vol. 9, no. 4, pp. 339–349, 2017.

[233] C. H. Chuang, R. Z. Lin, J. M. Melero-Martin, and Y. C. Chen, "Comparison of covalently and physically cross-linked collagen hydrogels on mediating vascular network formation for engineering adipose tissue," *Artificial Cells, Nanomedicine, and Biotechnology*, vol. 46, no. sup3, pp. S434–S447, 2018.

[234] S. L. Rowe and J. P. Stegemann, "Interpenetrating Collagen-Fibrin Composite Matrices with Varying Protein Contents and Ratios," *Biomacromolecules*,

vol. 7, no. 11, pp. 2942–2948, 2006.

[235] O. Moreno-Arotzena, J. Meier, C. del Amo, and J. García-Aznar, "Characterization of Fibrin and Collagen Gels for Engineering Wound Healing Models," *Materials*, vol. 8, no. 4, pp. 1636–1651, 2015.

[236] C. Valero, H. Amaveda, M. Mora, and J. M. García-Aznar, "Combined experimental and computational characterization of crosslinked collagen-based hydrogels," *PLOS ONE*, vol. 13, no. 4, p. e0195820, 2018.

[237] C. A. Mullen, M. G. Haugh, M. B. Schaffler, R. J. Majeska, and L. M. McNamara, "Osteocyte differentiation is regulated by extracellular matrix stiffness and intercellular separation," *Journal of the Mechanical Behavior of Biomedical Materials*, vol. 28, pp. 183–194, 2013.

[238] M. Linkert, C. T. Rueden, C. Allan, J. Burel, W. Moore, A. Patterson, B. Loranger, J. Moore, C. Neves, D. MacDonald, A. Tarkowska, C. Sticco, E. Hill, M. Rossner, K. W. Eliceiri, and J. R. Swedlow, "Metadata matters: access to image data in the real world," *The Journal of Cell Biology*, vol. 189, no. 5, pp. 777–782, 2010.

[239] S. van der Walt, J. L. Schönberger, J. Nunez-Iglesias, F. Boulogne, J. D. Warner, N. Yager, E. Gouillart, and T. Yu, "scikit-image: image processing in Python," *PeerJ*, vol. 2, p. e453, 2014.

[240] J. E. Coleman, "Structure and Mechanism of Alkaline Phosphatase," *Annual Review of Biophysics and Biomolecular Structure*, vol. 21, no. 1, pp. 441–483, 1992.

[241] E. E. Golub and K. Boesze-Battaglia, "The role of alkaline phosphatase in mineralization," *Current Opinion in Orthopaedics*, vol. 18, no. 5, pp. 444–448, 2007.

[242] E. Birmingham, G. L. Niebur, P. E. Mchugh, G. Shaw, F. P. Barry, and L. M. McNamara, "Osteogenic differentiation of mesenchymal stem cells is regulated by osteocyte and osteoblast cells in a simplified bone niche," *European Cells and Materials*, vol. 23, pp. 13–27, 2012.

[243] J. Schiavi, L. Keller, D. N. Morand, N. D. Isla, O. Huck, J. C. Lutz, D. Mainard, P. Schwinté, and N. Benkirane-Jessel, "Active implant combining human stem cell microtissues and growth factors for bone-regenerative nanomedicine," *Nanomedicine*, vol. 10, no. 5, pp. 753–763, 2015.

[244] J. Almodóvar, T. Crouzier, Š. Selimović, T. Boudou, A. Khademhosseini, and C. Picart, "Gradients of physical and biochemical cues on polyelectrolyte multilayer films generated via microfluidics," *Lab on a Chip*, vol. 13, no. 8, p. 1562, 2013.

[245] K. W. Eliceiri, M. R. Berthold, I. G. Goldberg, L. Ibáñez, B. S. Manjunath, M. E. Martone, R. F. Murphy, H. Peng, A. L. Plant, B. Roysam, N. Stuurmann, J. R. Swedlow, P. Tomancak, and A. E. Carpenter, "Biological imaging software tools," *Nature Methods*, vol. 9, no. 7, pp. 697–710, 2012.

[246] K. Zhang, C. Barragan-Adjemian, L. Ye, S. Kotha, M. Dallas, Y. Lu, S. Zhao, M. Harris, S. E. Harris, J. Q. Feng, and L. F. Bonewald, "E11/gp38 Selective Expression in Osteocytes: Regulation by Mechanical Strain and Role in Dendrite Elongation," *Molecular and Cellular Biology*, vol. 26, no. 12, pp. 4539–4552, 2006.

[247] J. Clover and M. Gowen, "Are MG-63 and HOS TE85 human osteosarcoma cell lines representative models of the osteoblastic phenotype?," *Bone*, vol. 15, no. 6, pp. 585–591, 1994.

[248] K. Jang, K. Sato, K. Igawa, U. I. Chung, and T. Kitamori, "Development of an osteoblast-based 3D continuous-perfusion microfluidic system for drug screening," *Analytical and Bioanalytical Chemistry*, vol. 390, no. 3, pp. 825–832, 2008.

[249] S. C. A. Yeh, K. Wilk, C. P. Lin, and G. Intini, "In Vivo 3D Histomorphometry Quantifies Bone Apposition and Skeletal Progenitor Cell Differentiation," *Scientific Reports*, vol. 8, no. 1, 2018.

[250] W. Zhang, Y. Gu, Y. Hao, Q. Sun, K. Konior, H. Wang, J. Zilberberg, and W. Y. Lee, "Well plate-based perfusion culture device for tissue and tumor microenvironment replication," *Lab on a Chip*, vol. 15, no. 13, pp. 2854–2863, 2015.

[251] G. Agrawal, A. Aung, and S. Varghese, "Skeletal muscle-on-a-chip: an in vitro model to evaluate tissue formation and injury," *Lab on a Chip*, vol. 17, no. 20, pp. 3447–3461, 2017.

[252] J. Park, B. K. Lee, G. S. Jeong, J. K. Hyun, C. J. Lee, and S.-h. Lee, "Three-dimensional brain-on-a-chip with an interstitial level of flow and its application as an in vitro model of Alzheimer's disease," *Lab on a Chip*, vol. 15, no. 1, pp. 141–150, 2015.

[253] S. Li, P. Glynne-Jones, O. G. Andriotis, K. Y. Ching, U. S. Jonnalagadda, R. O. C. Oreffo, M. Hill, and R. S. Tare, "Application of an acoustofluidic perfusion bioreactor for cartilage tissue engineering," *Lab Chip*, vol. 14, no. 23, pp. 4475–4485, 2014.

[254] C. Kim, K. S. Lee, J. H. Bang, Y. E. Kim, M.-C. Kim, K. W. Oh, S. H. Lee, and J. Y. Kang, "3-Dimensional cell culture for on-chip differentiation of stem cells in embryoid body," *Lab on a Chip*, vol. 11, no. 5, p. 874, 2011.

[255] Y. Liu, A. Beyer, and R. Aebersold, "On the Dependency of Cellular Protein Levels on mRNA Abundance.," *Cell*, vol. 165, no. 3, pp. 535–50, 2016.

[256] J. Van der Stok, O. P. Van der Jagt, S. Amin Yavari, M. F. P. De Haas, J. H. Waarsing, H. Jahr, E. M. M. Van Lieshout, P. Patka, J. A. N. Verhaar, A. A. Zadpoor, and H. Weinans, "Selective laser melting-produced porous titanium scaffolds regenerate bone in critical size cortical bone defects," *Journal of Orthopaedic Research*, vol. 31, no. 5, pp. 792–799, 2013.

[257] H. Shao, X. Ke, A. Liu, M. Sun, Y. He, X. Yang, J. Fu, Y. Liu, L. Zhang, G. Yang, S. Xu, and Z. Gou, "Bone regeneration in 3D printing bioactive ceramic scaffolds with improved tissue/material interface pore architecture in thin-wall bone defect," *Biofabrication*, vol. 9, no. 2, p. 025003, 2017.

[258] Y. Zhang, L. Xia, D. Zhai, M. Shi, Y. Luo, C. Feng, B. Fang, J. Yin, J. Chang, and C. Wu, "Mesoporous bioactive glass nanolayer-functionalized 3D-printed scaffolds for accelerating osteogenesis and angiogenesis," *Nanoscale*, vol. 7, no. 45, pp. 19207–19221, 2015.

[259] J. Wieding, T. Lindner, P. Bergschmidt, and R. Bader, "Biomechanical stability of novel mechanically adapted open-porous titanium scaffolds in metatarsal bone defects of sheep," *Biomaterials*, vol. 46, pp. 35–47, 2015.

[260] P. Cortellini and M. S. Tonetti, "Clinical concepts for regenerative therapy in intrabony defects," *Periodontology 2000*, vol. 68, no. 1, pp. 282–307, 2015.

[261] L. Claes, S. Recknagel, and A. Ignatius, "Fracture healing under healthy and inflammatory conditions," *Nature Reviews Rheumatology*, vol. 8, no. 3, pp. 133–143, 2012.

[262] E. Czekanska, M. Stoddart, R. Richards, and J. Hayes, "In search of an osteoblast cell model for in vitro research," *European Cells and Materials*, vol. 24, pp. 1–17, 2012.

[263] P. Chao, T. Maguire, E. Novik, K.-C. Cheng, and M. Yarmush, "Evaluation of a microfluidic based cell culture platform with primary human hepatocytes for the prediction of hepatic clearance in human," *Biochemical Pharmacology*, vol. 78, no. 6, pp. 625–632, 2009.

[264] M. Jasty, C. Bragdon, D. Burke, D. O'Connor, J. Lowenstein, and W. H. Harris, "In Vivo Skeletal Responses to Porous-Surfaced Implants Subjected to Small Induced Motions*," *The Journal of Bone and Joint Surgery (American Volume)*, vol. 79, no. 5, pp. 707–714, 1997.

[265] M. Cross, G. Roger, and J. Spycher, "Cementless fixation techniques and challenges in joint replacement*Note: This chapter is an updated version of Chapter 9 from the first edition of Joint replacement technology edited by P. A. Revell and published by Woodhead Publishing 2008*," in *Joint Replacement Technology*, pp. 186–211, Elsevier, 2014.

[266] J. Pitocchi, M. Wesseling, G. H. van Lenthe, and M. A. Pérez, "Finite Element Analysis of Custom Shoulder Implants Provides Accurate Prediction of Initial Stability," *Mathematics*, vol. 8, no. 7, p. 1113, 2020.

[267] R. M. Meneghini, A. D. Stultz, J. S. Watson, M. Ziemba-Davis, and C. A. Buckley, "Does Ischial Screw Fixation Improve Mechanical Stability in Revision Total Hip Arthroplasty?," *The Journal of Arthroplasty*, vol. 25, no. 7, pp. 1157–1161, 2010.

[268] M. P. Hoenig, B. Loeffler, S. Brown, R. Peindl, J. Fleischli, P. Connor, and D. D'Alessandro, "Reverse glenoid component fixation: Is a posterior

screw necessary?," *Journal of Shoulder and Elbow Surgery*, vol. 19, no. 4, pp. 544–549, 2010.

[269] F. Bobbert, K. Lietaert, A. Eftekhari, B. Pouran, S. Ahmadi, H. Weinans, and A. Zadpoor, "Additively manufactured metallic porous biomaterials based on minimal surfaces: A unique combination of topological, mechanical, and mass transport properties," *Acta Biomaterialia*, vol. 53, pp. 572–584, 2017.

[270] H. Seyednejad, D. Gawlitta, R. V. Kuiper, A. de Bruin, C. F. van Nostrum, T. Vermonden, W. J. Dhert, and W. E. Hennink, "In vivo biocompatibility and biodegradation of 3D-printed porous scaffolds based on a hydroxyl-functionalized poly(ϵ-caprolactone)," *Biomaterials*, vol. 33, no. 17, pp. 4309–4318, 2012.

[271] Y. Lai, Y. Li, H. Cao, J. Long, X. Wang, L. Li, C. Li, Q. Jia, B. Teng, T. Tang, J. Peng, D. Eglin, M. Alini, D. W. Grijpma, G. Richards, and L. Qin, "Osteogenic magnesium incorporated into PLGA/TCP porous scaffold by 3D printing for repairing challenging bone defect," *Biomaterials*, vol. 197, pp. 207–219, 2019.

[272] J.-A. Kim, J. Lim, R. Naren, H.-s. Yun, and E. K. Park, "Effect of the biodegradation rate controlled by pore structures in magnesium phosphate ceramic scaffolds on bone tissue regeneration in vivo," *Acta Biomaterialia*, vol. 44, pp. 155–167, 2016.

[273] S. Janbaz, K. Narooei, T. van Manen, and A. A. Zadpoor, "Strain rate–dependent mechanical metamaterials," *Science Advances*, vol. 6, no. 25, p. eaba0616, 2020.

[274] A. A. Zadpoor, "Meta-biomaterials," *Biomaterials Science*, vol. 8, no. 1, pp. 18–38, 2020.

[275] K. Bobe, E. Willbold, I. Morgenthal, O. Andersen, T. Studnitzky, J. Nellesen, W. Tillmann, C. Vogt, K. Vano, and F. Witte, "In vitro and in vivo evaluation of biodegradable, open-porous scaffolds made of sintered magnesium W4 short fibres," *Acta Biomaterialia*, vol. 9, no. 10, pp. 8611–8623, 2013.

[276] J. A. Inzana, D. Olvera, S. M. Fuller, J. P. Kelly, O. A. Graeve, E. M. Schwarz, S. L. Kates, and H. A. Awad, "3D printing of composite calcium phosphate and collagen scaffolds for bone regeneration," *Biomaterials*, vol. 35, no. 13, pp. 4026–4034, 2014.

[277] N. Golafshan, E. Vorndran, S. Zaharievski, H. Brommer, F. B. Kadumudi, A. Dolatshahi-Pirouz, U. Gbureck, R. van Weeren, M. Castilho, and J. Malda, "Tough magnesium phosphate-based 3D-printed implants induce bone regeneration in an equine defect model," *Biomaterials*, vol. 261, p. 120302, 2020.

[278] Y. Li, P. Pavanram, J. Zhou, K. Lietaert, F. S. L. Bobbert, Y. Kubo, M. A. Leeflang, H. Jahr, and A. A. Zadpoor, "Additively manufactured functionally

graded biodegradable porous zinc," *Biomaterials Science*, vol. 8, no. 9, pp. 2404–2419, 2020.

[279] H. Gholipour, A. Meimandi-Parizi, A. Oryan, and A. Bigham Sadegh, "The effects of gelatin, fibrin-platelet glue and their combination on healing of the experimental critical bone defect in a rat model: radiological, histological, scanning ultrastructural and biomechanical evaluation," *Cell and Tissue Banking*, vol. 19, no. 3, pp. 341–356, 2018.

[280] P. Simpson-Haidaris and B. Rybarczyk, "Tumors and Fibrinogen," *Annals of the New York Academy of Sciences*, vol. 936, pp. 406–425, jan 2006.

[281] Y. Li, W.-J. Tseng, C. M. de Bakker, H. Zhao, R. Chung, and X. S. Liu, "Peak trabecular bone microstructure predicts rate of estrogen-deficiency-induced bone loss in rats," *Bone*, vol. 145, p. 115862, 2021.

[282] W. J. Polacheck, R. Li, S. G. M. Uzel, and R. D. Kamm, "Microfluidic platforms for mechanobiology," *Lab on a Chip*, vol. 13, no. 12, p. 2252, 2013.

Curriculum vitae

Research experience

- **KU Leuven**, Leuven, Belgium.
  Doctoral Researcher, September 2020 - Ongoing.
- **Materialise NV**, Leuven, Belgium.
  Early Stage Researcher, January 2019 - September 2020.
- **The RJAH Orthopaedic Hospital**, Oswestry, United Kingdom.
  Visiting Researcher, August 2019.
- **NUI Galway**, Galway, Ireland.
  Visiting Researcher, February 2018 - April 2018.
- **Universidad de Zaragoza**, Zaragoza, Spain.
  Early Stage Researcher, September 2017 - December 2018.
- **McGowan Institute for Regenerative Medicine**, Pittsburgh, Pennsylvania.
  Visiting Scholar, September 2016 - April 2017.
- **McGowan Institute for Regenerative Medicine**, Pittsburgh, Pennsylvania.
  Visiting Scholar, February 2014 - April 2014.

Education

- **Master Degree in Biomedical Engineering**
  Politecnico di Milano, Milano, Italy. *110/110 cum laude*.
- **Bachelor Degree in Mechanical Engineering**
  Università degli Studi di Palermo, Palermo, Italy. *110/110 cum laude*.

Publications

Journal articles

The following publications in international peer reviewed journals have arisen from the work presented in this thesis:

- **Nasello, G.**, Alamán-Díez, P., Schiavi, J., Pérez, M. Á., McNamara, L. and García-Aznar, J. M., 2020 Primary human osteoblasts cultured in a 3D microenvironment create a unique representative model of their differentiation into osteocytes. *Frontiers in Bioengineering and Biotechnology, 8*, p.336.
- **Nasello, G.**, Vautrin, A., Pitocchi, J., Wesseling, M., Kuiper, J. H., Pérez, M. Á. and García-Aznar, J. M., 2021 Mechano-driven regeneration predicts scaffold mineralization patterns in large animal model based on implantation site mechanics and individual sensitivity. *Bone, 144*, p.115769.
- García-Aznar, J. M., **Nasello, G.**, Hervas-Raluy, S., Pérez, M. Á. and Gómez-Benito, M. J., 2021 Multiscale Modeling of Bone Tissue Mechanobiology. *Submitted to Bone*.
- **Nasello, G.**, Cóndor, M., Vaughan, T. and Schiavi, J., 2021 Designing hydrogel-based bone-on-chips for personalized medicine. *Submitted to Applied Sciences*.

Other publications:

- D'Amore, A., **Nasello, G.**, Luketich, S.K., Denisenko, D., Jacobs, D.L., Hoff, R., Gibson, G., Bruno, A., Raimondi, M.T. and Wagner, W.R., 2018. Meso-scale topological cues influence extracellular matrix production in a large deformation, elastomeric scaffold model. *Soft matter, 14(42)*, pp.8483-8495.

Conference presentations

Oral presentations:

- **Nasello, G.**, 2019 Micro-engineered platform to study osteoblast-osteocyte transition. *European Network of BioAdhesives*. 18th September, Leuven, Belgium.
- **Nasello, G.**, Pérez, M. Á., Asín, J., Wirix-Speetjens, R. and García-Aznar, J. M., 2019 Mechanically-driven osteointegration: a numerical model for bone regeneration in porous scaffolds. *25th Congress of the European Society of Biomechanics*. 8th July, Vienna, Austria.
- **Nasello, G.**, Alamán-Díez, P., Schiavi, J., Pérez, M. Á., McNamara, L. and García-Aznar, J. M., 2019 Osteoblast-osteocyte differentiation in microfluidic devices. *TERMIS European Chapter Meeting 2019*. 29th May, Rhodes, Greece.
- **Nasello, G.**, Pérez, M. Á., Wirix-Speetjens, R. and García-Aznar, J. M., 2018 Multiphysic Approach for Bicomponent Tissue Engineered Bone Grafts. *Virtual Physiological Human Conference 2018*. 6th September, Zaragoza, Spain.

Poster presentations:

- **Nasello, G.**, Pitocchi, J., Pérez, M. Á., and García-Aznar, J. M., 2019 Finite element model predicts the effect of scaffold location in bone ingrowth distribution. *National Day on Biomedical Engineering 2019*. 29th November, Brussel, Belgium.
- **Nasello, G.**, Alamán-Díez, P., Schiavi, J., Pérez, M. Á., McNamara, L. and García-Aznar, J. M., 2019 Microfluidic platform as minimal functional unit for mature bone tissue formation. *7th Belgian Symposium on Tissue Engineering*. 15th November, Hasselt, Belgium.
- **Nasello, G.**, Alamán-Díez, P., Schiavi, J., Pérez, M. Á., McNamara, L. and García-Aznar, J. M., 2019 Osteoblast-osteocyte differentiation in microfluidic devices. *7th TERMIS Winterschool 2019*. 15th January, Radstadt, Austria.
- **Nasello, G.**, Pérez, M. and García-Aznar, J. M., 2019 Integration of models and experiments for bone tissue formation. *24th Congress of the European Society of Biomechanics*. 8th July, Dublin, Ireland.